

Supernova environments in J-PLUS

Normalized Cumulative Rank distributions and stellar population synthesis, combining narrow- and broad-band filters

Raul González-Díaz^{1,2*}, Lluís Galbany^{1,3}, Tuomas Kangas^{4,5}, Rubén García-Benito⁶,
Joseph P. Anderson^{7,8}, Joseph Lyman⁹, Jesús Varela¹⁰, Lamberto Oltra¹, Rafael Logroño García¹⁰,
Gonzalo Vilella Rojo¹⁰, Carlos López-Sanjuan¹⁰, Miguel Ángel Pérez-Torres⁶, Fabián Rosales-Ortega²,
Seppo Mattila^{4,5}, Hanindyo Kuncarayakti^{4,5}, Phil James¹¹, Stacey Habergham¹¹, José Manuel Vílchez⁶,
Jailson Alcaniz¹², Raul E. Angulo¹³, Javier Cenarro¹⁰, David Cristóbal-Hornillos¹⁰, Renato Dupke¹²,
Alessandro Ederoclite¹⁰, Carlos Hernández-Monteagudo¹⁰, Antonio Marín-Franch¹⁰, Mariano Moles¹⁰,
Laerte Sodré Jr.¹⁴, and Héctor Vázquez Ramió¹⁰

¹ Institute of Space Sciences (ICE-CSIC), Campus UAB, Carrer de Can Magrans, s/n, E-08193 Barcelona, Spain.

² Instituto Nacional de Astrofísica, Óptica y Electrónica (INAOE-CONAHCyT), Luis E. Erro 1, 72840 Tonantzintla, Puebla, México.

³ Institut d'Estudis Espacials de Catalunya (IEEC), E-08034 Barcelona, Spain.

⁴ Finnish Centre for Astronomy with ESO (FINCA), FI-20014 University of Turku, Finland

⁵ Tuorla Observatory, Department of Physics and Astronomy, FI-20014 University of Turku, Finland

⁶ Instituto de Astrofísica de Andalucía (CSIC), Glorieta de la Astronomía s/n, Aptdo. 3004, E-18080-Granada, Spain.

⁷ European Southern Observatory, Alonso de Córdova 3107, Casilla 19, Santiago, Chile.

⁸ Millennium Institute of Astrophysics MAS, Nuncio Monsenor Sotero Sanz 100, Off. 104, Providencia, Santiago, Chile.

⁹ Department of Physics, University of Warwick, Coventry CV4 7AL, UK.

¹⁰ Centro de Estudios de Física del Cosmos de Aragón (CEFCA), Unidad Asociada al CSIC, P. San Juan, 1, 44001 Teruel, Spain

¹¹ Astrophysics Research Institute, Liverpool John Moores University, IC2, 146 Brownlow Hill, Liverpool L3 5RF, UK

¹² Observatorio Nacional, Rua Gal. José Cristina 77, Rio de Janeiro, 20921-400, RJ, Brazil.

¹³ Donostia International Physics Center, Paseo Manuel de Lardizabal 4, 20018, Donostia-San Sebastian, Spain.

¹⁴ Instituto de Astronomia, Geofísica e Ciencias Atmosféricas, U. São Paulo, R. do Matão 1226, São Paulo, 05508-090, SP, Brazil.

Received ... ; accepted ...

ABSTRACT

We investigate the local environmental properties of 418 supernovae (SNe) of all types using data from the Javalambre Photometric Local Universe Survey (J-PLUS), which includes five broad- and seven narrow-band imaging filters. Our study involves two independent analyses: 1) the Normalized Cumulative Rank (NCR) method, which utilizes all 12 single bands along with five continuum-subtracted narrow-band emission and absorption bands, and 2) simple stellar population (SSP) synthesis, where we build spectral energy distributions (SED) of the surrounding 1 kpc^2 SN environment using the 12 broad- and narrow-band filters. Improvements over previous works include: (i) the extension of the NCR technique to other filters (broad and narrow) and using a set of homogeneous data (same telescope/instrument); (ii) a correction for extinction to all bands based on the relation between the $g - i$ color and the color excess $E(B - V)$; and (iii) a correction for the contamination of the [N II] $\lambda 6583$ line that falls within the $\text{H}\alpha$ filter. All NCR distributions in the broad-band filters, tracing the overall light distribution in each galaxy, are similar to each other. The main difference is that type Ia, II and I Ib SNe are preferably located in redder environments than the other SN types. The radial distribution of the SNe shows that type I Ib SNe seem to have a preference for occurring in the inner regions of galaxies, whereas other types of SNe occur throughout the galaxy without a distinct preference for a specific location. For the $\text{H}\alpha$ filter we recover the sequence from SNe Ic with the highest NCR to SNe Ia with the lowest, which is interpreted as a sequence in progenitor mass and age. All core-collapse SN types are strongly correlated to the [O II] emission, which also traces SFR, following the same sequence as in $\text{H}\alpha$. The NCR distributions of the Ca II triplet show a clear division between II/I Ib/Ia and Ib/Ic/IIn subtypes, which is interpreted as a difference in the environmental metallicity. Regarding the SSP synthesis, we found that including the seven J-PLUS narrow filters in the fitting process has a more significant effect for the core-collapse SN environmental parameters than for SNe Ia, shifting their values towards more extincted, younger, and more star-forming environments, due to the presence of strong emission-lines and stellar absorptions in those narrow-bands.

Key words. galaxies: general – (stars:) supernovae: general – techniques: photometric – galaxies: photometry – methods: statistical – methods: observational

1. Introduction

Supernovae (SNe) are one of the final stages in stellar evolution, being key in driving chemical evolution of galaxies. Classical SNe (excluding superluminous) are basically divided in two main types: thermonuclear (those of type Ia) and core-collapse (CC). Type Ia SNe are those triggered by the thermonuclear explosion of a carbon and oxygen white dwarf (WD; Hoyle & Fowler 1960). Different progenitor scenarios, such as WDs reaching the Chandrasekhar limit ($M_{Ch} \sim 1.44M_{\odot}$) by mass accretion in a binary system or mergers of WDs, and explosion mechanisms, such as internal detonations of M_{Ch} WD or surface explosions on WDs with masses lower than M_{Ch} , have been proposed to explain how the WD explode (see review by e.g. Maoz et al. 2014). No direct progenitor detection has been reported to date (but see McCully et al. 2014), but all cases, the main spectral features are the lack of H lines and the presence of strong Si II lines up to a couple of weeks after maximum brightness (Filippenko 1997). SNe Ia occur in galaxies of all types, including elliptical galaxies which only contain old stellar populations, providing strong evidence that SNe Ia have long-lived, low-mass progenitors (Han et al. 2010). SNe Ia are more luminous than CC SNe, comprising about 30% of the observed SNe (Graur et al. 2017). Their distinctive feature lies in the fact that generally normal SNe Ia exhibit similar spectra and light curves, making them valuable for tracing cosmological distances (e.g. Phillips et al. 1999; Riess et al. 1996; Perlmutter et al. 1997, 1999; Astier et al. 2006).

CC SNe are those resulting from the gravitational collapse of the iron core of a massive star ($> 8M_{\odot}$; Arnett et al. 1989). CCSNe are divided into 3 main sub-types depending on their spectral features, which reflect the state of the outer layers of the progenitor star at the moment of explosion. Type II SNe show H lines because their progenitors have kept the H-rich outer envelope intact, type Ib SNe show He but no H since the progenitor has lost the H envelope, and type Ic SNe lack both H and He lines due to the loss of both H- and He-rich layers (Filippenko 1997). Additionally, SNe IIn show narrow H emission lines most probably due to interaction with circumstellar material (Smith et al. 2011), and SNe I Ib are those intermediate between SNe II and Ib, that show H only for a few days after explosion indicating that there was still a thin H layer before explosion (Filippenko 1988; Nomoto et al. 1993). There is a debate on the process responsible for the mass-loss leading to stripped envelope (SE) SN types (Ib, Ic, I Ib). Mass-loss through radiation-driven wind from single hot massive stars or removal of the outer envelope via tidal stripping by a less massive companion in a binary are the two most viable possibilities (Filippenko 1997; Gal-Yam 2017; Prentice & Mazzali 2017; Shivvers et al. 2017; Taddia et al. 2018).

One of the outstanding questions in the field of massive stellar evolution is the link between the nature of the progenitor and the resultant SN. Direct constraints on the nature of SN progenitors are limited. The bulk of these come from the small number of nearby events where deep, high-resolution (usually from the Hubble Space Telescope) pre-explosion imaging exists to directly image the progenitor star (e.g. Maund et al. 2013; Smartt 2015; Van Dyk 2017). For almost all discovered SNe, this is unfeasible. As such, methods investigating statistical properties of SNe have been developed to exploit the large numbers of observed SN environments (pre-SN or once the SN has faded), including historical ones. One of those statistical methods is the Normalised Cumulative Rank (NCR; Fruchter et al. 2006; James & Anderson 2006). The NCR, when applied to H α narrow imaging, measures the correlation between SN locations and star formation inten-

Table 1: J-PLUS photometric system properties. Transmission curves can be found at the J-PLUS website: <http://www.j-plus.es/survey/instrumentation>.

Filter name	Central λ (nm)	FWHM (nm)	Comments
uJAVA	348.5	50.8	ultraviolet continuum
J0378	378.5	16.8	[OII] emission
J0395	395.0	10.0	Ca H+K absorption
J0410	410.0	20.0	H δ emission
J0430	430.0	20.0	G-band absorption
gSDSS	480.3	140.9	SDSS green continuum
J0515	515.0	20.0	Mgb Triplet absorption
rSDSS	625.4	138.8	SDSS red continuum
J0660	660.0	14.5	H α emission
iSDSS	766.8	153.5	SDSS near infrared continuum
J0861	861.0	40.0	Ca II triplet absorption
zSDSS	911.4	140.9	SDSS near infrared continuum

sity (i.e. H α emission) in their host galaxies. The strength of this correlation is an indicator of the progenitor lifetime, a proxy for the initial mass of the progenitor. The method has been employed on samples of SNe to deduce a sequence of ascending mass for the common SN types Ia, II, Ib, and Ic (Anderson & James 2008; Anderson et al. 2012; Kangas et al. 2013). Subsequently, Kangas et al. 2017 established a connection between the NCRs of these SNe and those of massive stars in the LMC and M33. This linkage indicated initial masses of approximately $> 20M_{\odot}$ for SN Ic progenitors and $> 9M_{\odot}$ for SNe II and SNe Ib. For the stripped envelope SN types, Ic and Ib, these findings would imply that single Wolf-Rayet stars and/or massive binaries are the most probable progenitors for the former, while for the latter interacting relatively low-mass binary systems, such as the directly detected 10–12 M_{\odot} progenitor of the SN Ib iPTF13bvn (Eldridge & Maund 2016), would be dominant.

Another method that has proved useful to put constraints on SN progenitors is the study of the stellar populations at SN locations. Galbany et al. (2014, 2016) presented the first statistical study using Integral Field Spectroscopy of nearby SN host galaxies provided by the CALIFA survey, which consists of 132 SN of all types in 115 galaxies, and that was later extended to 272 SNe in 232 galaxies in Galbany et al. (2018). Stellar parameters were inferred by fitting a set of single stellar population (SSP) models to the spectra of the locations where SNe occurred. They found that CC SNe tend to explode at positions with younger stellar populations than the galaxy average, while at SN Ia locations local properties were on average the same as global. They also found a sequence from higher to lower metallicity, from SN Ia to SN Ic-BL, and significant increasing relative number of SNe Ic at higher metallicities compared to other CC SN types, which supports a large fraction of this SN subtype occurring under the single star scenario (also see Kuncarayakti et al. 2013, 2018).

In this paper, we present a comprehensive analysis of 418 supernova (SN) environments using the 12 filter system of the Javalambre Photometric Local Universe Survey (J-PLUS¹; Cenarro et al. 2019), whose spatial resolution ($\lesssim 382$ pc, corresponding to an angular resolution of 1.14 arcsec at $z = 0.016$) and overall data quality of this dataset allow us to study the SN environments. Our investigation involves two main methodologies: the NCR analysis and the SSP synthesis. Compared to previous works in the literature, our study offers several advancements. Firstly, we extend the NCR technique to a number of broad- and narrow-band filters other than H α , which enables us to explore correlations with new spectral lines. This extension opens up possibilities to probe additional environmental factors, such

* Raul.GonzalezD@autonomia.cat

¹ www.j-plus.es

Table 2: Pivot wavelengths and Zero Points of the J-PLUS bands.

Filter	uJAVA	J0378	J0395	J0410	J0430	gSDSS
λ_{pivot} (nm)	352.29	378.64	395.06	410.07	430.04	474.46
ZP (AB mag)	21.078 (049)	20.416 (036)	20.332 (037)	21.283 (029)	21.380 (028)	23.553 (035)
Filter	J0515	rSDSS	J0660	iSDSS	J0861	zSDSS
λ_{pivot} (nm)	514.98	622.98	659.98	767.65	860.25	892.20
ZP (AB mag)	21.500 (040)	23.494 (023)	20.953 (023)	23.136 (023)	21.439 (007)	22.498 (007)

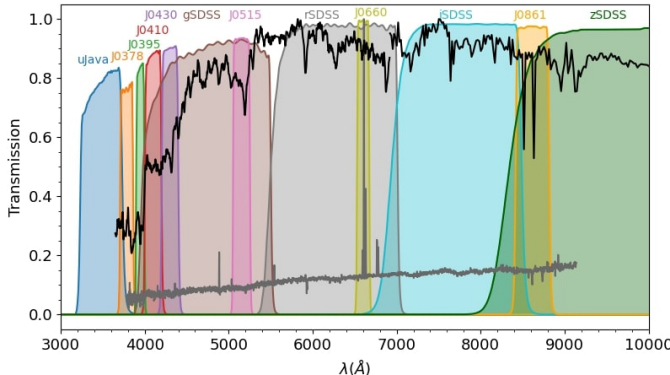


Fig. 1: Transmission of the 12 J-PLUS filters, on top of a typical star-forming (in grey) and passive galaxy (in black) spectra. Labels, which represent the filter names, highlight the main spectral features covered by the intermediate and narrow band filters.

as stellar population metallicity or age. Previous studies, such as Kangas et al. (2013, with UV imaging) and Anderson et al. (2015, with NIR imaging), have explored these factors to some extent. However, our research operates on a much larger scale and utilizes a set of homogeneous data acquired from the same telescope and instrument. Another improvement over past works is the correction for the contamination from the [N II] $\lambda 6583$ line that falls within the H α filter. Vilella-Rojo et al. (2015) presented a method to correct for such extra emission by combining narrow and broad-band data, and providing pure H α emission from J-PLUS observations. This method can also be extended to other narrow-band filters.

2. Data

2.1. J-PLUS

J-PLUS is designed to observe 8500 deg^2 of the northern sky from the Observatorio Astrofísico de Javalambre (OAJ, Teruel, Spain; Cenarro et al. 2014) with the 83 cm Javalambre Auxiliary Survey Telescope (JAST80) and T80Cam, a panoramic camera of $9.2\text{k} \times 9.2\text{k}$ pixels that provides a 2 deg^2 field of view (FoV) with a pixel scale of $0.55 \text{ arcsec pix}^{-1}$ (Marín-Franch et al. 2015). The J-PLUS filter system comprises the 12 broad, intermediate and narrow band optical filters. J-PLUS is particularly designed to carry out the photometric calibration of the Javalambre Physics of the Accelerating Universe Astrophysical Survey (J-PAS²; Benítez et al. 2014), which has been observe the northern sky from Javalambre using 59 optical narrow band filters. For this reason, some J-PLUS filters are located at key stellar spectral features that allow to retrieve very accurate spectral energy distributions (SED) for more than five millions of stars in our galaxy. The

12 filters of J-PLUS are listed in Table 1 and their transmission is shown in Figure 1, together with two template spectra of a star-forming and a passive galaxies to highlight the regions of interest covered by the intermediate and narrow band filters. The third J-PLUS Data Release (DR3³) was made public in December 2022, comprising 1642 pointings observed in the twelve optical bands amounting to $\sim 3200 \text{ sq. deg}$ with around 30 million sources detected at magnitudes $r < 21$. We cross-matched all SN coordinates from the Open Supernova Catalogue (OSC; Guillochon et al. 2017) to the central coordinates of all J-PLUS DR3 tiles, and found 2168 SNe positions within the 2 sq. deg of the J-PLUS tile. The width of the narrow H α filter (J0660 filter; $\sim 150 \text{ Å}$) puts an upper limit to the redshift of galaxies that are useful for a NCR study at $z \sim 0.0163$ (or about 60 Mpc), since the J0660 transmission falls down dramatically at 6672 Å . Thus, in order to keep the H α emission of the SN host galaxy within the coverage of the J-PLUS J0660 filter, we excluded all objects with a redshift larger than 0.0163. Moreover, NCR becomes less useful with distance, and samples at significantly different median distances may not be directly comparable (Kangas et al. 2017). This redshift cut is passed by 282 SNe of the following types: 88 SNe Ia, 126 SNe II, 7 SNe IIn, 22 SNe Ib, 17 SNe Ic, 17 SNe IIb and other 5 type Ibc SNe.

2.2. A dedicated SN host galaxy programme at JAST80

To reach a significantly large number of SNe that cover all types compared to previous studies, and within the redshift limit imposed by the J-PLUS H α filter width, we had to include objects outside the J-PLUS footprint taking special care to increase the number of less represented subtypes (Ic, Ib, IIb, IIn). With this objective in mind, we initiated a dedicated program to acquire 73 additional fields using the same instrumental configuration and exposure times as in J-PLUS, which involves T80 and 12 filters. These fields encompassed the positions and host galaxies of 136 SNe. For each of the 12 filters, we obtained three individual frames, all of which were subsequently processed using the same J-PLUS pipeline (Cenarro et al. 2019).

Summing up the observations from the main survey and our dedicated programme, 418 SNe are included in our sample, and are listed in Table A.1. Taking into account the main SN types, we have 156 SNe II, 20 SN IIn, 108 SN Ia, 51 SN Ib, 49 SN Ic, 27 SN IIb and 7 other type Ibc SNe. The analysis is carried out with the sample divided into these seven main SN types, where SNe Ibc include Ib, Ic, IIb and other Ibc.

3. Generation of individual 3D datacubes

Starting from the initial 12 images per field, one for each filter, we perform a number of steps to produce one 3D datacube per galaxy, namely galaxy cutout, flux calibration, correction for

² <http://www.j-pas.org/survey>

³ http://www.j-plus.es/datareleases/data_release_dr3

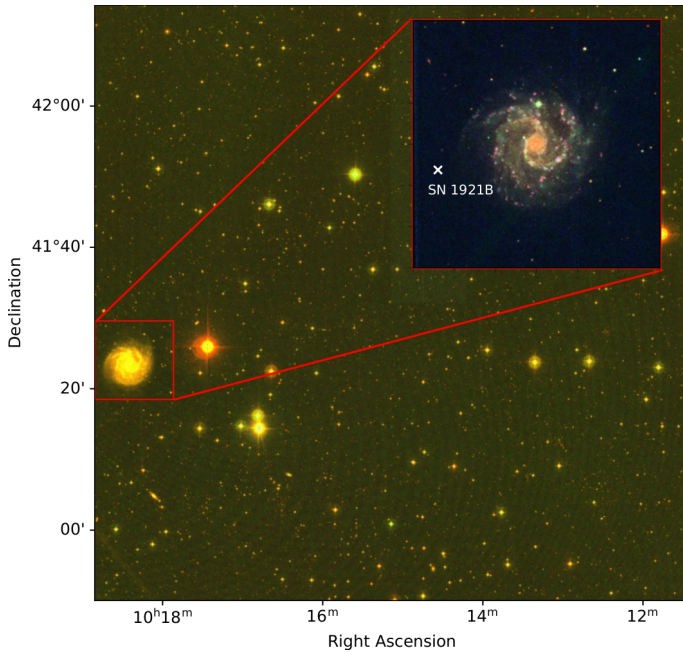


Fig. 2: Example of J-PLUS field frame. The zoom corresponds to the cutout of the galaxy NGC 3184 that contains the SN 1921B, marked in white. The images were constructed combining the uJAVA (blue), gSDSS (green) and rSDSS (red) images as fake colors.

dust extinction, and continuum subtraction. All these steps are described in the following subsections.

3.1. Galaxy cutouts

J-PLUS images cover around ~ 2 sq. deg of the sky with a pixel scale of 0.55 arcsec, with a median seeing of 1.14 arcsec, corresponding to $\lesssim 382$ pc at $z = 0.016$. After registering all 12 images to the same reference frame, we take a squared cutout of a size that includes the full extent of the SN host galaxy centered at its core, defining the size by visual inspection (see Fig. 2). The 12 cutouts are then stored in a 3D cube, mimicking integral field spectroscopy observations, where 2 spatial dimensions correspond to RA and Dec, and the 3rd dimension provides a spectral energy distribution (SED) at any position within the cutout.

3.2. Flux calibration

To convert the electronic counts stored in each pixel to radiative flux we use the expression from Logroño-García et al. (2019),

$$F_\lambda = C \cdot 10^{-0.4(ZP+48.6)} \frac{c}{\lambda_{\text{pivot}}^2}, \quad (1)$$

where C is the number counts in the pixel, c is the speed of light, ZP is the zero point of the band used for the calibration to the standard AB magnitude system, and λ_{pivot} is the pivot wavelength of the filter, which is a source-independent measurement of the characteristic wavelength of a given passband by,

$$\lambda_{\text{pivot}}^2 = \frac{\int T(\lambda) d\lambda}{\int T(\lambda) \lambda^{-2} d\lambda}, \quad (2)$$

where $T(\lambda)$ represents the transmission curve of the filter. The values of ZP and pivot wavelength are given in Table 2.

3.3. Dust extinction correction

The Milky Way interstellar dust reddening was corrected using the python code DUSTMAPS (Green 2018) and the *Gaia Total Galactic Extinction* map (Delchambre et al. 2023) as the source to obtain the $E(B-V)$ color excess for every galaxy. In addition, we applied a correction to the reddening due to dust in the SN host galaxy. Following Calzetti et al. (2000), the difference between the intrinsic and observed flux due to extinction is given by,

$$F_i(\lambda) = F_0(\lambda) 10^{0.4E(B-V)k'(\lambda)}, \quad (3)$$

where $F_i(\lambda)$ and $F_0(\lambda)$ are the intrinsic and observed fluxes at a wavelength λ , $E(B-V)$ is the color excess, and $k'(\lambda)$ is the extinction law, an empirical relationship between the amount of extinction and wavelength. We employ the Calzetti et al. (2000) extinction law, defined as:

$$k'(\lambda) = \begin{cases} 2.659(-1.857 + 1.040/\lambda) + R'_V & \text{for } 0.63 \mu\text{m} \leq \lambda \leq 2.20 \mu\text{m} \\ 2.659(-2.156 + 1.509/\lambda - 0.198/\lambda^2 + 0.011/\lambda^3) + R'_V & \text{for } 0.12 \mu\text{m} \leq \lambda \leq 0.63 \mu\text{m} \end{cases} \quad (4)$$

where R'_V is the obscuration in the V band. Here, we use the same value found by Calzetti et al. (2000), $R'_V = 4.05 \pm 0.80$ for stellar extinction⁴. To estimate the color excess $E(B-V)$, we follow Vilella-Rojo et al. (2015) who found a relation between the observed $g' - i'$ colour and the spectroscopically measured $E(B-V)$ obtained after convolving the SDSS spectra with the J-PLUS photometric system. These authors obtained the following expression by fitting a power-law function,

$$E(B-V) = 0.206(g' - i')^{1.68} - 0.0457, \quad (5)$$

and assuming $E(B-V) = 0$ for $g' - i' < 0.4$.

This is an empirical expression for the gas extinction. Vilella-Rojo et al. (2015) mix in the same process of correction to the stellar and gas component for all the J-PLUS data, so, we use the same method to be coherent. The gas extinction is, at minimum, the same as the stellar extinction. However, on average, the extinction in HII regions can be twice as high (Cid Fernandes et al. 2005). Therefore, it's essential to note that the extinction correction applied by this method represents a conservative lower bound.

With all these ingredients, we correct the fluxes of the 12 images for all SNe in our sample, pixel by pixel. This improvement results in a change in our NCR values compared to studies that do not apply this correction to the fluxes. Hence, we caution to not make direct comparisons of NCR values to previous works that employed different methodologies.

3.4. J0660 continuum subtraction

J-PLUS narrow band filters were designed to cover wavelength regions of a number of emission lines of interest. However, they also include flux of the underlying stellar continuum that needs to measure exclusively the gas-phase component. In particular, both $rSDSS$ and $J0660$ filters are collecting the flux of the $H\alpha$ emission line, so to study the $H\alpha$ emission, which is a tracer of

⁴ The stellar extinction mainly affects those filters without emission lines, and gas extinction mainly affects those with emission lines (Thomas et al. 2013).

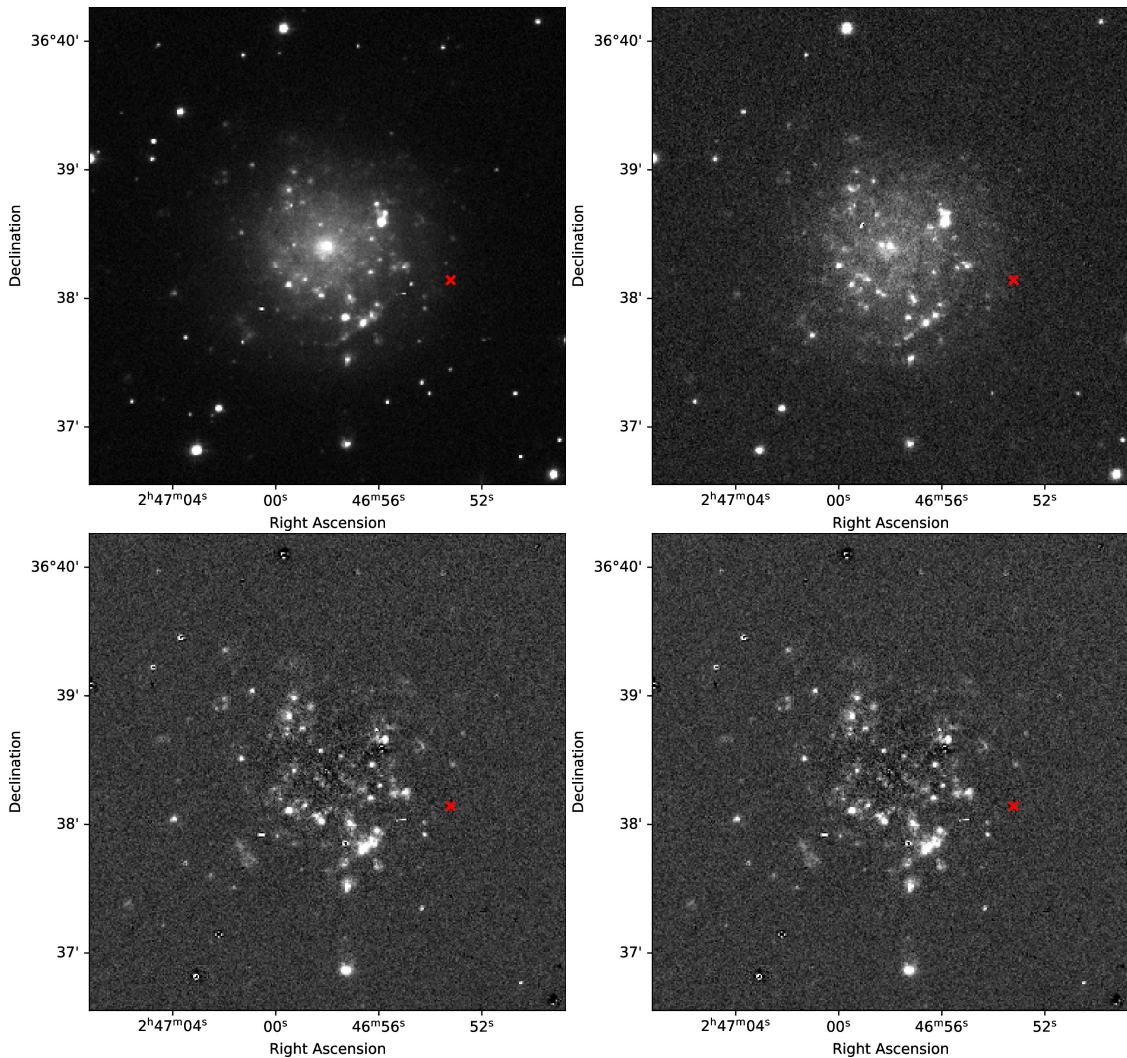


Fig. 3: J-PLUS NGC1058 J0660 image with the type II SN1961V marked in red. Top left: Before dust extinction correction. Top right: After dust extinction correction. Bottom left: After continuum subtraction. Bottom right: After [NII] removal.

the star formation, we have to subtract the stellar continuum from the J0660 flux.

Vilella-Rojo et al. (2015) presented two methods to remove the underlying continuum from a narrow band filter. The simplest is by combining the narrow band that contains the emission with an adjacent or overlapping broad filter that traces the continuum. For H α , we can use the J0660 and the rSDSS filters, but taking into account that J0660 also includes the contribution of the forbidden transition of [N II] doublet (at 654.8 nm and 658.5 nm). Assuming a flat continuum, the flux of the three emission lines can be recovered using the following expression,

$$F_{H\alpha+[NII]} = \Delta_{J0660} \frac{\bar{F}_{J0660} - \bar{F}_{rSDSS}}{1 - \frac{\Delta_{J0660}}{\Delta_{rSDSS}}}, \quad (6)$$

where \bar{F}_{J0660} and \bar{F}_{rSDSS} correspond to the average fluxed inside the J0660 and rSDSS filters, respectively, and Δ_x is defined for any passband x at any wavelength of interest λ_s as

$$\Delta_x \equiv \frac{\int P_x(\lambda) \lambda d\lambda}{P_x(\lambda = \lambda_s) \lambda_s}, \quad (7)$$

where P_x is the transmission of the passband x as a function of wavelength. In our case, we take $\lambda_s = \lambda_{H\alpha}$.

This method assumes a linear continuum, so the H α absorption is not taken into account resulting in an overall bias of approximately 9% in all the results (Vilella-Rojo et al. 2015). When including more filters, such as those available in J-PAS, this method of continuum subtraction improve significantly (Martínez-Solaeche et al. 2021).

3.5. [N II] removal

The continuum-subtracted J0660 flux includes both the H α and the [N II] doublet emission. To remove the [N II] contribution we use the bi-modal empirical relation between the spectroscopic dust corrected H α flux and the total H α +[N II] flux found by Vilella-Rojo et al. (2015). This bi-modality can be disentangled by using the same $g' - i'$ colour used for the dust correction. Vilella-Rojo et al. (2015) obtained the following expressions by fitting a line to each branch,

$$\log(F_{H\alpha}) = \begin{cases} 0.989 \log(F_{H\alpha+[NII]}) - 0.193, & \text{if } g' - i' \leq 0.5 \\ 0.954 \log(F_{H\alpha+[NII]}) - 0.753, & \text{if } g' - i' > 0.5. \end{cases} \quad (8)$$

In addition, we can easily obtain the [N II] flux by simply taking the difference between the H α flux and $F_{H\alpha+[NII]}$,

$$F_{[NII]} = F_{H\alpha+[NII]} - F_{H\alpha}. \quad (9)$$

We do not apply this procedure for SNe at $z > 0.014$, since the [N II] $\lambda 6583$ line is outside the J0660 filter range at a higher redshift and a subtraction of this line can not be correctly performed. Therefore we assume all emission in the J0660 filter coming from H α flux for $z > 0.014$.

3.6. Other continuum subtractions

We repeated the subtraction procedure for other narrow filters by applying a different method that was presented in Pascual et al. (2007) and Vilella-Rojo et al. (2015), in which three instead of two filters were used, one narrow filter that contain the feature of interest and two filters (one at each side if the main feature) to trace the continuum,

$$F_{cs} = \frac{(\bar{F}_{B1} - \bar{F}_{B2}) - \left(\frac{\alpha_{B1} - \alpha_{B2}}{\alpha_N - \alpha_{B2}} \right) (\bar{F}_N - \bar{F}_{B2})}{\beta_{B1} - \beta_N \left(\frac{\alpha_{B1} - \alpha_{B2}}{\alpha_N - \alpha_{B2}} \right)}, \quad (10)$$

where F_{cs} is the flux of the narrow filter with the continuum subtracted, \bar{F}_x is the average flux, and β and α^5 are defined as,

$$\beta_x \equiv \frac{P_x(\lambda = \lambda_s)\lambda_s}{\int P_x(\lambda)\lambda d\lambda} \quad ; \quad \alpha_x \equiv \frac{\int P_x(\lambda)\lambda^2 d\lambda}{\int P_x(\lambda)\lambda d\lambda}. \quad (11)$$

The subindices $B1$, $B2$ and N refer to the first broad filter, the second, and the narrow filter respectively. We note that in this case the continuum is not flat, but has a slope defined by the two reference filters. Similarly to the method of subtracting the continuum described above, this method also improves significantly when additional filters are incorporated (Martínez-Solaeche et al. 2021).

We use this method to subtract the continuum of the J0378 and J0861 filter using the $uJAVA$ and $gSDSS$, and the $iSDSS$ and $zSDSS$ filters, respectively. In the latter case, this is an estimate of the Calcium triplet absorption. More negative NCR values for absorption filters indicate deeper absorption. Therefore, we invert the sign of the resulting fluxes when constructing the NCR with this continuum-subtraction method to maintain coherence during analysis.

3.7. Error calculation

Throughout the preceding calculations, it is essential to consider the respective error estimation through robust propagation.

The total uncertainty in our measurements of the flux (Eq. 1) for a source and a given filter (Molino et al. 2014, Logroño-García et al. 2017) is given by,

$$\sigma_{F_\lambda} = \sqrt{\left(\frac{\partial F_\lambda}{\partial ZP} \sigma_{ZP} \right)^2 + \left(\frac{\partial F_\lambda}{\partial C} \sigma_{bn} \right)^2 + \left(\frac{\partial F_\lambda}{\partial C} \sigma_{ec} \right)^2}, \quad (12)$$

σ_{ZP} being the error of the zero point reflected in table 2, σ_{ec} the uncertainly in the electron counting of the CCD and σ_{bn} the large scale background noise variation, the last two given by,

$$\sigma_{ec} = \sqrt{\frac{C}{G}}, \quad \sigma_{bn} = S_{fit} \sqrt{N_{pix}} \left(a_{fit} + b_{fit} \sqrt{N_{pix}} \right), \quad (13)$$

⁵ We need to make a calculation that involves an integration of the transmission curve of the passband; the data of the transmission curve are the same and can be found in the J-PLUS webpage.

where G is the gain of the detector, N_{pix} the number of pixels; S_{fit} , a_{fit} and b_{fit} are the resulting coefficients from the fitting. This information is found within headers of each image.

We calculate the error of the other magnitudes by a quadratic propagation of errors. The error of the flux with the dust correction (Eq. 3) is given by,

$$\sigma_{F_i(\lambda)} = \sqrt{(D_{F_0} \cdot \sigma_{F_0(\lambda)})^2 + (D_{k'} \cdot \sigma_{k'(\lambda)})^2 + (D_E \cdot \sigma_{E(B-V)})^2}, \quad (14)$$

where $D_{F_0} = \frac{\partial F_i(\lambda)}{\partial F_0(\lambda)}$, $D_{k'} = \frac{\partial F_i(\lambda)}{\partial k'(\lambda)}$ and $D_E = \frac{\partial F_i(\lambda)}{\partial E(B-V)}$. $\sigma_{E(B-V)}$ and $\sigma_{k'(\lambda)}$ are the errors of the color excess (Eq. 5) and the error given for the extinction law (Eq. 4) respectively, that are given by

$$\sigma_{E(B-V)} = \sqrt{\left(\frac{\partial E(B-V)}{\partial i'} \sigma_{i'} \right)^2 + \left(\frac{\partial E(B-V)}{\partial g'} \sigma_{g'} \right)^2}, \quad (15)$$

where $\sigma_{g'}$ and $\sigma_{i'}$ are the error of the flux in $gSDSS$ and $iSDSS$ bands given by the equation 12, and

$$\sigma_{k'(\lambda)} = \sqrt{\left(\frac{\partial k'(\lambda)}{\partial \lambda} \sigma_\lambda \right)^2 + \left(\frac{\partial k'(\lambda)}{\partial R'_V} \sigma_{R'_V} \right)^2}. \quad (16)$$

Knowing the error of the fluxes with the dust correction, we can now calculate the error of the continuum subtracted fluxes. In the case of the subtraction of the red continuum of the J0660 filter (Eq. 6) we have

$$\sigma_{F_{H\alpha+[NII]}} = \sqrt{\left(\frac{\partial F_{H\alpha+[NII]}}{\partial \bar{F}_{F600}} \sigma_{\bar{F}_{F600}} \right)^2 + \left(\frac{\partial F_{H\alpha+[NII]}}{\partial \bar{F}_{r'}} \sigma_{\bar{F}_{r'}} \right)^2}, \quad (17)$$

with $\sigma_{\bar{F}_{r'}}$ and $\sigma_{\bar{F}_{F600}}$ being the error of the extinction corrected flux of the J0660 and $rSDSS$ filters obtained by equation 14.

We can then calculate the error of the H α flux with the [NII] line subtracted (Eq. 8) and the error of the [NII] line flux (eEq. 9) as

$$\sigma_{F_{H\alpha}} = \frac{\partial F_{H\alpha}}{\partial F_{H\alpha+[NII]}} \sigma_{F_{H\alpha+[NII]}}, \quad (18)$$

and

$$\sigma_{F_{[NII]}} = \sqrt{\left(\frac{\partial F_{[NII]}}{\partial F_{H\alpha}} \sigma_{F_{H\alpha}} \right)^2 + \left(\frac{\partial F_{[NII]}}{\partial F_{H\alpha+[NII]}} \sigma_{F_{H\alpha+[NII]}} \right)^2}. \quad (19)$$

Finally, we can calculate the error of the J0378 and J0861 flux with the continuum subtracted (Eq. 10) as

$$\sigma_{F_{cs}} = \sqrt{\left(\frac{\partial F_{cs}}{\partial \bar{F}_N} \sigma_{\bar{F}_N} \right)^2 + \left(\frac{\partial F_{cs}}{\partial \bar{F}_{B1}} \sigma_{\bar{F}_{B1}} \right)^2 + \left(\frac{\partial F_{cs}}{\partial \bar{F}_{B2}} \sigma_{\bar{F}_{B2}} \right)^2}, \quad (20)$$

with the subindex B1, B2 and N being referred to the first broad filter, the second, and the narrow filter respectively. Errors on α_x , β_x and Δ_x are negligible and are therefore not included in the calculation in order to simplify the procedure.

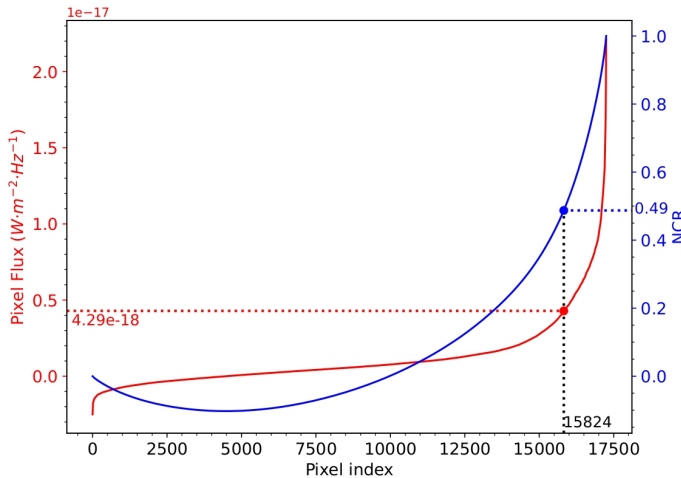


Fig. 4: Example of the calculation of the NCR value for a SN pixel. The red curve is the sorted pixel value (left flux scale), while the blue curve is the cumulative distribution of the flux values, i.e., the Normalized Cumulative Rank Pixel Value Function (NCRPV or NCR for simplicity). The blue dot represent the position and correspondent NCR value of the SN 2008az pixel, and the red dot represents the correspondent flux value.

3.8. Final 3D datacubes

Once all these corrections are applied, we store these newly generated images as new slices in the 3D datacube, where fluxes are in the primary and flux errors in the first extension. The final cube has 17 slices: 12 corresponding to the extinction-corrected images in the 12 J-PLUS filters, the H α +[N II] continuum subtracted flux, the J0378 and J0861 continuum subtracted flux, the flux corresponding only to the H α line, and the [N II] emission line flux.

Figure 3 shows the H α image of the same galaxy from Figure 2 at four different steps of the analysis: (a) the initial cutout from the observed image; (b) after dust reddening correction; (c) after r-band continuum subtraction; and (d) after [N II] emission removal.

4. Analysis

4.1. Normalized Cumulative Rank distributions

The NCR is obtained by sorting the flux values in increasing order (see Figure 4), constructing the cumulative distribution, and normalizing it to the total emission of the galaxy. This procedure associates each pixel with an NCR value between 0 and 1, where the brightest pixel in the galaxy has a NCR value of 1 and all pixels corresponding to sky have a 0 NCR. Then, the ranked value in this distribution corresponding to the pixel where the SN occurred⁶ is the NCR associated to the SN. By compiling significant numbers of NCR values for different SN types, we can build NCR distributions and study the differences among types and use this information to infer properties of their progenitors.

The NCR method has previously been applied to H α imaging of SN hosts. Assuming that the H α emission scales by the number of stars that are formed (Kennicutt 1998), a diagonal cumulative NCR distribution with a mean value of 0.5 indicates that the population traces the observed light, and the SN type follows the

number of stars formed and mapped by that particular SF tracer. Therefore, if SNe explode predominantly in locations with high SFR, they will favour higher NCRs. On the other hand, SNe that explode in random locations over the galaxy favor low NCRs.

Following James & Anderson (2006), we included all negative flux values in the construction of the NCR function, that are the result of a background subtraction during the processing with the J-PLUS pipeline (Cenarro et al. 2019). This NCR calculation is applied independently to the 17 images of the 418 SN host galaxies.

4.2. SN environment SED fitting

To extract the main properties of SN environments, we construct spectral energy distributions (SEDs) by measuring aperture photometry in all 12 J-PLUS bands in circular apertures of 1 kpc² centered at SN locations. To ensure the analysis yields meaningful results, the fluxes need to be only corrected for Milky Way extinction, so here we use the constructed 3D cubes with only this correction applied (at the stage outlined in Section 3.3). The size of the aperture is selected so that the flux contained in the aperture is of enough signal-to-noise to reliably obtain SSP parameters, and calculated using the host galaxy redshift obtained from the OSC, and assuming a flat Λ CDM cosmology with $H_0 = 70 \text{ km s}^{-1} \text{ Mpc}^{-1}$. Within the redshift range of our sample this translates into apertures of 26 to 2 arcsec radius. Figure 5 shows a couple of examples of the $rSDSS$ filter galaxy cutout and the SED from the 12 J-PLUS bands. We note how the SED shape of a SN environment with ongoing star formation (SN 1997dq on top) shows a bluer continuum with a clear H α emission, while the SED of a SN environment in a passive galaxy (SN 1957B on the bottom) looks redder and smoother.

Once the 418 SEDs are built, we use FAST++ (Schreiber et al. 2018)⁷, a C++ implementation of FAST (Kriek et al. 2009), to fit them and obtain a number of galaxy physical properties. Given galaxy photometry, FAST++ determines the best-fit SED from a library of simple stellar population (SSP) models. These models are initially synthesized in composite stellar populations (CSPs) on a five-dimensional grid, with each grid point corresponding to a CSP SED with age t_* , stellar metallicity Z_* , V band extinction A_V , time scale τ , and star formation history (SFH) at some redshift z . At each point on the grid a χ^2 value is calculated as,

$$\chi_F^2 = \sum_i \frac{[F_{\lambda,i} - F_{\lambda,\text{mod}}(t_*, \tau, A_V, Z_*, z)]^2}{\sigma_i^2}, \quad (21)$$

where N is the number of photometric points and σ_i is the error for point i . One sigma confidence intervals for parameters and derived quantities (such as stellar mass and SFR) are determined using Monte Carlo sampling of the grid around the lowest χ^2 . In this work, we used the BC03 (Bruzual & Charlot 2003) SSP library calculated using a delayed exponential (delayed- τ) SFH parametrization and a Chabrier (2003) initial mass function. Dust extinction is modelled with a Calzetti et al. (2000) dust extinction law with a uniform and constant foreground dust screen. In all fits, the redshift was fixed to the reported spectroscopic redshift of the SN host galaxy.

The output of FAST++ includes the distribution of stellar populations of different age and metallicity present at that location. Although several degeneracies are at play, with large enough samples one can disentangle the underlying differences between the average properties of these parent populations for different

⁶ The precision of SN locations is lower than the image resolution (see Section 1), so what we are measuring is the immediate SNe environment.

⁷ Available at <https://github.com/cschrreib/fastpp>

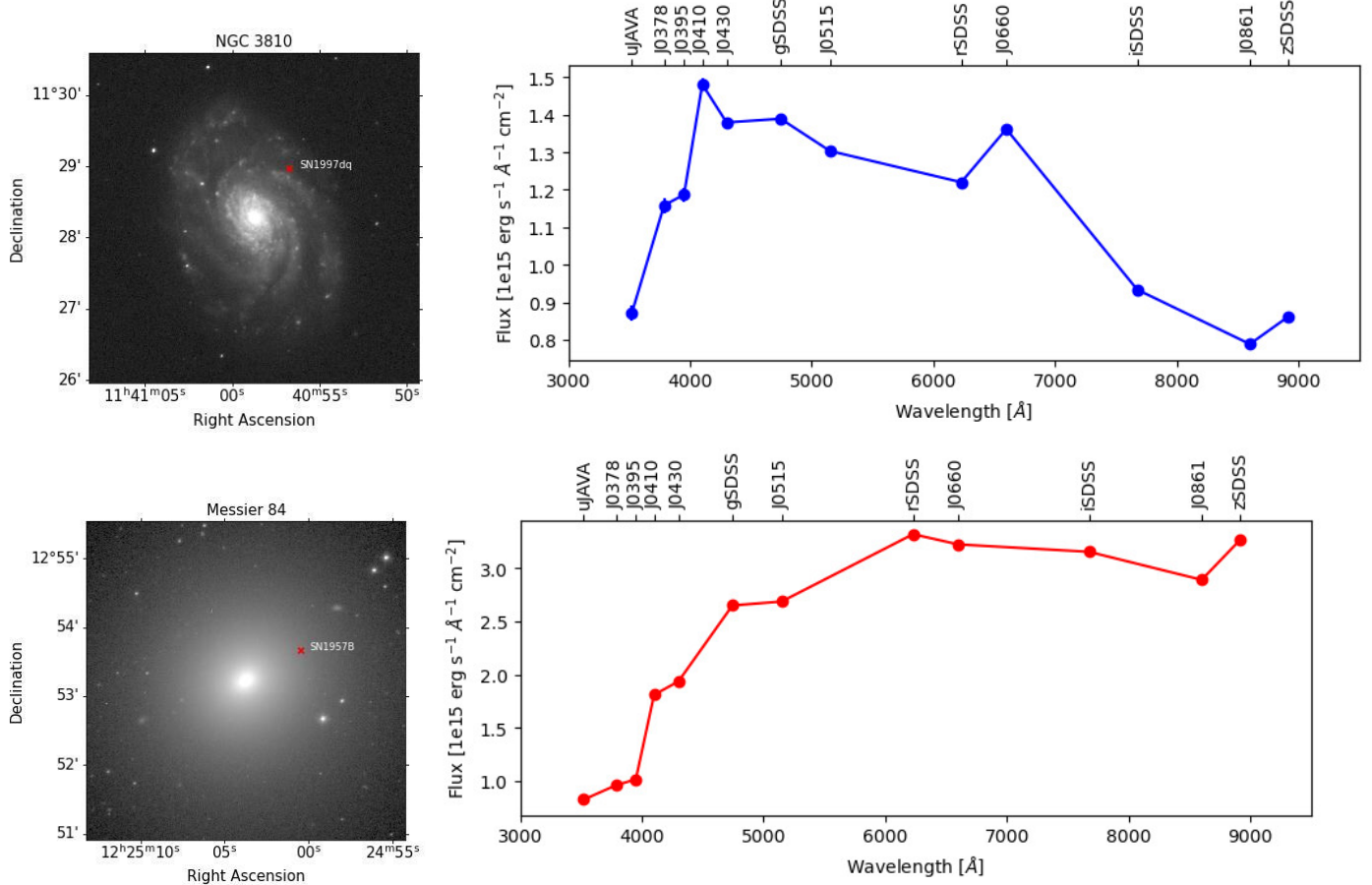


Fig. 5: Example of two SEDs of the SN local environments of 1 squared kpc extracted from J-PLUS observations. On top, the star-forming environment of SN 1997dq in its host galaxy NGC 3810 clearly shows a blue continuum based on the five broad-band filters and increased flux for the narrow-band filters where the main emission-lines fall. On the bottom, for SN 1957B in the Messier 84 galaxy, a smooth red continuum is seen with no bumps at the narrow-band filter wavelengths.

SN types. In particular, we mainly focus on stellar population age, dust extinction, stellar mass, and star formation rate (SFR).

5. Results

5.1. NCR distributions

The resulting NCRs for all individual SNe are provided in Tables A.2, A.3 and A.4. With the NCR and error for all SNe in our sample, we construct cumulative distributions for all SN types and in all 17 frames of the data cubes as follows. We build a probability distribution for every NCR using 30000 NCR trials of the form $NCR + (\sigma_{NCR} \cdot \alpha)$, α being a random variable between -1 and 1. We sort all the NCRs in increasing order, and then the median and 1 sigma of those distributions of 30000 NCRs are shown in the plots. In Figure 6 we show the 12 panels, one for each broad- and narrow- band, with the corresponding NCR distributions for the seven SN types.

In general, we observe that as we move to redder wavelengths (from $gSDSS$ to $zSDSS$), all SN type distribution tend to be equal, following the black diagonal distribution, with an average $NCR \gtrsim 0.4$ for every distribution. Type II, IIb and Ia SN distributions begin to separate from the diagonal and those of types Ib, Ic and IIn at bluer wavelengths. Also, type Ib SNe distribution gets closer to the diagonal as we move to bluer bands. The order Ia-II-IIb-IIn-Ibc remains mostly equal in all filters, however,

IIn and IIb types presents higher and lower NCRs in red bands respectively.

We conducted Kolmogorov–Smirnov (KS) tests to compare two samples and assess the probability of both being drawn from the same probability distribution. By setting a significance level of 0.05, if the p-value computed by the KS test falls below this threshold, it means the rejection of the null hypothesis. In other words, it indicates they are originated from different populations. Table 3 shows the p-value for every pair of NCR distributions and the diagonal hypothetical distribution which accurately traces the respective flux ([1:1]), and also for every filter. The Table summarises what is visually shown in Figure 6. For the 12 J-PLUS filters, all distributions for filters redder than $J0410$ show p-values > 0.05 (with the exception of the combination of II vs Ibc types for $J0515$ and Ia vs Ibc for $J0410$). For $uJAVA$, $J0378$ and $J0395$, Ia and II/Ib/IIn shows p-value > 0.05 . Only combinations of CC-types with Ia, and combinations of II with Ib, Ic and Ibc presents p-values < 0.05 , indicating that types Ia, II, IIb and IIn come from different possible progenitors than those SNe of types Ib, Ic and Ibc that are located in redder environments in comparison with the rest of the types.

The distributions of the five continuum-subtracted narrow-band filters are presented in Figure 7. We note again that SN with $z > 0.014$ are not included in the N II distributions as explained in section 3.5. The most significant characteristic is the high number of zero NCR values in all cases. As we discuss later (section 6), we

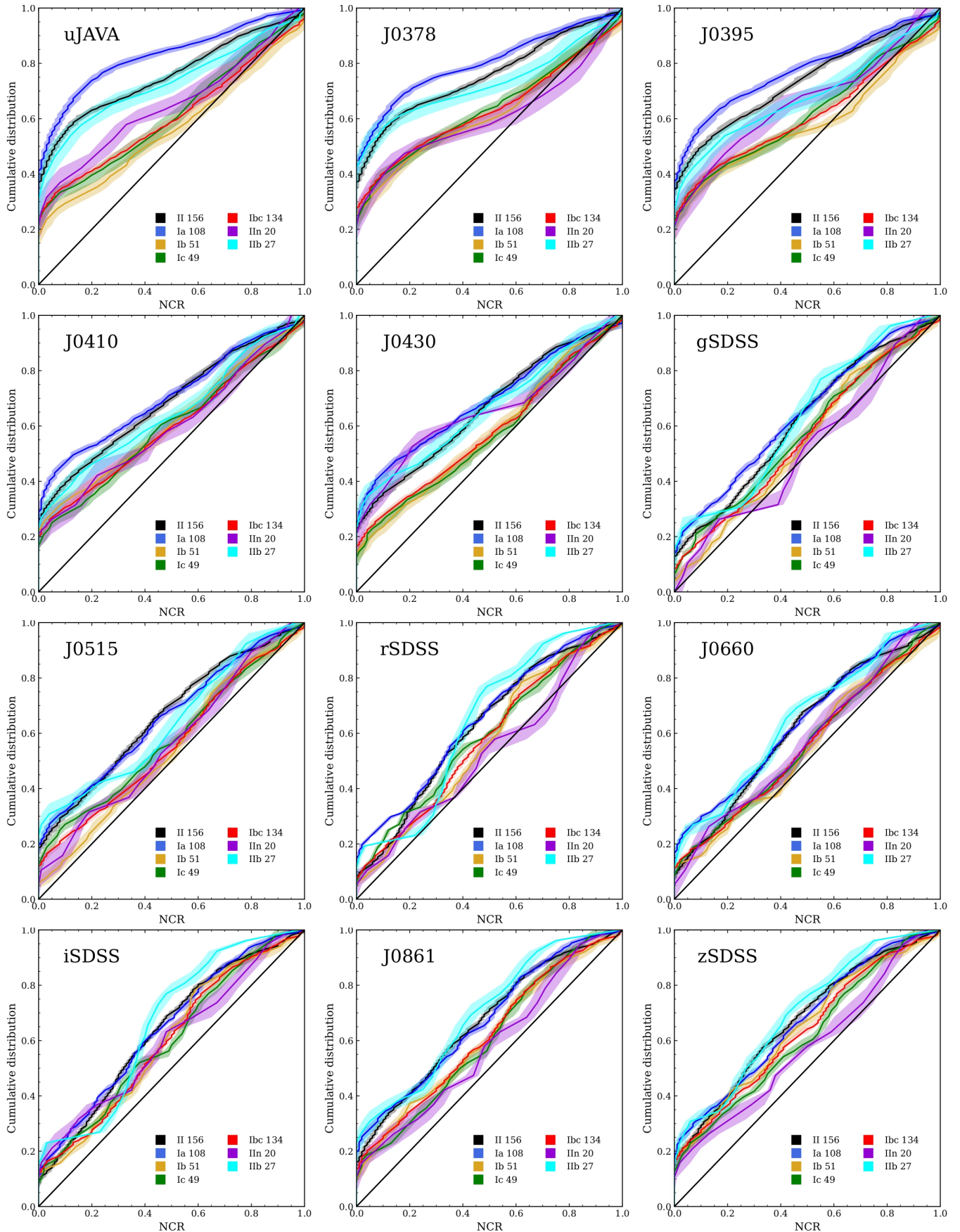


Fig. 6: Cumulative NCR distributions of the 12 broad- and narrow-band filters. The straight black diagonal line represents a hypothetical distribution, infinite in size, which accurately traces the respective observed flux. Each SN distribution corresponds to the median and one sigma of the 30000 NCR trials distributions as detailed in section 5.1 of Lyman et al. (2020). It can be observed that as we move to redder filters (from gSDSS to zSDSS), the distributions for each type tend to become more similar along the diagonal. In contrast, there is a clearer distinction between them in the blue filters with more zero values.

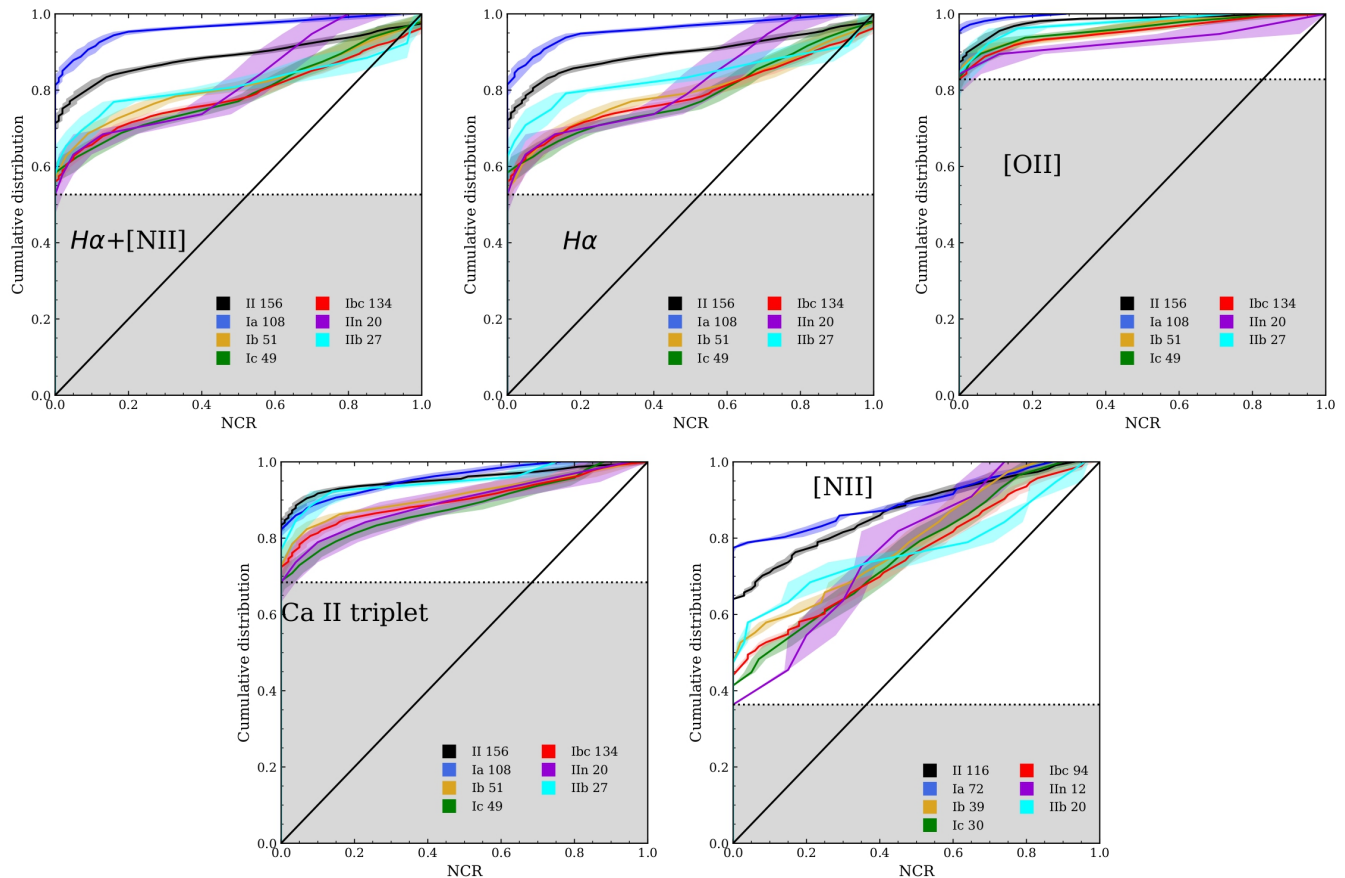


Fig. 7: Cumulative NCR distributions of the five constructed filters. $H\alpha+[\text{N II}]$, $[\text{O II}]$ and Ca II triplet distributions correspond to the J0660, J0378 and J0861 continuum subtracted filters respectively. The $H\alpha$ filter is the result of removing the $[\text{N II}]$ contribution, which is only applied to SNe with $z < 0.014$. All distributions correspond to the median and one sigma of the 30000 NCR trial distributions as outlined in section 5.1 (Lyman et al. 2020). The straight black diagonal line represents a hypothetical distribution, infinite in size, which accurately traces the respective observed flux. The gray shade marks the lowest values of zeros in a distribution in each filter.

associate part of the zero values found to the small aperture of the JAST80 telescope and the exposure times of the images used, that is not enough to collect enough photons to provide high signal-to-noise (S/N) in these continuum-subtracted images for all galaxies. Moreover, $H\alpha$ is associated with stars of $M > 15 - 20M_\odot$, so many SN progenitors are not expected to be associated with this emission, contributing to more zero NCRs in the distributions. The removal of the $[\text{N II}]$ line has no appreciable effect on the NCR distributions, with the plots of $H\alpha+[\text{N II}]$, $H\alpha$ and $[\text{N II}]$ being similar. In any case, we observe a similar scenario between the broad and narrow-band filters, where the type Ia distribution is clearly the one with the lowest NCRs in all cases, followed by type II. The $[\text{O II}]$ emission also traces the star formation rate (Kennicutt 1998), similarly to $H\alpha$. With the change of signs in Ca II triplet fluxes, higher NCR after subtracting the continuum suggests deeper absorption, analogous to high NCR values in emission line filters indicating strong emission (see section 3.6). The order of the distributions appears to remain consistent, with Ia, II, and IIb displaying lower NCR values, distinguishing them from the other SN types. However, the large amount of zero values makes the analysis difficult in these cases.

5.2. SN environment parameter distributions

The local stellar population parameters A_V , t_* , SFR and sSFR for all 418 SN environments are reported in Table A.5. Additionally, their distributions are illustrated in Figure 8 segregated according to the same seven SN groups. These have been constructed in a similar way as in the previous section, by performing 30000 different distributions where in each realization the best output values from the best FAST++ fits are randomly varied within their 1σ uncertainty, and the median and the 1σ variation of all realizations is taken as the final distribution.

We recover previous trends already found in the literature. The average local A_V is larger for SNe Ibc (1.13 ± 0.08 mag) compared to SNe Ia (0.63 ± 0.09 mag), with the SNII distribution being in the middle of the two (0.85 ± 0.07 mag), as previously reported by Galbany et al. (2017). This trend is driven by the SNIb and SNIc distributions, which are clearly shifted to higher values compared to all others. Similarly, all CC SN distributions show younger average ages (38 ± 10 Myr for SNe II and 43 ± 13 Myr for SNe Ibc) compared to those of SNe Ia environments (222 ± 73 Myr), and CC SN environments have both higher SFR (0.08 ± 0.06 and $0.16 \pm 0.04 M_\odot \text{yr}^{-1}$ for SNe Ibc and SNe II, respectively) and sSFR (1.88 ± 1.40 and $4.35 \pm 1.29 \cdot 10^{-8} \text{ yr}^{-1}$ for SNe Ibc and SNe II, respectively) than SNe Ia (0.01 ± 0.01

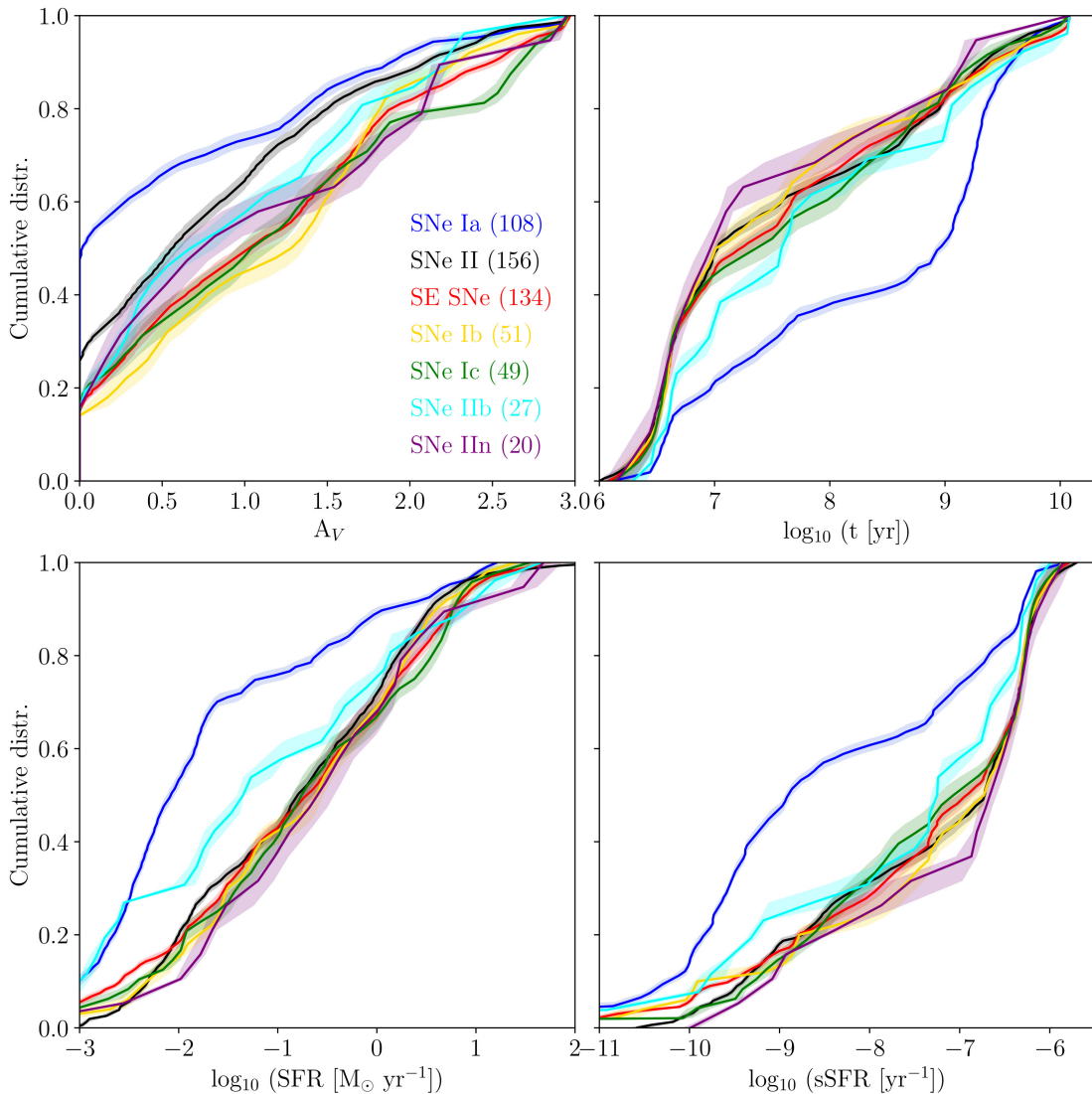


Fig. 8: Cumulative distributions of each of the three main SN types for the main environmental parameters obtained from the best FAST++ fits to the SED: extinction A_V , average stellar age $\langle t \rangle$, star-formation rate $\log_{10} \text{SFR}$, and specific star-formation rate $\log_{10} \text{SFR/Mass}$.

$M_\odot \text{yr}^{-1}$ and $0.19 \pm 0.16 10^{-8} \text{ yr}^{-1}$) that occur in more passive local environments (Galbany et al. 2018).

5.3. Radial distributions of the SNe

To investigate potential correlations between the emission of a specific band and the distribution of SNe in galaxies, we calculated two parameters: the Normalized Galactocentric Distance (NGCD) and the fraction of the r-band emission flux (F_r ; Anderson & James 2009; Habergham et al. 2010). Our approach involved fitting an elliptical 2D Gaussian model to the $r\text{SDSS}$ images of the galaxies to determine the shape and size of each galaxy. If the SN was located at the center of the ellipse, NGCD was assigned a value of 0; if the SN was positioned at the outer ellipse's edge, NGCD equaled 1. We then fitted a second ellipse, with the same parameters as the first one, but scaled to place the SN at the edge of this second ellipse. F_r was subsequently computed as the ratio between the integrated fluxes in the $r\text{SDSS}$ band of the second and first ellipses.

We find in Figure 9 that all SN types exhibit nearly identical distributions with respect to each other, except for type IIb SNe, which appear to be concentrated in the inner regions of galaxies (within the range of 0.2 to 0.6 in NGCD). For the other SN types, there does not seem to be a preference for any specific location within the galaxies.

The F_r are also similar between all SN types, and close to the diagonal, tracing the $r\text{SDSS}$ emission as the NCR distributions of Figure 6 do. Since all J-PLUS bands present the NCR distributions close to the diagonal, and there is no preference in the location of the SN, we are only tracing the general shape and size of the galaxies.

6. Discussion

6.1. NCR results

Concerning the NCR distributions of the broad- and narrow-band filters and the average NCR values, it is worth noting that the broad filters exhibit slightly lower errors than the narrow-band filters, particularly for those where the continuum has been

Combination	uJAVA	J0378	J0395	J0410	J0430	gSDSS	J0515	rSDSS	J0660	iSDSS	J0861	zSDSS	Hα+[N II]	[O II]	Ca II triplet	Hα	[N II]
II vs Ia	0.213	0.740	0.709	0.757	0.646	0.896	0.999	0.442	0.408	0.997	0.974	0.973	0.076	0.013	0.990	0.399	0.527
II vs Ib	0.002	0.096	0.023	0.638	0.392	0.386	0.083	0.279	0.169	0.496	0.632	0.925	0.095	0.347	0.158	0.037	0.017
II vs Ic	0.021	0.164	0.184	0.438	0.251	0.810	0.318	0.777	0.298	0.421	0.367	0.391	0.017	0.461	0.001	0.001	0.002
II vs Ibc	0.001	0.037	0.019	0.194	0.073	0.289	0.023	0.229	0.117	0.399	0.380	0.495	0.000	0.134	0.003	0.000	0.000
II vs IIn	0.410	0.321	0.773	0.695	0.819	0.343	0.487	0.211	0.750	0.814	0.446	0.434	0.193	0.364	0.109	0.069	0.026
II vs IIb	0.998	0.918	0.817	0.899	0.995	0.985	0.751	0.695	0.889	0.805	0.971	0.987	0.421	0.848	0.903	0.859	0.543
Ia vs Ib	0.000	0.017	0.021	0.334	0.117	0.270	0.135	0.224	0.173	0.614	0.777	0.977	0.000	0.009	0.256	0.001	0.002
Ia vs Ic	0.000	0.027	0.046	0.104	0.165	0.770	0.525	0.669	0.439	0.704	0.588	0.740	0.000	0.003	0.014	0.000	0.000
Ia vs Ibc	0.000	0.003	0.006	0.046	0.074	0.217	0.092	0.342	0.217	0.506	0.697	0.959	0.000	0.000	0.026	0.000	0.000
Ia vs IIn	0.086	0.184	0.362	0.449	0.926	0.155	0.595	0.271	0.774	0.832	0.557	0.557	0.006	0.076	0.263	0.014	0.010
Ia vs IIb	0.627	0.837	0.700	0.938	0.999	0.837	0.893	0.700	0.999	0.771	0.996	0.999	0.018	0.043	0.965	0.310	0.121
Ib vs Ic	0.988	0.999	0.926	0.999	1.000	0.879	0.701	0.890	0.999	0.994	0.991	0.984	0.990	1.000	0.409	0.380	0.895
Ib vs Ibc	0.967	1.000	0.975	1.000	0.999	0.985	0.924	0.998	0.999	1.000	1.000	0.999	0.989	0.997	0.998	0.978	0.995
Ib vs IIn	0.806	0.999	0.889	0.999	0.405	0.851	0.987	0.494	0.999	0.947	0.967	0.687	0.903	0.707	0.947	0.754	0.754
Ib vs IIb	0.131	0.352	0.862	0.987	0.553	0.528	0.221	0.295	0.271	0.624	0.760	0.972	0.964	0.964	0.770	0.630	0.630
Ic vs Ibc	1.000	1.000	0.999	1.000	1.000	0.999	0.999	0.991	1.000	0.999	0.999	0.999	0.997	0.999	0.744	0.827	0.995
Ic vs IIn	0.934	0.997	0.966	0.999	0.469	0.731	0.975	0.789	0.999	0.995	0.951	0.951	0.857	0.707	0.984	0.681	0.883
Ic vs IIb	0.286	0.349	0.897	0.835	0.620	0.793	0.865	0.512	0.438	0.280	0.488	0.512	0.798	0.964	0.118	0.179	0.335
Ibc vs IIn	0.965	0.995	0.927	1.000	0.466	0.853	0.999	0.579	0.999	0.973	0.903	0.772	0.569	0.652	0.999	0.840	0.813
Ibc vs IIb	0.264	0.393	0.927	0.957	0.732	0.673	0.613	0.393	0.346	0.443	0.673	0.788	0.810	0.880	0.372	0.314	0.487
IIn vs IIb	0.890	0.688	0.996	0.996	0.996	0.551	0.749	0.284	0.565	0.714	0.376	0.578	0.549	0.873	0.498	0.553	0.553
II vs [1:1]	0	0	0	0	0	0.000038	0	0	0	0	0	0	0	0	0	0	0
Ia vs [1:1]	0	0	0	0	0	0.00125	0	0	0.00028	0.00055	0	0	0	0	0	0	0
Ib vs [1:1]	0.014	0.001	0.001	0.003	0.128	0.357	0.667	0.107	0.311	0.035	0.060	0.019	0.047	0.056	0.003	0.100	0.004
Ic vs [1:1]	0.002	0.000	0.001	0.022	0.071	0.257	0.069	0.213	0.339	0.216	0.144	0.071	0.295	0.018	0.278	0.908	0.193
Ibc vs [1:1]	0.000	0.000	0.000	0.000	0.000	0.146	0.016	0.031	0.036	0.004	0.002	0.000	0.011	0.001	0.000	0.053	0.000
IIn vs [1:1]	0.028	0.021	0.036	0.146	0.016	0.855	0.643	0.952	0.568	0.366	0.496	0.496	0.396	0.473	0.317	0.711	0.554
IIb vs [1:1]	0.000	0.000	0.001	0.016	0.005	0.107	0.017	0.020	0.068	0.015	0.023	0.023	0.037	0.017	0.000	0.007	0.001

Table 3: p-values of the Kolmogorov-Smirnov test for every SN type combination and filter. We also included the p-values for the SN types and the diagonal hypothetical distribution which accurately traces the respective flux ([1:1]). Black font boxed values represent those distributions without an underlying causative relationship, i.e., we reject the null hypothesis that the two samples were drawn from the same probability distribution (p-value < 0.05), and both NCR distributions come from different populations. The distribution used for the five continuum subtracted filters have been rebuilt by removing proportionally the number of zero NCR values in each distribution that correspond to the lowest observed fraction of zeros in an individual distribution (see section 6).

subtracted. The errors for the *uJAVA* filter are higher than the rest of the broad-band filters. This is what we expected since the broad filters have higher S/N, and the *uJAVA* filter has the lower FWHM of all J-PLUS broad-band filters. We also observe approximately the same sequence between the main types in all panels in Figure 6, being type Ibc between II and Ia for bluer wavelengths, moving upward in the cumulative plot, downward for NCR, for redder wavelengths. This shift of the Ibc distribution is due to the Ib contribution, that correlates more with bluer bands, similarly to what was reported by Kangas et al. (2013). Kelly & Kirshner (2012) also found that the environments of SN Ib exists preferentially in environments with bluer surface brightness, specially in ultraviolet band. In our case, we also found that the filter that best distinguishes the type Ib distribution is *uJAVA*.

By looking at continuum-subtracted filters, the main characteristic is the large amount of zeros present in all distributions. For instance, in the Hα plot we have a noticeable amount of zero NCR values: ∼ 35% for Ibc, ∼ 53% for II, and ∼ 65% for Ia. This is partly because many SNe do not follow the Hα emission. However, this fraction of zeros is larger than in previous studies (e.g., Anderson et al. 2012 found ∼ 25% for Ibc, ∼ 39% for II, and ∼ 58% for Ia). Since these filters represent the residual flux once a pseudo-continuum (from broad-band filters) has been subtracted from a narrow-band filter, and since the diagonal line assume a population that specifically traces the observed light, the distribution will include a fraction of zeros that depends on the image depth. Therefore, we have two explanations that can drive this large amount of zeros: either most of the flux collected by the narrow-band filters is due to the underlying continuum, or the combination of a small telescope aperture (0.8m) and low exposure time was not enough to get significant contrast in these continuum-subtracted filters.

To further analyse this, we rebuilt the NCR distributions, this time removing proportionally the number of zero NCR values in

each distribution that correspond to the lowest observed fraction of zeros in an individual distribution, following a procedure similar to Ransome et al. (2022). This can be done as all our images are of a similar depth, since all the images have been obtained using the same telescope, under the same conditions, exposure time and instrument configuration. This is equivalent of excluding the shaded region in all panels of Figure 7, because we assume we have reached the background level at that point, and tracing the diagonal from the intersection of the dotted horizontal line with the zero NCR to the upper-right corner. This assumption is grounded in the fact that we have successfully retrieved a certain level of signal, and anything below that threshold corresponds to the background we couldn't recover due to the combination of the telescope and exposure time used, as previously mentioned.

In Figure 10 we show the resulting distributions. Hα+[N II], Hα and [N II] plots still shows similar distributions, the main type that correlates the emission is the Ic, with the highest NCR values on average (Figure 11). For the J0660 (Figure 6) and Hα (Figure 10) panels for type Ia, II and all Ibc combined, we recovered the tendency of the distributions seen in previous works (e.g. Anderson & James 2008), where type Ic/Ibc SNe is the closest distribution to the diagonal line, followed by type II and type Ia. This has been interpreted as a sequence in progenitor age, then we infer from this a sequence of progenitor mass, those distributions closer to the diagonal being the SN type with higher mass progenitors (Kuncarayakti et al. 2018).

Type IIn SN distribution also correlates with the Hα emission, with lower NCR values than Ic (∼ 0.05 on average), which is also consistent with the literature (Ransome et al. 2022), with the same methodology), however, our non-zero IIn sample is reduced to only 7 SNe. All CCSN types are strongly correlated to the [O II] emission, that also traces SFR (Kennicutt 1998) following the sequence of Ia-II-IIb-Ic-Ibc-Ib-IIn. If we exclude the bias in the IIn type, which is limited to only 4 SNe and not being numerous enough to perform reliable statistics, we can observe that type

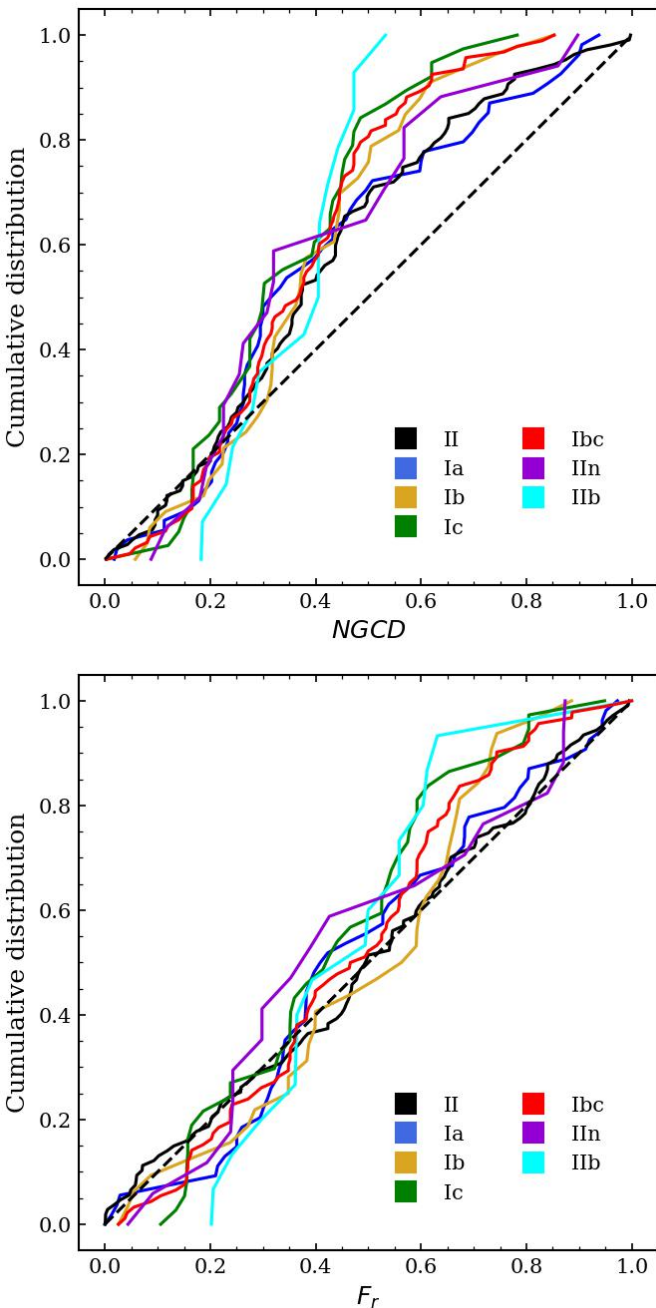


Fig. 9: Cumulative distributions of normalized galactocentric distances (top) and F_r (bottom) for every SN type.

Ib exhibits the most pronounced correlation with this emission, primarily because this type of SN is more closely associated with bluer bands, as previously mentioned. The same correlations between SN types are found for the $H\alpha+[N\text{ II}]$, $H\alpha$ and $[N\text{ II}]$ filters. Besides, the Ia, IIb and IIIn types are correlated when the $[N\text{ II}]$ is subtracted, being $p\text{-value} > 0.05$ after the removal.

The Ca II triplet distribution makes a clear division between types II, IIb and Ia and types Ib/Ic/IIIn (closer to the diagonal because of the change in the sign). These differences between populations are also evident when computing the p -value of the KS test (Table 3): II vs Ic, II vs Ibc, Ia vs Ic and Ia vs Ibc presents p -values < 0.05 for the Ca II triplet NCRs, II vs Ia, II vs IIb and Ia vs IIb presents p -values > 0.05 , as well as the rest of CC-SN between each other. The interpretation of the intensity of

the Ca II triplet absorption is not trivial. Some works (e.g. Diaz et al. 1989; Garcia-Vargas et al. 1998) have shown that the Ca II triplet equivalent width (EW) present a degeneracy between stellar population age and metallicity. At high metallicity the Ca II EW reaches its maximum value for stellar populations of approximately ~ 10 Myr, primarily attributed to the presence of Red Supergiant (RSG) stars. A secondary, lower peak emerges around 100 Myr, driven by stars in the Asymptotic Giant Branch (AGB) phase. Furthermore, for ages older than 1 Gyr, the Ca II EW becomes a reliable indicator of increasing metallicity. Based on our results, and compared to SNII that explode in low Ca II NCR environments, one possible interpretation would be to attribute the higher values for Ib/Ic to young progenitors exploding at locations with metal-rich older populations. For SNIIn, although with low numbers, our results are in line with these progenitors being a combination of very young (~ 10 Myr peak) and older (~ 100 Myr peak) stars (Galbany et al. 2018).

Finally, in Figure 11 we show the average NCR values in all filters for the 7 SN types. In the left panel, we see that on average, through the 12 J-PLUS filters, SNe Ia present the lower NCR values (between 0.10 ± 0.02 and 0.33 ± 0.02), followed by II < IIb < IIIn < Ibc, being the highest NCR values for Ibc/Ib/Ic types, ranging between 0.36 ± 0.01 and 0.48 ± 0.01 . The IIIn oscillates between the Ia/II/IIb types and Ibc, getting values from 0.35 ± 0.02 up to 0.49 ± 0.01 in $gSDSS$ and $rSDSS$ bands. Moreover, all NCRs of the Ia, II and IIb types tend to increase as we move to redder wavelengths (up to 0.2 in NCR), while Ib, Ic and Ibc tend to remain constant.

For the 5 continuum subtracted filters, shown in the right panel of Figure 11, SNe Ic tend to have higher NCR values on average in comparison with the correspondent J-PLUS bands, the average NCR being, for instance, 0.39 ± 0.02 in $J0660$ filter and 0.54 ± 0.05 in $H\alpha$, and ~ 0.5 for the rest, except the $[O\text{ II}]$ whose average NCR falls to 0.26 ± 0.02 . Moreover, the Figure illustrates the low NCR values on average for SNe Ia in comparison with the rest of the SN types, being especially low for $[O\text{ II}]$. It is also evident the insignificant effect of the $[N\text{ II}]$ removal from the $J0660$ filter for the rest of the SN types, since the average NCR values for $H\alpha$ and $H\alpha+[N\text{ II}]$ are similar in all distributions (except in type Ic, whose difference is ~ 0.1). The IIIn type is the next in terms of highest NCRs. For $H\alpha$, it presents a value of 0.45 ± 0.11 , consistent with the 0.521 ± 0.038 that (Ransome et al. 2022) found, however, we need to take into account that we have only 7 type IIIn SN in our non-zero sample. The ordination of SN types between $J0378$ and $[O\text{ II}]$ and between $J0861$ and Ca II triplet remains the same, but with systematically lower NCRs after subtracting the continuum.

6.2. SED fitting

We recovered the same relations between the main SN types previously found in other works. Although the main focus of this work was to construct NCR distributions of the narrow band filters, the fact that we recover these relations proves that the data is good enough to perform this kind of studies. However, to our knowledge, this is the first time that SED fitting is performed adding these 7 narrow band filters on top of the main 5 SDSS broad bands.

To see how much information these narrow band filters carry that is not included in the broad bands, we repeated the FAST++ fits this time only using the 5 broad band filters. In Figure 12, we show the differences between the 12- and 5-filter SED fits for the 4 main environmental parameters. Individual dots show the difference for each individual SN environment, the big dot

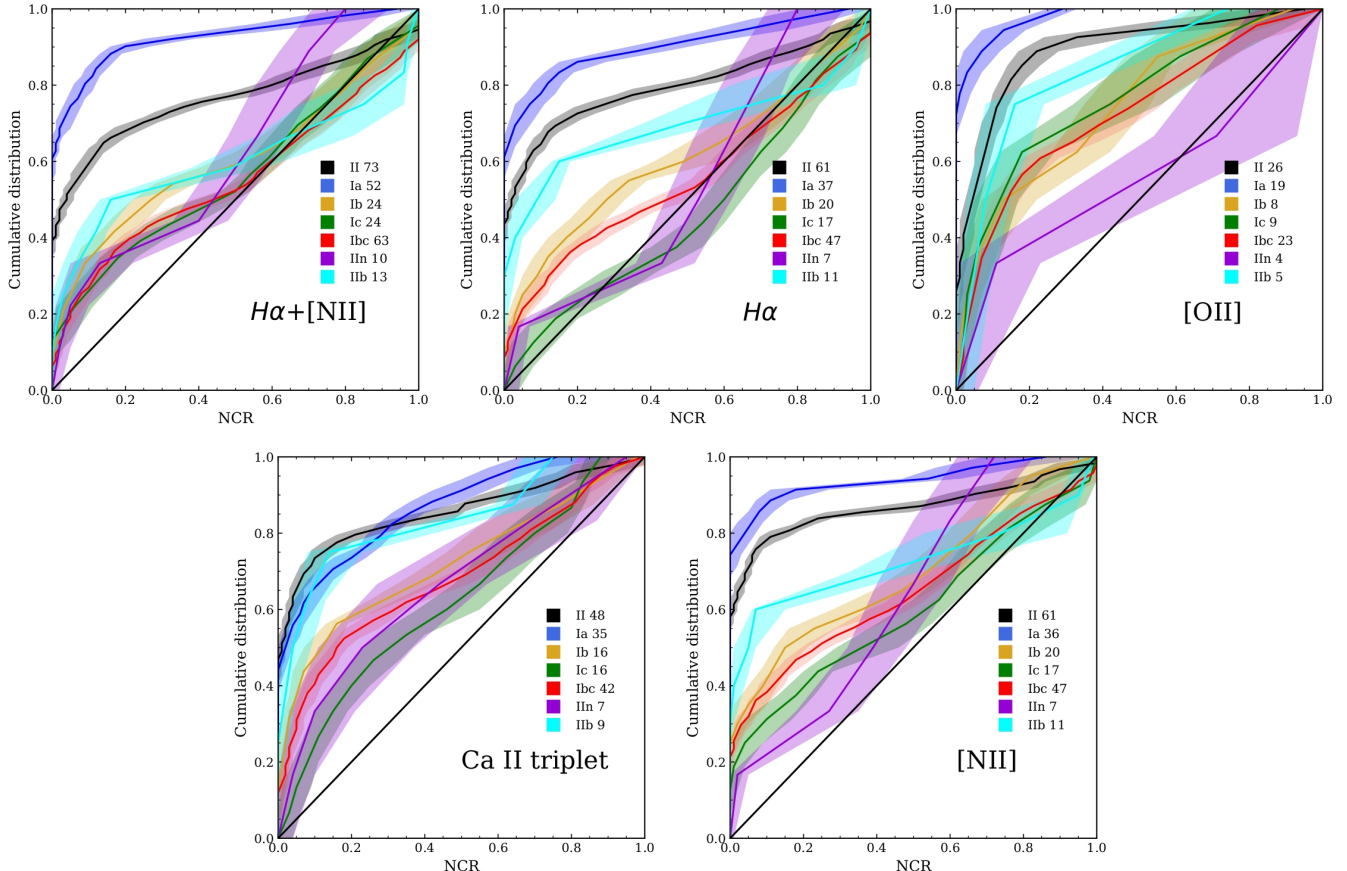


Fig. 10: The same as figure 7, but rebuilding the NCR distributions removing proportionally the number of zero NCR values in each distribution that correspond to the lowest observed fraction of zeros in an individual distribution.

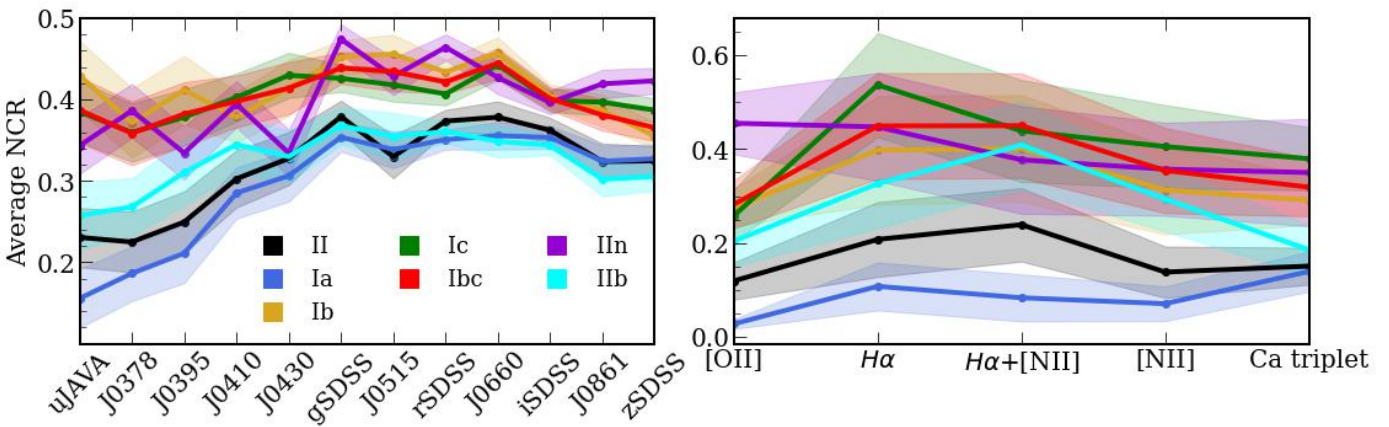


Fig. 11: Average NCR distributions as a function of the wavelength, for every SN type. The distributions are built averaging the NCR values for every J-PLUS photometric filter from the bluer to the redder filter (left panel). The right plot is built as the left one, but using the continuum-subtracted filters and removing proportionally the number of zero NCR values in each distribution that correspond to the lowest fraction of zeros in a distribution in each filter, as performed in section 6.1.

represent the average of all differences, and the violin plots represent the shape of the distributions. While all violins show the most populated value, similar to the median, compatible with zero difference, the average values show small shifts, which are more significant for the two CC SN types with respect to SNe Ia. Given that the narrow filters are chosen so that they cover some of the the main emission lines in galaxy spectra, these shifts for CC SNe are expected because they occur next to HII regions that

have intense emission lines. On the other hand, SNe Ia occur in all environments, most of them being non star-forming without emission lines, so the narrow band filters are not supposed to change significantly the SED and the results of the fitting.

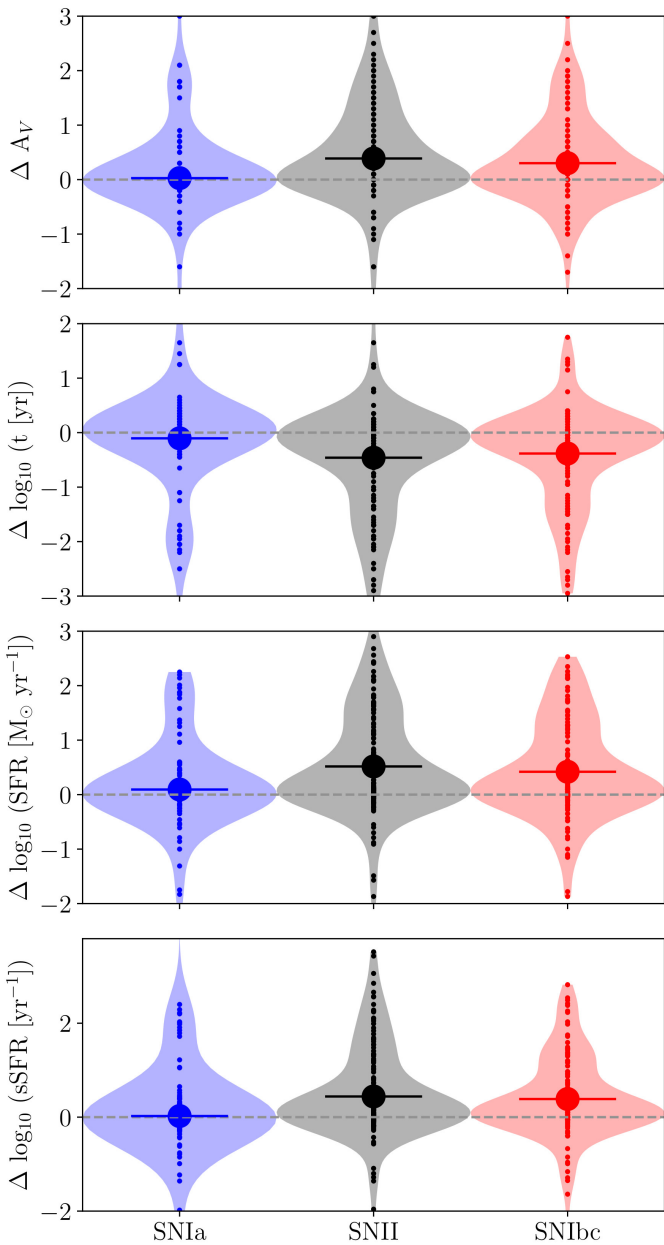


Fig. 12: Difference between the FAST++ SED fits once all the 12 J-PLUS filters are used and those only using the 5 broad band SDSS filters, for the four main environmental parameters. Individual dots represent the difference of each parameter for each individual SN environment, while the big dot represent the average of all differences. Violin plots represent the shape of the distributions.

7. Conclusions

We presented a study of 418 environments of different supernova types using broad- and narrow-band images obtained by the J-PLUS collaboration with the JAST80 telescope. We measured the Normalized Cumulative Rank (NCR) value for each SN and constructed NCR distributions by SN type. Improvements over previous works include the extension of the original H α NCR analysis to other optical bands, the homogeneity of the data of those 418 environments using the same telescope, instrument configuration, spatial resolution and image depth, and a better handling

of the extinction correction and the stellar-continuum subtraction for the narrow-band filters. In addition, we constructed spectral energy distributions (SED) of all these nearby environments and performed simple stellar population (SSP) synthesis to estimate parameters such as star-formation rate, stellar age, and extinction.

Regarding the NCR analysis on the J-PLUS filters, all broad band distributions are quite similar, being all close to the diagonal. The fact that almost all broad band distributions are close to the diagonal, along with the absence of a clear location preference for the SNe in the galaxies with respect to both NGCD and the fraction of r_{SDSS} flux (with the exception of the IIb type, that occur preferably in the inner part of the galaxies, between 0.2 and 0.5), suggests that we are primarily tracing the overall shape of the galaxy. The bluer bands ($uJAVA$, $J0378$ and $J0395$) show the only difference with respect the others; Ia, II and IIb types presents lower NCRs on average. When performing KS tests, the p-values indicate that the underlying populations of Ia-II-IIb-IIIn and Ibc-Ib-Ic are different, indicating that Ia-II-IIb progenitors trace better the redder wavelengths, also shown in the average NCR distributions.

The average NCR distributions for the 5 continuum-subtracted filters show a large fraction of zero values. For instance, in the H α emission, we have $\sim 35\%$ for Ibc, $\sim 53\%$ for II, and $\sim 65\%$ for Ia. This is partly because many SNe do not follow the H α emission. However, it is worth noting that there are more instances of zero values compared to previous studies (Anderson et al. 2012). We attribute those extra zero values to the low signal-to-noise ratio in the narrow-band filters due to the combination of a small telescope aperture (0.8m) and low exposure time was not enough to get significant contrast in these continuum-subtracted filters. For this reason, the fraction of zero values are not directly comparable with other studies that use images with different depths.

After considering the lowest percent of zeros among the 7 SN type distributions as our background, and removing proportionally the number of zero NCR values in each distribution that correspond to the lowest fraction of zeros in a distribution in each filter, we constructed new background-free NCR distributions, as performed by Ransome et al. (2022). The SN Ic distribution correlates most strongly with H α emission. It is followed by IIIn, Ibc, Ib, IIb, II and Ia, showing that the progenitors of the Ic types are younger and more massive than type II, while SNe Ia progenitors are even older, recovering results shown by previous works. However, it is important to note that the distribution for type IIIn is based on only 7 SNe in this panel. All core-collapse types strongly correlate with the [O II] emission, which also traces SFR following the sequence of Ia-II-IIb-Ic-Ibc-Ib (excluding IIIn since we have only 4 SNe). Besides, the Ca II triplet makes a clear division between II/IIb/Ia and Ib/Ic/IIIn progenitors, which we interpret as a difference in environmental stellar metallicity. The KS test performed for the 5 continuum subtracted filters also shows that II vs Ic, II vs Ibc, Ia vs Ic and Ia vs Ibc come from different populations. The opposite occurs with II vs Ia, II vs IIb and Ia vs IIb, as well as the rest of CC-SN between each other. In addition, after the [N II] removal, the distinction between the underlying populations of the Ia, IIb, and IIIn types, as revealed in the KS test, disappears, but the NCRs remain unchanged. We should note that the removal of [N II] is oversimplified and may potentially introduce noise into this aspect of the analysis.

Regarding the SED analysis, we have recovered the main relations previously reported between SN types for all parameters. Moreover, we found out that including the J-PLUS narrow filters in the SED fitting has a more significant effect for the CC SN environmental parameters, shifting all parameters, due to the

presence of strong emission-lines in their typical star-forming regions.

The JAST80 telescope with J-PLUS filters has allowed us to study SN host galaxies in the northern sky up to $z = 0.0163$. The H α emission from galaxies at higher redshifts falls outside the width covered by the J0660 filter. In the near future, using the next generation of narrow band wide field surveys, such as J-PAS at the JST250 telescope (Benítez et al. 2014) and the PAU survey at the William Herschel Telescope (Padilla et al. 2019), with filters covering a contiguous range at redder wavelengths, we will be able to extend the redshift range by using the filter covering the observed H α emission at $6563 \times (1+z)$ Å.

Acknowledgements. Based on observations made with the JAST80 telescope and T80Cam camera for the J-PLUS project at the Observatorio Astrofísico de Javalambre (OAJ), in Teruel, owned, managed, and operated by the Centro de Estudios de Física del Cosmos de Aragón (CEFCA). We acknowledge the OAJ Data Processing and Archiving Unit (UPAD) for reducing the OAJ data used in this work. Funding for OAJ, UPAD, and CEFCA has been provided by the Governments of Spain and Aragón through the Fondo de Inversiones de Teruel and their general budgets; the Aragonese Government through the Research Groups E96, E103, E16_17R, E16_20R and E16_23R; the Spanish Ministry of Science and Innovation (MCIN/AEI/10.13039/501100011033 y FEDER, Una manera de hacer Europa) with grants PID2021-124918NB-C41, PID2021-124918NB-C42, PID2021-124918NA-C43, and PID2021-124918NB-C44; the Spanish Ministry of Science, Innovation and Universities (MCIU/AEI/FEDER, UE) with grant PGC2018-097585-B-C21; the Spanish Ministry of Economy and Competitiveness (MINECO) under AYA2015-66211-C2-1-P, AYA2015-66211-C2-2, AYA2012-30789, and ICTS-2009-14; and European FEDER funding (FCDD10-4E-867, FCDD13-4E-2685). The Brazilian agencies FINEP, FAPESP, and the National Observatory of Brazil have also contributed to this project. The SNICE research group acknowledges financial support from the Spanish Ministerio de Ciencia e Innovación (MCIN) and the Agencia Estatal de Investigación (AEI) 10.13039/501100011033 under the PID2020-115253GA-100 HOSTFLOWS project, from Centro Superior de Investigaciones Científicas (CSIC) under the PIE project 20215AT016, and the program Unidad de Excelencia María de Maeztu CEX2020-001058-M. L.G. is also funded by the European Social Fund (ESF) "Investing in your future" under the 2019 Ramón y Cajal program RYC2019-027683-I. RGB acknowledges financial support from the Severo Ochoa grant CEX2021-001131-S funded by MCIN/AEI/10.13039/501100011033. Based on observations made with the JAST80 telescope/s at the Observatorio Astrofísico de Javalambre, in Teruel, owned, managed and operated by the Centro de Estudios de Física del Cosmos de Aragón, under proposals 1800146, 1900154, 1900165, 2000177, and 2000182. We thank the OAJ Data Processing and Archiving Unit (UPAD) for reducing and calibrating the OAJ data used in this work. This work was funded by ANID, Millennium Science Initiative, ICN12_009.

- Gal-Yam A., 2017, in Alsabti A. W., Murdin P., eds, , Handbook of Supernovae. p. 195, doi:10.1007/978-3-319-21846-5_35
- Galbany L., et al., 2014, *A&A*, **572**, A38
- Galbany L., et al., 2016, *A&A*, **591**, A48
- Galbany L., et al., 2017, *MNRAS*, **468**, 628
- Galbany L., et al., 2018, *ApJ*, **855**, 107
- Garcia-Vargas M. L., Molla M., Bressan A., 1998, *A&AS*, **130**, 513
- Graur O., Bianco F. B., Modjaz M., Shivvers I., Filippenko A. V., Li W., Smith N., 2017, *ApJ*, **837**, 121
- Green G., 2018, *The Journal of Open Source Software*, **3**, 695
- Guillochon J., Parrent J., Kelley L. Z., Margutti R., 2017, *ApJ*, **835**, 64
- Habergham S. M., Anderson J. P., James P. A., 2010, *ApJ*, **717**, 342
- Han D.-H., Park C., Choi Y.-Y., Park M.-G., 2010, *ApJ*, **724**, 502
- Hoyle F., Fowler W. A., 1960, *ApJ*, **132**, 565
- James P. A., Anderson J. P., 2006, *A&A*, **453**, 57
- Kangas T., Mattila S., Kankare E., Kotilainen J. K., Väistänen P., Greimel R., Takalo A., 2013, *MNRAS*, **436**, 3464
- Kangas T., et al., 2017, *A&A*, **597**, A92
- Kelly P. L., Kirshner R. P., 2012, *ApJ*, **759**, 107
- Kennicutt Robert C. J., 1998, *ApJ*, **498**, 541
- Kriek M., van Dokkum P. G., Labbé I., Franx M., Illingworth G. D., Marchesini D., Quadri R. F., 2009, *ApJ*, **700**, 221
- Kuncarayakti H., et al., 2013, *AJ*, **146**, 30
- Kuncarayakti H., et al., 2018, *A&A*, **613**, A35
- Logroño-García R., Vilella-Rojo G., López-Sanjuan C., Varela J., Muniesa D., Lamadrid J. L., Cenarro A. J., J-PLUS T., 2017, in Arribas S., Alonso-Herrero A., Figueras F., Hernández-Monteagudo C., Sánchez-Lavega A., Pérez-Hoyos S., eds, Highlights on Spanish Astrophysics IX. pp 283–283
- Logroño-García R., et al., 2019, *A&A*, **622**, A180
- Lyman J. D., Galbany L., Sánchez S. F., Anderson J. P., Kuncarayakti H., Prieto J. L., 2020, *MNRAS*, **495**, 992
- Maoz D., Mannucci F., Nelemans G., 2014, *ARA&A*, **52**, 107
- Marín-Franch A., Taylor K., Cenarro J., Cristobal-Hornillos D., Moles M., 2015, in IAU General Assembly. p. 2257381
- Martínez-Solaeche G., et al., 2021, *A&A*, **647**, A158
- Maund J. R., et al., 2013, *MNRAS*, **431**, L102
- McCully C., et al., 2014, *Nature*, **512**, 54
- Molino A., et al., 2014, *MNRAS*, **441**, 2891
- Nomoto K., Suzuki T., Shigeyama T., Kumagai S., Yamaoka H., Saio H., 1993, *Nature*, **364**, 507
- Padilla C., et al., 2019, *AJ*, **157**, 246
- Pascual S., Gallego J., Zamorano J., 2007, *PASP*, **119**, 30
- Perlmutter S., et al., 1997, *ApJ*, **483**, 565
- Perlmutter S., et al., 1999, *ApJ*, **517**, 565
- Phillips M. M., Lira P., Suntzeff N. B., Schommer R. A., Hamuy M., Maza J., 1999, *AJ*, **118**, 1766
- Prentice S. J., Mazzali P. A., 2017, *MNRAS*, **469**, 2672
- Ransom C. L., Habergham-Mawson S. M., Darnley M. J., James P. A., Percival S. M., 2022, *MNRAS*, **513**, 3564
- Riess A. G., Press W. H., Kirshner R. P., 1996, *ApJ*, **473**, 88
- Schreiber C., et al., 2018, *A&A*, **618**, A85
- Shivvers I., et al., 2017, *PASP*, **129**, 054201
- Smartt S. J., 2015, *PASA*, **32**, e016
- Smith N., Li W., Filippenko A. V., Chornock R., 2011, *MNRAS*, **412**, 1522
- Taddia F., et al., 2018, *A&A*, **609**, A136
- Thomas D., et al., 2013, in Thomas D., Pasquali A., Ferreras I., eds, IAU Symposium Vol. 295, The Intriguing Life of Massive Galaxies. pp 129–132, doi:10.1017/S174392131300450X
- Van Dyk S. D., 2017, *Philosophical Transactions of the Royal Society of London Series A*, **375**, 20160277
- Vilella-Rojo G., et al., 2015, *A&A*, **580**, A47

References

- Anderson J. P., James P. A., 2008, *MNRAS*, **390**, 1527
- Anderson J. P., James P. A., 2009, *MNRAS*, **399**, 559
- Anderson J. P., Habergham S. M., James P. A., Hamuy M., 2012, *MNRAS*, **424**, 1372
- Anderson J. P., James P. A., Habergham S. M., Galbany L., Kuncarayakti H., 2015, *PASA*, **32**, e019
- Arnett W. D., Schramm D. N., Truran J. W., 1989, *ApJ*, **339**, L25
- Astier P., et al., 2006, *A&A*, **447**, 31
- Benítez N., et al., 2014, arXiv e-prints, p. arXiv:1403.5237
- Bruzual G., Charlot S., 2003, *MNRAS*, **344**, 1000
- Calzetti D., Armus L., Bohlin R. C., Kinney A. L., Koornneef J., Storchi-Bergmann T., 2000, *ApJ*, **533**, 682
- Cenarro A. J., et al., 2014, in Observatory Operations: Strategies, Processes, and Systems V. p. 91491I, doi:10.1117/12.2055455
- Cenarro A. J., et al., 2019, *A&A*, **622**, A176
- Chabrier G., 2003, *PASP*, **115**, 763
- Cid Fernandes R., Mateus A., Sodré L., Stasińska G., Gomes J. M., 2005, *MNRAS*, **358**, 363
- Delchambre L., et al., 2023, *A&A*, **674**, A31
- Díaz A. I., Terlevich E., Terlevich R., 1989, *MNRAS*, **239**, 325
- Eldridge J. J., Maund J. R., 2016, *MNRAS*, **461**, L117
- Filippenko A. V., 1988, *AJ*, **96**, 1941
- Filippenko A. V., 1997, *ARA&A*, **35**, 309
- Fruchter A. S., et al., 2006, *Nature*, **441**, 463

Appendix A: Sample list and NCRs

Table A.1: Supernovae sample. Name of the SN, Type, Right ascension, Declination and redshift.

NAME	TYPE	RA	DEC	z	NAME	TYPE	RA	DEC	z
SN2014ge	Ib	181.2146	26.9963	0.0019	SN2001fv	II	166.0069	28.0321	0.0046
SN2017igf	Ia	175.7069	77.3702	0.0060	SN1941C	II	182.3375	29.9083	0.0020
SN2019clq	Ib	114.1563	74.4465	0.0120	SN2006M	II	201.8323	31.7874	0.0156
SN2019tdf	Ia	266.6207	30.7069	0.0155	SN1961F	II	147.1597	33.4264	0.0047
SN2019upq	II	217.2838	27.4502	0.0143	SN2010ie	II	107.0988	35.1698	0.0158
SN2019xdf	II	141.9661	68.4119	0.0130	SN1998Y	II	114.2372	35.2433	0.0126
SN2020aapr	II	112.0179	66.3748	0.0150	SN2019ovr	II	112.2094	35.5476	0.0131
SN2020acac	II	217.7526	25.4889	0.0151	SN2017hbg	II	111.9055	35.6085	0.0160
SN2020akf	Ia	142.1653	38.5631	0.0125	SN2018aoq	II	182.6591	39.3964	0.0033
SN2020dr1	II	112.0481	72.5781	0.0121	SN2020dvt	II	234.4522	38.1465	0.0140
SN2020xqj	II	180.9564	29.7171	0.0106	SN1975T	II	174.1750	54.2867	0.0043
SN2021aan	Ia	342.5469	30.3633	0.0123	SN1980D	II	173.7422	54.8819	0.0043
SN2021afkk	II	37.4999	28.6342	0.0138	SN1978H	II	174.8486	56.2669	0.0080
SN2021afsj	Ia	134.1768	52.1080	0.0122	SN2001dc	II	222.8173	58.9841	0.0071
SN2021ass	II	27.5422	27.6452	0.0118	SN2006at	II	198.1713	63.2793	0.0150
SN2021bbm	II	146.2804	68.5915	0.0150	SN2014F	II	277.6325	67.9916	0.0086
SN2021eay	II	273.5339	64.7788	0.0090	SN2013ej	II	24.2007	15.7586	0.0022
SN2021gmg	Ia	334.8448	32.9579	0.0121	SN2019fyd	II	348.8172	19.0417	0.0158
SN2021jag	Ia	181.6873	67.1649	0.0084	SN2009ga	II	352.1116	22.4140	0.0116
SN2021mxz	Ic	284.2136	36.6223	0.0097	SN1995Z	II	20.9098	32.6314	0.0158
SN2021qvr	II	352.1110	22.4200	0.0116	iPTF13dkz	II	24.0483	33.6171	0.0160
SN2021wcu	Ia	110.1047	32.8515	0.0160	SN2000dj	II	29.1693	34.1701	0.0154
SN2021yok	II	112.2311	20.5861	0.0149	SN2006Q	II	24.5781	35.3651	0.0160
SN2022aaq	Ia	216.6334	56.5842	0.0065	ASASSN-14kg	II	26.1599	35.8057	0.0145
SN2022acfz	II	114.3969	35.6055	0.0133	SN1999dj	II	27.0456	35.3964	0.0144
SN2022bdu	Ic	144.2174	37.6942	0.0150	SN2004dw	II	285.9094	27.6151	0.0141
SN2022hkc	Ia	114.6578	37.6314	0.0130	SN2015U	Ibn	112.2245	33.8196	0.0138
SN2022mji	II	145.7253	31.8510	0.0040	SN2001ej	Ib	110.9301	33.4439	0.0135
SN2022mjk	Ia	21.4223	1.7615	0.0150	SN2015Q	Ib	176.8962	55.9708	0.0080
SN2022ngb	IIb	284.2145	36.6188	0.0090	SN1997dc	Ib	352.1184	22.4231	0.0116
SN2022oqm	Ic	227.2842	52.5348	0.0120	SN2006ep	Ib	10.3537	25.4963	0.0151
SN2022prv	II	235.0323	20.6755	0.0151	SN2005kf	Ic	116.8600	26.9257	0.0150
SN2022sje	II	275.5222	66.6245	0.0155	SN2000C	Ic	114.2379	35.2441	0.0126
SN2022zkd	II	174.2199	54.8940	0.0140	SN2006dg	Ic	356.4766	12.0664	0.0142
SN2023jo	IIn	121.8533	39.1938	0.0130	SN2006ei	Ic	29.1548	34.1771	0.0154
SN1997bm	Ia	173.2380	50.2454	0.0098	SN2018dbg	Ibc	214.4953	26.4124	0.0148
SN1963K	Ia	170.9154	53.8369	0.0096	SN2016bmd	IIb	110.1007	32.8507	0.0142
SN1990L	Ia	234.1000	22.5017	0.0144	SN2006iv	IIb	177.0515	54.9874	0.0081
SN2020fcw	Ia	217.1334	27.4083	0.0144	SN2004C	IIb	171.8738	56.8801	0.0063
SN1989A	Ia	171.9959	29.5059	0.0084	SN2018fpb	IIb	359.9283	34.3444	0.0148
SN1999gr	Ia	182.2971	29.2763	0.0129	SN2005db	IIn	10.3616	25.4977	0.0151
SN1982C	Ia	183.3458	28.4917	0.0130	SN2019el	IIn	0.7363	32.5479	0.0005
SN2017iji	Ia	183.1121	29.1492	0.0134	SN2014cn	II	182.2981	29.1725	0.0120
SN2013hg	Ia	182.4820	29.8976	0.0128	SN2020noe	II	154.7773	34.6540	0.0155
SN1991bi	Ia	200.9332	31.5641	0.0160	SN2018fmf	II	144.6223	76.3199	0.0076
SN2010jv	Ia	111.8603	33.8116	0.0135	SN2004dd	II	6.9707	-1.8129	0.0135
SN1995al	Ia	147.7332	33.5526	0.0051	SN2003gd	II	24.1777	15.7389	0.0022
SN2011hd	Ia	149.7013	34.7843	0.0150	SN1997ef	Ic	119.2620	49.5615	0.0117
SN2020hni	Ia	111.5922	36.2337	0.0150	SN2002ap	Ic	24.0994	15.7537	0.0022
SN1999da	Ia	263.8457	60.8137	0.0127	SN2002fb	Ia	29.4538	36.3406	0.0156
SN1989P	Ia	275.5075	66.6034	0.0141	SN1988E	II	193.3700	2.1730	0.0035
SN2003hm	Ia	42.2433	3.1688	0.0139	SN1981B	Ia	188.6230	2.1998	0.0060
ASASSN-15mc	Ia	42.2482	3.1696	0.0139	SN2011hy	II	71.2719	72.7841	0.0159
SN2009nq	Ia	348.8207	19.0229	0.0158	SN2019ccm	Ib	70.2724	73.6731	0.0149
SN2002dp	Ia	352.1255	22.4274	0.0116	SN2012eg	II	47.3207	38.6391	0.0114
SN2017haf	Ia	359.0910	32.4567	0.0094	SN1991bg	Ia	186.2650	12.8710	0.0034
SN1999ej	Ia	20.7391	33.4661	0.0137	SN1957B	Ia	186.2580	12.9000	0.0034
SN2016F	Ia	24.8835	33.8267	0.0160	SN2013am	II	169.7370	13.0637	0.0027
SN2011gb	Ia	23.4289	34.8103	0.0142	SN2001ez	II	85.6568	69.2374	0.0129
SN2006td	Ia	29.5657	36.3494	0.0160	ASASSN-15ti	Ia	46.2859	37.9002	0.0160
SN2005cx	Ia	29.7283	36.6763	0.0160	SN2003cg	Ia	153.5670	3.4674	0.0041
SN2006W	II	216.8587	25.5194	0.0157	SN1984E	II	153.5460	3.4703	0.0041
SN2019hyk	II	214.4912	26.4215	0.0147	SN2003ef	II	192.4260	-11.0915	0.0139
					SN2016cvn	Ia	92.4223	-11.0929	0.0139
					SN2005bo	Ia	192.4210	-11.0965	0.0139
					SN2006eg	Ib-c	38.2232	19.2592	0.0133
					SN1969L	II	40.9389	37.3109	0.0017
					SN1961V	II	40.9019	37.3453	0.0017

NAME	TYPE	RA	DEC	z
SN2015ab	Ia	37.1369	20.2856	0.0137
SN2007ap	Ia	239.0960	16.5161	0.0157
SN2003gt	Ia	308.2460	9.8720	0.0152
ASASSN-15tw	II	192.6170	-10.8414	0.0080
SN1986E	II	185.4220	14.6319	0.0037
SN2003gk	Ib	345.4290	2.2691	0.0106
SN2015ah	Ib	345.1030	1.6269	0.0161
SN2004ao	Ib	262.0390	7.4154	0.0056
SN2006D	Ia	193.1410	-9.7752	0.0085
SN2012au	Ib	193.7170	-10.2473	0.0000
SN2007C	Ib	197.2050	-6.7836	0.0056
SN2002jz	Ib	63.3022	13.4187	0.0052
SN2018ow	IIb	42.7684	9.1123	0.0100
SN2016G	Ic	45.9904	43.4010	0.0091
SN2016coi	Ic	329.7670	18.1862	0.0036
SN2014ad	Ic	179.4350	-10.1710	0.0057
SN2009iz	Ib	40.5642	42.3972	0.0142
SN2007ru	Ic	346.8460	43.5927	0.0155
SN2007iq	Ic	93.3847	69.7303	0.0134
SN2007gr	Ic	40.8665	37.3457	0.0017
SN2006F	Ib	37.0474	19.6038	0.0139
SN2005da	Ic	279.4450	17.5431	0.0150
SN1999ed	II	102.5040	25.6318	0.0155
SN2004ge	Ic	102.5010	25.6339	0.0155
SN2000eo	IIIn	47.2840	-10.2987	0.0105
SN1984L	Ib	38.8773	-7.1584	0.0051
SN1962L	Ic	40.9197	1.3978	0.0040
PS15cwt	IIIn	38.3177	19.2568	0.0135
SN2018ebt	Ic	310.4790	64.2146	0.0100
SN2017jfs	IIIn	187.4070	7.8264	0.0078
SN2014L	Ic	184.7030	14.4121	0.0080
SN1986I	II	184.7170	14.4122	0.0080
SN1967H	II	184.7300	14.4122	0.0080
SN1972Q	II	184.7120	14.4444	0.0080
SN2012cw	Ic	153.4500	3.4341	0.0039
SN2011jm	Ic	193.7130	2.6541	0.0033
SN2008aq	II-IIb	192.6270	-10.8671	0.0080
SN2016aaI	II	192.6170	-10.8414	0.0080
SN2015P	II	192.6280	-10.8778	0.0080
SN2008ao	Ic	46.9444	38.3684	0.0154
SN2005kj	IIIn	130.0380	-5.6006	0.0168
SN2005ip	IIIn	143.0270	8.4457	0.0071
SN2005ek	Ic	46.4540	36.7696	0.0166
SN2004dk	Ib	245.4540	-2.2715	0.0052
SN2020hvp	Ib	245.4390	-2.2893	0.0052
SN2017jbl	IIb	53.3030	36.1902	0.0151
SN2017ewx	Ib	210.5690	7.6790	0.0152
SN2013ha	IIIn	93.9577	66.8387	0.0136
SN2010X	Ic	72.1162	73.4708	0.0150
SN2010jl	IIIn	145.7220	9.4949	0.0107
SN2009lj	Ic	48.1354	39.3117	0.0146
SN2017lf	Ia	48.1400	39.3209	0.0146
SN2008im	Ib	60.2590	74.0968	0.0083
SN2008eb	Ic	272.9670	14.9807	0.0076
SN2008du	Ic	344.0490	3.9265	0.0161
SN2007rz	Ic	67.7952	7.6310	0.0130
SN2006bo	IIIn	307.6750	9.1947	0.0153
SN2005aj	Ic	44.7035	75.7538	0.0085
SN2004gn	Ib	188.5500	2.6596	0.0058
SN1991T	Ia	188.5430	2.6657	0.0058
SN2001B	Ib	74.3302	78.1879	0.0052
SN2002ji	Ib	170.7210	16.5861	0.0050
SN2000fn	Ib	121.7410	8.0054	0.0154
SN2000H	IIb	102.7820	12.9218	0.0132
SN2018imj	II	102.7740	12.9154	0.0132
SN1999el	IIIn	309.3240	66.1032	0.0048
SN2020dpw	II	309.2940	66.1030	0.0048
SN2000E	Ia	309.3070	66.0973	0.0048

NAME	TYPE	RA	DEC	z
SN2015G	Ib	309.3570	66.1199	0.0048
PTF09dfk	Ib	347.3060	7.8043	0.0160
SN1999dn	Ib	354.0610	2.1524	0.0093
SN2007fo	Ib	354.0580	2.1584	0.0093
SN1998ey	Ic	322.5030	26.7226	0.0161
PTF12gzk	Ic	333.1730	0.5120	0.0138
ASASSN14az	IIb	356.1970	-2.1165	0.0067
SN2017gas	IIIn	304.2970	58.2025	0.0123
SN2017hyh	IIb	107.6710	6.4615	0.0120
SN2012ej	Ic	96.7125	59.0841	0.0089
SN2011an	IIIn	119.8520	16.4189	0.0163
SN2018afm	IIIn	119.8540	16.4265	0.0163
SN2016P	Ic	209.3800	6.0975	0.0145
SN2010do	Ic	209.3670	6.0968	0.0145
SN2003bl	II	209.3780	6.0934	0.0145
SN2004gk	Ic	186.3880	12.2611	-0.0005
SN2003aa	Ic	161.6530	13.7589	0.0101
SN2007am	II	161.6400	13.7526	0.0101
SN1986A	Ia	161.6520	13.7502	0.0101
SN2018kp	Ia	161.6380	13.7419	0.0101
SN1992C	II	161.6510	13.7446	0.0101
SN2001is	Ib	85.5378	69.3652	0.0131
SN1998eb	Ia	85.5501	69.3740	0.0131
SN2013cc	II	85.4948	69.3614	0.0131
SN2001ef	Ic	71.1190	75.6418	0.0083
SN2000ew	Ib	175.2440	11.4655	0.0033
SN1997dq	Ic	175.2330	11.4794	0.0033
SN1998cc	Ib	202.3300	17.0451	0.0134
SN2001R	II	202.3210	17.0448	0.0134
SN1997bs	IIIn	170.0590	12.9721	0.0024
SN1989B	Ia	170.0580	13.0052	0.0024
SN2009hd	II	170.0710	12.9796	0.0024
SN1973R	II	170.0480	12.9964	0.0024
SN2016cok	II	170.0800	12.9822	0.0024
SN1990B	Ic	189.1410	11.2416	0.0074
SN2004cc	Ib	189.1430	11.2424	0.0074
SN2020fqv	IIb	189.1390	11.2316	0.0074
SN1989M	Ia	189.4200	11.8237	0.0051
SN1988A	II	189.4310	11.8054	0.0051
SN1961H	Ia	189.1140	11.4397	0.0038
SN1976B	Ib	186.5510	13.1127	0.0008
iPTF13bvn	Ib	225.0010	1.8814	0.0045
SN2012P	Ib-c	224.9960	1.8901	0.0045
SN2004dg	II	224.9960	1.8904	0.0045
SN2017gpn	IIb	54.4386	72.5330	0.0074
SN2008dv	Ic	54.4643	72.5727	0.0074
CSS141028081814044553	Ib	124.5580	4.7646	0.0139
ASASSN15bd	IIb	238.6600	16.6106	0.0080
SN2006my	II	190.9200	16.3873	0.0027
SN1987K	IIb	190.9220	16.3958	0.0027
SN2015cz	II	22.9977	33.4794	0.0145
SN2020lkb	II	22.9795	33.4723	0.0145
SN2017fgc	Ia	20.0602	3.4028	0.0077
SN2008ij	II	274.9660	74.5653	0.0050
SN2005ai	Ia	107.6360	75.3581	0.0128
AT2020drl	II	112.0480	72.5781	0.0102
SN2014J	Ia	148.9250	69.6739	0.0009
SN2004am	II	148.9440	69.6773	0.0009
SN2008iz	II	148.9650	69.6794	0.0009
SN2018lkg	II	106.6450	63.8491	0.0142
SN2017jav	Ia	105.7310	62.7725	0.0152
SN2007sa	Ia	165.7950	56.2240	0.0051
SN2019fmb	IIIn	186.6820	56.0758	0.0154
SN1999by	Ia	140.4670	51.0018	0.0021
SN1957A	Ia	140.4630	50.9978	0.0021
SN1972R	Ib	140.4830	50.9550	0.0021
SN2015ba	II	218.1220	49.8929	0.0079
SN1996cc	II	217.8690	49.9622	0.0069

NAME	TYPE	RA	DEC	z	NAME	TYPE	RA	DEC	z
SN2016iuh	Ia	184.8810	49.8178	0.0137	SN1994I	Ic	202.4750	47.1918	0.0015
SN2019arb	Ia	184.8800	49.8142	0.0137	SN1985F	Ib	190.3880	41.1516	0.0018
SN2005cs	II	202.4720	47.1745	0.0015	SN2008ax	IIb	187.6700	41.6378	0.0019
SN1945A	I	202.4880	47.2717	0.0015	SN1954A	Ib	183.9380	36.2700	0.0010
SN1999bw	II	154.9450	45.5264	0.0022	SN2010gk	Ic	210.6500	32.5085	0.0145
SN1966J	Ia	154.9380	45.5033	0.0022	SN2007uy	Ib	137.3980	33.1194	0.0065
SN2020tlf	II	220.0420	42.7777	0.0022	SN2008D	Ib	137.3780	33.1389	0.0065
SN1982F	II	187.6700	41.6378	0.0019	SN1999eh	Ib	137.3860	33.1214	0.0065
SN1921B	II	154.5960	41.3500	0.0019	SN2002cw	Ib	281.5100	32.2842	0.0153
SN2020sec	Ia	138.5370	40.0781	0.0085	AT2014ge	Ib	181.2150	26.9963	0.0019
SN2020rue	II	109.5030	39.8368	0.0150	SN2018cow	Ic	244.0010	22.2680	0.0141
SN2006lv	Ib-c	173.0140	36.7010	0.0083	SN1988ac	Ibc	179.4280	32.2839	0.0109
ASASSN-16eu	II	131.0460	34.7156	0.0142	SN1991ar	Ib	10.9863	1.8538	0.0152
SN2006lt	Ib	34.2495	30.6993	0.0160	SN2000dv	Ib	134.1810	52.1037	0.0122
SN2012C	Ic	144.3770	32.8421	0.0145	SN2012cd	IIb	200.6470	54.8132	0.0118
SN2015bh	II	137.3960	33.1223	0.0065	SN2006jc	Ibn	139.3370	41.9091	0.0056
SN2020jhf	Ia	198.7230	27.0086	0.0155	SN2006ld	Ib	8.8659	2.9308	0.0141
SN2019ltw	IIb	244.6600	21.9731	0.0161	SN2010gr	Ib-c	38.4957	44.3473	0.0169
SN2018cyg	II	233.5350	56.6970	0.0113	SN2011it	Ic	330.6850	31.6968	0.0159
SN2001cm	II	233.5280	56.6906	0.0113	SN2011jf	IbPec	39.7275	27.8469	0.0153
SN1991F	Ia	164.0090	57.1134	0.0063	SN2015ap	Ib-c	31.3055	6.1023	0.0114
SN1975G	Ia	210.3250	54.4250	0.0063	SN2017hcb	Ib	39.0988	31.7097	0.0162
SN2019gsc	Ia	219.4380	52.7268	0.0113	SN2009lw	II-Ilb	37.0504	31.3129	0.0166
SN2007T	II	225.1910	49.9901	0.0135	SN1940A	II	229.0460	56.2383	0.0022
SN2019cth	Ia	221.4480	50.3969	0.0134	SN2014C	Ib	339.2730	34.4089	0.0027
SN2014bc	II	184.7400	47.3031	0.0015	SN1954C	II	227.4380	57.0017	0.0026
SN1981K	II	184.7480	47.3253	0.0015	SN1959D	II	339.2580	34.4190	0.0027
SN2002cs	Ia	281.7500	45.7055	0.0158	SN1976F	II	39.4042	33.6633	0.0090
SN2002bu	II	184.4050	45.6465	0.0017	SN1994ak	II	138.5060	40.1060	0.0085
SN2017czd	II	222.9460	43.6447	0.0084	SN1999A	II	226.9800	54.7611	0.0105
SN2018acj	II	207.1690	43.4180	0.0078	SN2000ez	II	179.4410	32.2970	0.0109
SN1971I	Ia	198.9570	41.9875	0.0017	SN2002A	II	110.6510	71.5949	0.0096
SN1937F	II	154.5670	41.3750	0.0019	SN2003G	IIn	32.1172	6.3978	0.0117
SN1921C	I	154.5960	41.3500	0.0019	SN2003da	II	140.9480	42.1802	0.0138
SN1999gi	II	154.5690	41.4412	0.0019	SN2004cm	II	211.8540	55.1030	0.0046
SN2016bkv	II	154.5800	41.4276	0.0019	SN2005Ix	II	35.6625	28.2520	0.0170
SN2015V	II	267.3630	36.1433	0.0046	SN2005mg	II	4.1842	7.0722	0.0132
SN2018ccb	II	277.7390	29.8798	0.0158	SN2006G	IIb	21.1493	1.7211	0.0167
SN2005dv	Ia	205.2690	67.6723	0.0101	SN2007cm	II	190.6880	55.1492	0.0164
SN2018fru	II	204.0160	66.3012	0.0103	SN2007pk	IIn	22.9461	33.6150	0.0167
ASASSN-15lf	II	181.6900	67.1567	0.0085	SN2008az	II	257.1080	25.5172	0.0097
SN2002kg	II	114.2580	65.5748	0.0004	SN2010ic	II	334.7680	33.3297	0.0163
SN2004dj	II	114.3210	65.5994	0.0004	SN2011hn	II	135.8230	30.5934	0.0142
SN1954J	II	114.2340	65.6312	0.0004	SN2013bu	II	339.2590	34.4014	0.0027
iPTF13akc	Ia	113.2350	64.9112	0.0139	SN2014cv	IIP	239.7650	51.3050	0.0125
SDSS-IIISN14215	II	18.6553	1.1776	-0.0000	SN2015X	II	109.1770	29.8563	0.0107
SN2019bxq	IIn	254.4940	78.6038	0.0142	SN2015am	II	32.2912	31.9976	0.0167
SN2010gi	II	260.4420	75.8457	0.0041	SN2016bam	II	116.7200	39.0227	0.0135
SN2017hkp	II	25.6737	28.7206	0.0075	SN2016bkx	IIP	112.0460	72.5754	0.0102
SN2013fs	II	349.9360	10.1847	0.0119	SN2016bme	II	134.1630	52.1023	0.0122
SN1964H	II	337.1000	30.2899	0.0033	SN2016brw	II	257.1110	25.5143	0.0097
SN2002jg	Ia	334.8700	29.3846	0.0150	SN2016ccf	II	131.0460	34.7155	0.0142
SN1992az	II	32.1957	38.7726	0.0142	SN2016hrv	II	128.3420	52.5309	0.0166
SN2002dl	Ia	335.2250	33.2927	0.0163	SN2017gtd	IIP	35.6674	28.2569	0.0170
SN1991ao	II	6.9850	32.7783	0.0164	SN1938A	I	39.4042	34.4417	0.0164
SN2000fd	Ia	7.3004	33.1082	0.0161	SN1966G	I	21.1542	1.7350	0.0167
SN2005B	II	268.7030	71.5429	0.0144	SN1970L	I	145.8330	31.9517	0.0051
SN1998ar	II	143.7450	21.7160	0.0124	SN1976G	Ia	20.4417	5.2267	0.0076
SN2016iyC	Ib	332.3100	21.5215	0.0127	SN1982V	I	40.0787	32.2664	0.0149
SN2008ie	Ib	40.8367	4.9720	0.0136	SN1982W	Ia	211.7870	55.0187	0.0064
SN2018hdp	Ic	33.4378	4.1023	0.0115	SN1997dp	Ia	38.5270	32.9371	0.0150
SN2018gj	Ib	248.0100	78.2114	0.0045	SN1998es	Iapec	24.3233	5.8807	0.0106
SN2008bo	Ib	274.9770	74.5725	0.0050	SN2001ed	Ia	27.9628	6.2909	0.0166
SN2018gwo	Ic	182.1620	68.7790	0.0074	SN2005ev	Ia	37.7705	27.7018	0.0153
SN1993J	Ib	148.8530	69.0205	-0.0001	SN2007J	Ia	34.7154	33.7287	0.0168
SN2002ho	Ic	183.8250	65.9820	0.0090	SN2009hr	Ia	10.1422	3.5414	0.0170
SN2017ati	Ib	147.4860	67.1832	0.0160	SN2010eb	Ia	20.4074	5.2944	0.0076
SN2011dh	Ib	202.5210	47.1697	0.0015	SN2011aa	Iapec	114.1780	74.4430	0.0125

NAME	TYPE	RA	DEC	z
SN2011hr	Ia-91T	133.6920	39.5378	0.0134
SN2013fb	Ia	35.6753	28.2670	0.0170
SN2014da	Ia-91bg	7.3130	2.8660	0.0141
SN2017glq	Ia	32.1167	6.3879	0.0117
SN2017gxq	Ia	196.3500	56.3242	0.0085
SN2017hjy	Ia	39.0107	43.4721	0.0070
SN2018bi	Ia	34.9720	29.0341	0.0166
iPTF13ebh	Ia	35.4999	33.2705	0.0132
SN2011fe	Ia	210.5120	54.4658	0.0008
SN1909A	II	210.5120	54.4658	0.0008
SN1951H	II	210.9730	54.3619	0.0008
SN1970G	II	210.7540	54.2426	0.0008
SN1995V	II	41.6115	-0.4988	0.0051
SN2004hx	II	40.3025	-0.8794	0.0140
SN2018ivc	II	40.6720	-0.0088	0.0038
SN1998dk	Ia	3.6340	-0.7364	0.0130
SN2009ig	Ia	39.5484	-1.3126	0.0088
SN2023ixf	II	210.9106	54.3116	0.000804

Table A.2: NCR values for all the sample with the broad-band filters.

Name(Type)	uJAVA	gSDSS	rSDSS	iSDSS	zSDSS
ASASSN-14kg(II)	0.484	0.775	0.745	0.749	0.780
ASASSN-15lf(II)	0.271	0.130	0.096	0.089	0.050
ASASSN-15tw(II)	0.571	0.324	0.305	0.269	0.232
ASASSN-16eu(II)	0.441	0.269	0.200	0.203	0.207
ASASSN14az(IIb)	0.603	0.185	0.122	0.087	0.077
ASASSN15bd(IIb)	0.819	0.661	0.576	0.578	0.569
AT2020drl(II)	0.062	0.000	0.034	0.016	0.160
PS15cwt(IIn)	0.355	0.362	0.327	0.272	0.283
SDSS-IIISN14215(II)	0.363	0.448	0.272	0.395	0.265
SN1909A(II)	0.120	0.000	0.000	0.000	0.000
SN1921B(II)	0.680	0.097	0.056	0.043	0.179
SN1937F(II)	0.510	0.085	0.099	0.137	0.133
SN1940A(II)	0.374	0.063	0.030	0.190	0.000
SN1941C(II)	0.429	0.283	0.196	0.177	0.202
SN1951H(II)	0.397	0.231	0.158	0.205	0.197
SN1954C(II)	0.456	0.476	0.426	0.426	0.364
SN1954J(II)	0.298	0.306	0.292	0.290	0.293
SN1959D(II)	0.579	0.426	0.409	0.407	0.423
SN1961F(II)	0.888	0.853	0.771	0.712	0.687
SN1961V(II)	0.155	0.096	0.084	0.052	0.044
SN1964H(II)	0.503	0.372	0.301	0.334	0.329
SN1967H(II)	0.655	0.503	0.513	0.418	0.410
SN1969L(II)	0.129	0.045	0.009	0.050	0.000
SN1970G(II)	0.505	0.371	0.298	0.280	0.250
SN1972Q(II)	0.416	0.350	0.280	0.264	0.224
SN1973R(II)	0.271	0.293	0.306	0.301	0.310
SN1975T(II)	0.507	0.109	0.067	0.085	0.107
SN1976F(II)	0.551	0.304	0.000	0.216	0.000
SN1978H(II)	0.454	0.687	0.655	0.659	0.646
SN1980D(II)	0.000	0.116	0.082	0.032	0.106
SN1981K(II)	0.562	0.608	0.572	0.586	0.575
SN1982F(II)	0.320	0.439	0.490	0.538	0.540
SN1984E(II)	0.154	0.158	0.165	0.147	0.140
SN1986E(II)	0.107	0.233	0.277	0.266	0.253
SN1986I(II)	0.746	0.677	0.634	0.602	0.591
SN1987K(IIb)	0.988	0.972	0.972	0.981	0.988
SN1988A(II)	0.513	0.468	0.452	0.446	0.433
SN1988E(II)	0.679	0.681	0.668	0.660	0.651
SN1991ao(II)	0.018	0.026	0.020	0.009	0.000
SN1992C(II)	0.258	0.280	0.267	0.273	0.256
SN1992az(II)	0.000	0.213	0.202	0.196	0.179
SN1993J(IIb)	0.468	0.358	0.330	0.296	0.290
SN1994ak(II)	0.000	0.228	0.264	0.264	0.245
SN1995V(II)	0.663	0.638	0.636	0.640	0.656
SN1995Z(II)	0.441	0.472	0.479	0.494	0.423
SN1996cc(II)	0.118	0.294	0.245	0.243	0.246
SN1997bs(IIn)	0.323	0.389	0.369	0.355	0.349
SN1998Y(II)	0.637	0.664	0.620	0.620	0.613
SN1998ar(II)	0.260	0.214	0.169	0.134	0.119
SN1999A(II)	0.000	0.389	0.387	0.360	0.240
SN1999bw(II)	0.015	0.218	0.216	0.219	0.162
SN1999dj(II)	0.347	0.179	0.154	0.162	0.144
SN1999ed(II)	0.549	0.404	0.344	0.307	0.305
SN1999el(IIn)	0.450	0.454	0.463	0.469	0.466
SN1999gi(II)	0.803	0.817	0.789	0.776	0.752
SN2000H(IIb)	0.267	0.238	0.237	0.238	0.226
SN2000dj(II)	0.309	0.235	0.156	0.131	0.133
SN2000eo(IIn)	0.259	0.160	0.133	0.118	0.116
SN2000ez(II)	0.676	0.623	0.523	0.525	0.527
SN2001R(II)	0.353	0.202	0.168	0.143	0.151
SN2001cm(II)	0.553	0.479	0.152	0.416	0.348
SN2001dc(II)	0.091	0.478	0.477	0.431	0.419
SN2001ez(II)	0.586	0.279	0.307	0.398	0.280

Name(Type)	uJAVA	gSDSS	rSDSS	iSDSS	zSDSS	Name(Type)	uJAVA	gSDSS	rSDSS	iSDSS	zSDSS
SN2001fv(II)	0.418	0.345	0.282	0.297	0.285	SN2015am(II)	0.387	0.500	0.513	0.564	0.418
SN2002A(II)	0.368	0.621	0.514	0.584	0.541	SN2015ba(II)	0.366	0.315	0.278	0.296	0.267
SN2002bu(II)	0.000	0.149	0.130	0.200	0.219	SN2015bh(II)	0.468	0.270	0.279	0.304	0.273
SN2002kg(II)	0.553	0.557	0.495	0.494	0.449	SN2015cz(II)	0.322	0.336	0.330	0.342	0.323
SN2003G(IIn)	0.337	0.660	0.699	0.691	0.547	SN2016aa(II)	0.425	0.271	0.231	0.255	0.180
SN2003bl(II)	0.214	0.253	0.241	0.216	0.206	SN2016bam(II)	0.445	0.321	0.258	0.217	0.154
SN2003da(II)	0.000	0.328	0.415	0.438	0.349	SN2016bkv(II)	0.651	0.731	0.743	0.765	0.752
SN2003ef(II)	0.566	0.719	0.700	0.700	0.693	SN2016bkx(IIP)	0.572	0.505	0.491	0.466	0.524
SN2003gd(II)	0.736	0.276	0.261	0.249	0.209	SN2016bmd(IIb)	0.000	0.472	0.426	0.388	0.434
SN2004C(IIB)	0.700	0.609	0.589	0.547	0.532	SN2016bme(II)	0.126	0.111	0.145	0.175	0.202
SN2004am(II)	0.538	0.550	0.602	0.650	0.676	SN2016brw(II)	0.545	0.452	0.452	0.444	0.510
SN2004cm(II)	0.937	0.961	0.933	0.942	0.904	SN2016ccf(II)	0.395	0.300	0.226	0.265	0.243
SN2004dd(II)	0.524	0.571	0.500	0.476	0.494	SN2016cok(II)	0.354	0.319	0.289	0.277	0.273
SN2004dg(II)	0.665	0.511	0.488	0.457	0.458	SN2016hrv(II)	0.727	0.763	0.664	0.749	0.634
SN2004dj(II)	0.370	0.428	0.388	0.387	0.359	SN2016iy(IIb)	0.394	0.313	0.289	0.306	0.304
SN2004dw(II)	0.083	0.049	0.069	0.082	0.087	SN2017ati(IIb)	0.363	0.211	0.000	0.177	0.357
SN2004hx(II)	0.000	0.270	0.000	0.000	0.000	SN2017czd(II)	0.750	0.816	0.789	0.708	0.624
SN2005B(II)	0.930	0.000	0.127	0.094	0.000	SN2017gas(IIn)	0.551	0.640	0.642	0.653	0.687
SN2005cs(II)	0.459	0.551	0.539	0.527	0.493	SN2017gpn(IIb)	0.276	0.015	0.038	0.011	0.040
SN2005db(IIn)	0.343	0.571	0.523	0.509	0.510	SN2017gt(IIIP)	0.477	0.878	0.838	0.834	0.803
SN2005ip(IIn)	0.560	0.442	0.420	0.390	0.373	SN2017hbg(II)	0.445	0.420	0.520	0.561	0.443
SN2005kj(IIn)	0.196	0.149	0.175	0.200	0.239	SN2017hkp(II)	0.074	0.091	0.090	0.103	0.082
SN2005lx(II)	0.027	0.239	0.192	0.208	0.157	SN2017hyh(IIb)	0.044	0.017	0.025	0.025	0.035
SN2005mg(II)	0.000	0.396	0.328	0.316	0.377	SN2017jbl(IIb)	0.393	0.535	0.614	0.000	0.701
SN2006G(IIB)	0.184	0.408	0.367	0.372	0.271	SN2017jfs(IIn)	0.737	0.761	0.744	0.726	0.715
SN2006M(II)	0.741	0.705	0.677	0.648	0.535	SN2018acj(II)	0.437	0.500	0.487	0.545	0.409
SN2006Q(II)	0.534	0.653	0.701	0.727	0.751	SN2018afm(IIn)	0.175	0.076	0.071	0.067	0.084
SN2006W(II)	0.000	0.583	0.480	0.420	0.434	SN2018aoq(II)	0.207	0.220	0.213	0.219	0.195
SN2006at(II)	0.044	0.004	0.009	0.013	0.016	SN2018ccb(II)	0.241	0.128	0.094	0.066	0.080
SN2006bo(IIn)	0.190	0.031	0.018	0.000	0.000	SN2018cyg(II)	0.587	0.687	0.364	0.530	0.512
SN2006iv(IIB)	0.645	0.367	0.337	0.305	0.263	SN2018fmf(II)	0.562	0.611	0.538	0.498	0.430
SN2006my(II)	0.881	0.910	0.911	0.934	0.954	SN2018fpb(IIb)	0.653	0.660	0.543	0.523	0.585
SN2007T(II)	0.487	0.318	0.241	0.271	0.273	SN2018fru(II)	0.663	0.949	0.934	0.883	0.895
SN2007am(II)	0.568	0.556	0.540	0.513	0.499	SN2018gj(IIb)	0.247	0.006	0.050	0.000	0.000
SN2007cm(II)	0.053	0.416	0.346	0.385	0.328	SN2018imj(II)	0.156	0.136	0.125	0.142	0.129
SN2007pk(IIn)	0.845	0.840	0.818	0.812	0.813	SN2018ivc(II)	0.496	0.581	0.580	0.578	0.578
SN2008aq(II-IIb)	0.598	0.457	0.364	0.361	0.288	SN2018lkg(II)	0.874	0.763	0.761	0.823	0.803
SN2008ax(IIB)	0.185	0.307	0.360	0.416	0.419	SN2018ow(IIb)	0.448	0.532	0.521	0.505	0.000
SN2008az(II)	0.545	0.452	0.452	0.444	0.510	SN2019bxq(IIn)	0.770	0.771	0.756	0.748	0.752
SN2008bo(IIB)	0.349	0.524	0.446	0.423	0.392	SN2019el(IIn)	0.000	0.374	0.299	0.258	0.000
SN2008ie(IIb)	0.626	0.364	0.338	0.377	0.309	SN2019fmb(IIn)	0.542	0.463	0.401	0.385	0.291
SN2008ij(II)	0.234	0.294	0.271	0.264	0.254	SN2019fy(II)	0.267	0.165	0.173	0.182	0.201
SN2008iz(II)	0.516	0.476	0.543	0.605	0.660	SN2019hyk(II)	0.445	0.214	0.160	0.173	0.125
SN2009ga(II)	0.347	0.348	0.309	0.260	0.242	SN2019ltw(IIb)	0.854	0.461	0.411	0.444	0.441
SN2009hd(II)	0.677	0.559	0.532	0.521	0.527	SN2019ovr(II)	0.629	0.565	0.474	0.487	0.501
SN2010gi(II)	0.098	0.086	0.103	0.108	0.104	SN2019upq(II)	0.000	0.139	0.129	0.321	0.664
SN2010ic(II)	0.000	0.121	0.151	0.177	0.230	SN2019xdf(II)	0.465	0.458	0.426	0.379	0.343
SN2010ie(II)	0.000	0.158	0.109	0.064	0.146	SN2020aap(II)	0.402	0.654	0.703	0.736	0.540
SN2010jl(IIn)	0.811	0.759	0.725	0.000	0.557	SN2020acac(II)	0.599	0.898	0.918	0.914	0.864
SN2011an(IIn)	0.169	0.162	0.161	0.152	0.166	SN2020dpw(II)	0.391	0.426	0.446	0.464	0.465
SN2011dh(IIB)	0.369	0.403	0.298	0.275	0.243	SN2020drl(II)	0.111	0.094	0.000	0.056	0.124
SN2011hn(II)	0.381	0.360	0.348	0.496	0.381	SN2020dvt(II)	0.489	0.487	0.571	0.597	0.000
SN2011hy(II)	0.288	0.212	0.220	0.221	0.000	SN2020fqv(IIb)	0.794	0.810	0.795	0.779	0.767
SN2012cd(IIB)	0.000	0.114	0.047	0.154	0.144	SN2020lkb(II)	0.144	0.173	0.126	0.130	0.048
SN2012eg(II)	0.000	0.152	0.131	0.128	0.139	SN2020noe(II)	0.521	0.970	0.938	0.850	0.363
SN2013am(II)	0.342	0.397	0.398	0.413	0.414	SN2020rue(II)	0.197	0.136	0.134	0.173	0.000
SN2013bu(II)	0.616	0.423	0.382	0.352	0.346	SN2020tlf(II)	0.510	0.377	0.308	0.311	0.317
SN2013cc(II)	0.557	0.479	0.388	0.343	0.311	SN2020xqj(II)	0.707	0.861	0.847	0.817	0.846
SN2013ej(II)	0.473	0.345	0.281	0.272	0.212	SN2021afkk(II)	0.762	0.930	0.930	0.924	0.917
SN2013fs(II)	0.628	0.245	0.170	0.239	0.193	SN2021ass(II)	0.674	0.528	0.477	0.423	0.418
SN2013ha(IIn)	0.552	0.664	0.719	0.760	0.772	SN2021bbm(II)	0.399	0.571	0.592	0.577	0.583
SN2014F(II)	0.558	0.165	0.244	0.205	0.201	SN2021eay(II)	0.482	0.652	0.688	0.000	0.726
SN2014bc(II)	0.936	0.871	0.880	0.899	0.902	SN2021qvr(II)	0.362	0.464	0.467	0.454	0.425
SN2014cn(II)	0.229	0.483	0.382	0.330	0.366	SN2021yok(II)	0.489	0.464	0.461	0.437	0.403
SN2014cv(IIP)	0.616	0.648	0.655	0.690	0.697	SN2022acfz(II)	0.812	0.884	0.895	0.915	0.921
SN2015P(II)	0.190	0.172	0.140	0.171	0.110	SN2022mji(II)	0.522	0.842	0.842	0.834	0.830
SN2015V(II)	0.547	0.507	0.525	0.542	0.531	SN2022ngb(IIn)	0.430	0.330	0.354	0.365	0.378
SN2015X(II)	0.327	0.233	0.218	0.183	0.170	SN2022prv(II)	0.729	0.307	0.289	0.278	0.263

Name(Type)	uJAVA	gSDSS	rSDSS	iSDSS	zSDSS	Name(Type)	uJAVA	gSDSS	rSDSS	iSDSS	zSDSS
SN2022sje(II)	0.292	0.074	0.063	0.055	0.061	SN2010jv(Ia)	0.520	0.617	0.613	0.614	0.618
SN2022zkd(II)	0.264	0.000	0.000	0.401	0.000	SN2011aa(Iapec)	0.000	0.251	0.156	0.274	0.337
SN2023jo(II)n	0.896	0.954	0.953	0.958	0.950	SN2011fe(Ia)	0.120	0.000	0.000	0.000	0.000
iPTF13dkz(II)	0.000	0.809	0.806	0.786	0.724	SN2011gb(Ia)	0.872	0.560	0.562	0.461	0.674
ASASSN-15mc(Ia)	0.721	0.750	0.717	0.711	0.700	SN2011hd(Ia)	0.022	0.255	0.034	0.207	0.231
ASASSN-15ti(Ia)	0.000	0.110	0.027	0.122	0.000	SN2011hr(Ia-91T)	0.695	0.319	0.305	0.377	0.359
SN1921C(I)	0.680	0.097	0.056	0.043	0.179	SN2013fb(Ia)	0.406	0.102	0.071	0.187	0.180
SN1938A(I)	0.187	0.000	0.033	0.063	0.075	SN2013hg(Ia)	0.166	0.152	0.095	0.106	0.060
SN1945A(I)	0.409	0.655	0.615	0.584	0.558	SN2014J(Ia)	0.442	0.422	0.478	0.507	0.508
SN1957A(Ia)	0.148	0.144	0.147	0.150	0.110	SN2014da(Ia-91bg)	0.755	0.794	0.767	0.777	0.777
SN1957B(Ia)	0.359	0.402	0.393	0.392	0.383	SN2015ab(Ia)	0.294	0.490	0.470	0.000	0.000
SN1961H(Ia)	0.862	0.806	0.795	0.790	0.786	SN2016F(Ia)	0.096	0.060	0.054	0.054	0.070
SN1963K(Ia)	0.158	0.212	0.255	0.294	0.291	SN2016cvn(Ia)	0.000	0.000	0.000	0.000	0.000
SN1966G(I)	0.459	0.315	0.263	0.281	0.271	SN2016iuh(Ia)	0.041	0.484	0.454	0.434	0.442
SN1966J(Ia)	0.201	0.116	0.070	0.073	0.043	SN2017fgc(Ia)	0.643	0.645	0.318	0.532	0.157
SN1970L(I)	0.000	0.105	0.062	0.094	0.161	SN2017glq(Ia)	0.814	0.908	0.863	0.746	0.685
SN1971I(Ia)	0.203	0.053	0.070	0.044	0.052	SN2017gxq(Ia)	0.505	0.671	0.663	0.694	0.688
SN1975G(Ia)	0.316	0.069	0.049	0.062	0.000	SN2017haf(Ia)	0.443	0.214	0.207	0.161	0.183
SN1976G(Ia)	0.068	0.128	0.101	0.105	0.101	SN2017hjy(Ia)	0.613	0.438	0.331	0.295	0.269
SN1981B(Ia)	0.167	0.190	0.180	0.183	0.137	SN2017igf(Ia)	0.462	0.583	0.603	0.622	0.574
SN1982C(Ia)	0.348	0.092	0.228	0.065	0.111	SN2017iji(Ia)	0.820	0.819	0.824	0.821	0.827
SN1982V(I)	0.355	0.592	0.587	0.597	0.461	SN2017jav(Ia)	0.146	0.094	0.101	0.123	0.148
SN1982W(Ia)	0.363	0.259	0.281	0.250	0.208	SN2017lf(Ia)	0.286	0.228	0.270	0.296	0.319
SN1986A(Ia)	0.648	0.627	0.603	0.585	0.563	SN2018bi(Ia)	0.000	0.619	0.631	0.559	0.475
SN1989A(Ia)	0.406	0.259	0.252	0.213	0.214	SN2018kp(Ia)	0.372	0.356	0.303	0.276	0.236
SN1989B(Ia)	0.737	0.636	0.605	0.594	0.597	SN2019arb(Ia)	0.688	0.553	0.523	0.503	0.510
SN1989M(Ia)	0.723	0.592	0.560	0.538	0.533	SN2019cth(Ia)	0.867	0.884	0.830	0.773	0.651
SN1989P(Ia)	0.079	0.027	0.022	0.031	0.024	SN2019gsc(Ia)	0.657	0.762	0.770	0.845	0.787
SN1990L(Ia)	0.000	0.121	0.000	0.000	0.147	SN2019tdf(Ia)	0.451	0.511	0.461	0.432	0.389
SN1991F(Ia)	0.523	0.348	0.350	0.369	0.363	SN2020akf(Ia)	0.440	0.602	0.635	0.587	0.532
SN1991T(Ia)	0.291	0.279	0.257	0.263	0.214	SN2020fcw(Ia)	0.474	0.628	0.665	0.714	0.747
SN1991bg(Ia)	0.257	0.363	0.361	0.353	0.353	SN2020hni(Ia)	0.479	0.626	0.690	0.682	0.665
SN1991bi(Ia)	0.496	0.657	0.619	0.612	0.600	SN2020jhf(Ia)	0.835	0.844	0.784	0.708	0.709
SN1995al(Ia)	0.328	0.362	0.365	0.376	0.379	SN2020scc(Ia)	0.219	0.070	0.085	0.121	0.190
SN1997bm(Ia)	0.504	0.280	0.274	0.233	0.149	SN2021aaan(Ia)	0.578	0.743	0.689	0.661	0.660
SN1997dp(Ia)	0.609	0.265	0.226	0.161	0.225	SN2021afs(Ia)	0.174	0.176	0.189	0.204	0.220
SN1998dk(Ia)	0.321	0.382	0.325	0.311	0.402	SN2021gmg(Ia)	0.577	0.609	0.570	0.578	0.597
SN1998eb(Ia)	0.344	0.381	0.387	0.398	0.395	SN2021jag(Ia)	0.645	0.711	0.668	0.645	0.635
SN1998es(Iapec)	0.374	0.425	0.399	0.443	0.426	SN2021wcu(Ia)	0.711	0.777	0.586	0.525	0.384
SN1999by(Ia)	0.286	0.185	0.183	0.178	0.153	SN2022aaq(Ia)	0.480	0.581	0.569	0.567	0.567
SN1999da(Ia)	0.104	0.084	0.063	0.071	0.040	SN2022hkc(Ia)	0.275	0.230	0.219	0.217	0.247
SN1999ej(Ia)	0.258	0.147	0.168	0.185	0.150	SN2022mjk(Ia)	0.000	0.000	0.014	0.300	0.000
SN1999gr(Ia)	0.000	0.375	0.000	0.000	0.582	iPTF13akc(Ia)	0.637	0.645	0.496	0.505	0.548
SN2000E(Ia)	0.382	0.307	0.324	0.326	0.325	iPTF13ebh(Ia)	0.289	0.315	0.372	0.364	0.374
SN2000fd(Ia)	0.000	0.128	0.073	0.021	0.116	AT2014ge(Ib)	0.532	0.399	0.371	0.366	0.372
SN2001ed(Ia)	0.859	0.795	0.746	0.706	0.681	CSS14(Ib)	0.636	0.384	0.353	0.312	0.225
SN2002cs(Ia)	0.241	0.280	0.294	0.321	0.282	PTF09dfk(Ib)	0.684	0.724	0.735	0.737	0.737
SN2002dl(Ia)	0.343	0.199	0.121	0.111	0.115	PTF12gzk(Ic)	0.625	0.687	0.652	0.623	0.784
SN2002dp(Ia)	0.253	0.076	0.074	0.073	0.063	SN1954A(Ib)	0.137	0.117	0.041	0.213	0.093
SN2002fb(Ia)	0.179	0.271	0.316	0.335	0.320	SN1962L(Ic)	0.432	0.231	0.267	0.282	0.128
SN2002jg(Ia)	0.393	0.363	0.312	0.306	0.311	SN1972R(Ib)	0.193	0.077	0.092	0.099	0.082
SN2003cg(Ia)	0.305	0.439	0.499	0.520	0.553	SN1976B(Ib)	0.698	0.562	0.487	0.468	0.436
SN2003gt(Ia)	0.517	0.454	0.424	0.389	0.366	SN1984L(Ib)	0.828	0.621	0.528	0.514	0.409
SN2003hm(Ia)	0.613	0.788	0.767	0.744	0.726	SN1985F(Ib)	0.982	0.987	0.990	0.986	0.985
SN2005ai(Ia)	0.243	0.000	0.058	0.148	0.040	SN1988ac(Ibc)	0.822	0.751	0.659	0.625	0.634
SN2005bo(Ia)	0.484	0.522	0.489	0.487	0.454	SN1990B(Ic)	0.818	0.865	0.866	0.857	0.842
SN2005cx(Ia)	0.123	0.112	0.170	0.203	0.189	SN1991ar(Ib)	0.176	0.506	0.538	0.622	0.438
SN2005dv(Ia)	0.557	0.608	0.504	0.537	0.543	SN1994I(Ic)	0.937	0.913	0.887	0.873	0.861
SN2005ev(Ia)	0.276	0.133	0.165	0.215	0.233	SN1997dc(Ib)	0.140	0.163	0.180	0.176	0.162
SN2006D(Ia)	0.163	0.168	0.193	0.178	0.177	SN1997dq(Ic)	0.300	0.285	0.253	0.229	0.209
SN2006td(Ia)	0.324	0.716	0.753	0.748	0.739	SN1997ef(Ic)	0.761	0.646	0.637	0.553	0.480
SN2007J(Ia)	0.341	0.257	0.205	0.220	0.273	SN1998cc(Ib)	0.462	0.250	0.220	0.204	0.191
SN2007ap(Ia)	0.213	0.060	0.041	0.035	0.060	SN1998ey(Ic)	0.187	0.143	0.176	0.178	0.191
SN2007sa(Ia)	0.846	0.491	0.419	0.383	0.369	SN1999dn(Ib)	0.686	0.633	0.580	0.576	0.574
SN2009hr(Ia)	0.523	0.736	0.000	0.378	0.523	SN1999eh(Ib)	0.563	0.330	0.308	0.329	0.253
SN2009ig(Ia)	0.405	0.477	0.475	0.425	0.362	SN2000C(Ic)	0.648	0.593	0.570	0.547	0.549
SN2009nq(Ia)	0.000	0.067	0.032	0.053	0.091	SN2000dv(Ib)	0.624	0.627	0.620	0.605	0.624
SN2010eb(Ia)	0.320	0.064	0.043	0.042	0.055	SN2000ew(Ib)	0.802	0.749	0.718	0.680	0.675

Name(Type)	uJAVA	gSDSS	rSDSS	iSDSS	zSDSS	Name(Type)	uJAVA	gSDSS	rSDSS	iSDSS	zSDSS
SN2000fn(Ib)	0.524	0.374	0.363	0.361	0.306	SN2016G(Ic)	0.406	0.294	0.306	0.312	0.293
SN2001B(Ib)	0.520	0.414	0.415	0.427	0.000	SN2016P(Ic)	0.842	0.737	0.663	0.531	0.481
SN2001ef(Ic)	0.448	0.568	0.585	0.594	0.614	SN2016coi(Ic)	0.564	0.447	0.322	0.312	0.384
SN2001ej(Ib)	0.371	0.540	0.571	0.587	0.594	SN2017ewx(Ib)	0.617	0.533	0.000	0.438	0.410
SN2001is(Ib)	0.402	0.351	0.313	0.300	0.300	SN2017hcb(Ib)	0.827	0.642	0.606	0.602	0.611
SN2002ap(Ic)	0.000	0.123	0.162	0.051	0.098	SN2018cow(Ic)	0.392	0.406	0.338	0.376	0.361
SN2002cw(Ib)	0.275	0.211	0.138	0.159	0.211	SN2018dbg(Ibc)	0.951	0.941	0.930	0.928	0.934
SN2002ho(Ic)	0.471	0.492	0.516	0.496	0.492	SN2018ebt(Ic)	0.338	0.150	0.105	0.102	0.095
SN2002ji(Ib)	0.294	0.240	0.230	0.000	0.207	SN2018gwo(Ic)	0.152	0.052	0.026	0.071	0.059
SN2002jz(Ib)	0.231	0.184	0.195	0.210	0.203	SN2018hdp(Ic)	0.550	0.589	0.594	0.581	0.578
SN2003aa(Ic)	0.404	0.298	0.309	0.300	0.268	SN2019ccm(Ib)	0.352	0.516	0.572	0.588	0.000
SN2003gk(Ib)	0.662	0.659	0.681	0.000	0.000	SN2019clq(Ib)	0.838	0.787	0.887	0.856	0.911
SN2004ao(Ib)	0.197	0.120	0.096	0.086	0.087	SN2020hvp(Ib)	0.631	0.708	0.736	0.748	0.761
SN2004cc(Ib)	0.884	0.914	0.899	0.885	0.871	SN2021mxx(Ic)	0.536	0.757	0.759	0.779	0.759
SN2004dk(Ib)	0.545	0.443	0.388	0.336	0.296	SN2022bdu(Ic)	0.620	0.541	0.528	0.529	0.564
SN2004ge(Ic)	0.423	0.493	0.526	0.554	0.585	SN2022oqm(Ic)	0.000	0.110	0.040	0.058	0.044
SN2004gk(Ic)	0.573	0.798	0.778	0.792	0.799	iPTF13bvn(Ib)	0.707	0.608	0.555	0.524	0.520
SN2004gn(Ib)	0.648	0.594	0.575	0.554	0.523	SN2023ixf(II)	0.296	0.191	0.146	0.178	0.171
SN2005aj(Ic)	0.066	0.063	0.073	0.089	0.116						
SN2005da(Ic)	0.000	0.015	0.038	0.016	0.035						
SN2005ek(Ic)	0.000	0.000	0.000	0.000	0.005						
SN2005kf(Ic)	0.475	0.599	0.595	0.610	0.643						
SN2006F(Ib)	0.320	0.163	0.125	0.000	0.000						
SN2006dg(Ic)	0.185	0.113	0.108	0.113	0.120						
SN2006eg(Ib-c)	0.530	0.642	0.643	0.648	0.646						
SN2006ei(Ic)	0.510	0.394	0.363	0.310	0.386						
SN2006ep(Ib)	0.290	0.133	0.082	0.070	0.148						
SN2006jc(Ibn)	0.000	0.104	0.142	0.201	0.073						
SN2006ld(Ib)	0.000	0.714	0.564	0.506	0.521						
SN2006lt(Ib)	0.201	0.168	0.229	0.357	0.231						
SN2006lv(Ib-c)	0.547	0.624	0.549	0.527	0.354						
SN2007C(Ib)	0.357	0.390	0.401	0.404	0.420						
SN2007fo(Ib)	0.683	0.618	0.580	0.567	0.564						
SN2007gr(Ic)	0.557	0.509	0.533	0.507	0.502						
SN2007iq(Ic)	0.170	0.249	0.199	0.182	0.117						
SN2007ru(Ic)	0.072	0.033	0.038	0.048	0.052						
SN2007rz(Ic)	0.711	0.689	0.662	0.629	0.610						
SN2007uy(Ib)	0.650	0.617	0.578	0.560	0.501						
SN2008D(Ib)	0.413	0.359	0.344	0.315	0.286						
SN2008ao(Ic)	0.147	0.074	0.071	0.074	0.000						
SN2008du(Ic)	0.536	0.512	0.000	0.496	0.483						
SN2008dv(Ic)	0.454	0.409	0.475	0.496	0.537						
SN2008eb(Ic)	0.451	0.459	0.452	0.450	0.459						
SN2008im(Ib)	0.394	0.152	0.130	0.157	0.127						
SN2009iz(Ib)	0.193	0.069	0.000	0.000	0.000						
SN2009lj(Ic)	0.073	0.107	0.094	0.093	0.063						
SN2009lw(Ib-IIb)	0.325	0.221	0.213	0.199	0.203						
SN2010X(Ic)	0.277	0.139	0.168	0.254	0.000						
SN2010do(Ic)	0.472	0.369	0.326	0.294	0.293						
SN2010gk(Ic)	0.793	0.830	0.775	0.741	0.696						
SN2010gr(Ib-c)	0.000	0.261	0.256	0.259	0.188						
SN2011it(Ic)	0.000	0.212	0.140	0.240	0.201						
SN2011jf(IbPec)	0.230	0.160	0.228	0.249	0.239						
SN2011jm(Ic)	0.968	0.935	0.895	0.795	0.735						
SN2012C(Ic)	0.657	0.571	0.552	0.560	0.578						
SN2012P(Ib-c)	0.770	0.565	0.543	0.489	0.480						
SN2012au(Ib)	0.804	0.755	0.717	0.714	0.730						
SN2012cw(Ic)	0.233	0.210	0.229	0.212	0.200						
SN2012ej(Ic)	0.370	0.348	0.324	0.313	0.286						
SN2014C(Ib)	0.701	0.566	0.570	0.578	0.601						
SN2014L(Ic)	0.755	0.714	0.715	0.701	0.705						
SN2014ad(Ic)	0.051	0.029	0.022	0.016	0.023						
SN2014ge(Ib)	0.595	0.424	0.367	0.328	0.353						
SN2015G(Ib)	0.221	0.138	0.082	0.092	0.053						
SN2015Q(Ib)	0.359	0.416	0.391	0.401	0.384						
SN2015U(Ibn)	0.334	0.447	0.522	0.559	0.587						
SN2015ah(Ib)	0.568	0.630	0.614	0.000	0.000						
SN2015ap(Ib-c)	0.665	0.927	0.825	0.764	0.641						

Table A.3: NCR values for all the sample with the narrow-band filters.

Name(Type)	J0378	J0395	J0410	J0430	J0515	J0660	J0861	Name(Type)	J0378	J0395	J0410	J0430	J0515	J0660	J0861
ASASSN-14kg(II)	0.691	0.666	0.589	0.689	0.749	0.740	0.738	SN2005B(II)	0.000	0.452	0.452	0.000	0.255	0.000	0.146
ASASSN-15lf(II)	0.120	0.262	0.044	0.122	0.110	0.097	0.081	SN2005cs(II)	0.470	0.544	0.537	0.596	0.577	0.530	0.521
ASASSN-15tw(II)	0.000	0.565	0.428	0.534	0.355	0.289	0.200	SN2005db(IIn)	0.519	0.398	0.523	0.513	0.582	0.567	0.523
ASASSN-16eu(II)	0.664	0.405	0.280	0.326	0.346	0.289	0.271	SN2005ip(IIn)	0.543	0.478	0.523	0.482	0.466	0.523	0.379
ASASSN14az(IIb)	0.000	0.184	0.316	0.157	0.131	0.162	0.120	SN2006Q(II)	0.562	0.546	0.552	0.609	0.666	0.714	0.744
ASASSN15bd(IIb)	0.821	0.773	0.732	0.736	0.707	0.623	0.551	SN2006W(II)	0.220	0.391	0.078	0.036	0.323	0.512	0.502
AT2020drl(II)	0.154	0.421	0.000	0.000	0.024	0.082	0.167	SN2006at(II)	0.002	0.035	0.015	0.000	0.006	0.010	0.019
PS15cwt(IIn)	0.270	0.277	0.391	0.331	0.317	0.263	0.307	SN2006bo(IIn)	0.070	0.116	0.000	0.106	0.036	0.039	0.000
SDSS-IIENS14215(II)	0.433	0.583	0.454	0.435	0.423	0.413	0.359	SN2006iv(IIb)	0.386	0.473	0.269	0.331	0.438	0.403	0.289
SN1909A(II)	0.000	0.347	0.057	0.326	0.198	0.000	0.000	SN2006my(II)	0.765	0.777	0.899	0.926	0.903	0.891	0.948
SN1921B(II)	0.000	0.240	0.252	0.170	0.252	0.050	0.081	SN2007T(II)	0.471	0.585	0.297	0.346	0.339	0.319	0.268
SN1937F(II)	0.290	0.250	0.299	0.325	0.423	0.164	0.125	SN2007am(II)	0.668	0.642	0.602	0.608	0.532	0.606	0.481
SN1940A(II)	0.057	0.000	0.335	0.000	0.000	0.157	0.109	SN2007cm(II)	0.344	0.000	0.174	0.308	0.432	0.330	0.319
SN1941C(II)	0.010	0.183	0.405	0.000	0.154	0.257	0.353	SN2007pk(IIn)	0.836	0.838	0.872	0.853	0.837	0.823	0.808
SN1951H(II)	0.358	0.380	0.382	0.468	0.155	0.197	0.069	SN2008aq(IIb)	0.000	0.570	0.605	0.595	0.576	0.583	0.238
SN1954C(II)	0.398	0.441	0.550	0.428	0.458	0.391	0.424	SN2008ax(IIb)	0.233	0.241	0.307	0.303	0.332	0.295	0.429
SN1954J(II)	0.377	0.362	0.265	0.291	0.265	0.241	0.280	SN2008az(II)	0.582	0.469	0.542	0.523	0.447	0.457	0.483
SN1959D(II)	0.391	0.548	0.299	0.494	0.356	0.445	0.410	SN2008bo(IIb)	0.497	0.570	0.560	0.525	0.484	0.409	0.401
SN1961F(II)	0.878	0.875	0.885	0.818	0.852	0.830	0.691	SN2008ie(IIb)	0.497	0.361	0.204	0.303	0.337	0.339	0.325
SN1961V(II)	0.204	0.055	0.077	0.127	0.082	0.129	0.047	SN2008ij(II)	0.363	0.438	0.319	0.368	0.293	0.325	0.283
SN1964H(II)	0.357	0.351	0.447	0.262	0.328	0.214	0.298	SN2008iz(II)	0.533	0.536	0.467	0.469	0.468	0.592	0.624
SN1967H(II)	0.671	0.607	0.536	0.550	0.500	0.689	0.402	SN2009ga(II)	0.314	0.319	0.337	0.318	0.330	0.329	0.254
SN1969L(II)	0.001	0.000	0.009	0.118	0.078	0.051	0.000	SN2009hd(II)	0.672	0.663	0.591	0.587	0.539	0.562	0.518
SN1970G(II)	0.517	0.412	0.477	0.571	0.237	0.420	0.144	SN2010gi(II)	0.079	0.068	0.077	0.070	0.077	0.100	0.109
SN1972Q(II)	0.411	0.440	0.397	0.383	0.325	0.258	0.239	SN2010ic(II)	0.342	0.000	0.000	0.292	0.247	0.183	0.260
SN1973R(II)	0.282	0.299	0.295	0.297	0.294	0.334	0.295	SN2010ie(II)	0.394	0.010	0.014	0.015	0.125	0.108	0.136
SN1975T(II)	0.613	0.000	0.359	0.204	0.152	0.116	0.144	SN2010jl(IIn)	0.798	0.791	0.000	0.805	0.730	0.000	0.584
SN1976F(II)	0.657	0.463	0.000	0.000	0.212	0.226	0.000	SN2011an(IIn)	0.190	0.193	0.169	0.153	0.160	0.154	0.135
SN1978H(II)	0.381	0.656	0.553	0.584	0.617	0.664	0.616	SN2011dh(IIb)	0.449	0.456	0.377	0.434	0.377	0.248	0.231
SN1980D(II)	0.269	0.184	0.057	0.118	0.128	0.172	0.168	SN2011hn(II)	0.406	0.461	0.641	0.000	0.465	0.434	0.342
SN1981K(II)	0.618	0.570	0.674	0.658	0.623	0.596	0.569	SN2011hy(II)	0.248	0.363	0.227	0.292	0.251	0.257	0.268
SN1982F(II)	0.392	0.376	0.456	0.437	0.482	0.422	0.564	SN2012cd(IIb)	0.000	0.193	0.050	0.241	0.000	0.160	0.230
SN1984E(II)	0.209	0.169	0.117	0.116	0.109	0.176	0.118	SN2012eg(II)	0.381	0.151	0.170	0.174	0.076	0.143	0.113
SN1986E(II)	0.163	0.319	0.197	0.148	0.243	0.277	0.250	SN2013am(II)	0.392	0.382	0.427	0.406	0.407	0.404	0.406
SN1986l(II)	0.764	0.777	0.718	0.714	0.660	0.619	0.589	SN2013bu(II)	0.404	0.548	0.255	0.477	0.377	0.429	0.336
SN1987K(IIb)	0.982	0.980	0.980	0.979	0.970	0.968	0.986	SN2013cc(II)	0.607	0.609	0.514	0.569	0.452	0.431	0.307
SN1988A(II)	0.491	0.516	0.500	0.483	0.488	0.432	0.434	SN2013ej(II)	0.249	0.354	0.314	0.355	0.275	0.250	0.195
SN1988E(II)	0.607	0.635	0.717	0.699	0.690	0.668	0.654	SN2013fs(II)	0.430	0.000	0.345	0.196	0.204	0.238	0.312
SN1991ao(II)	0.131	0.000	0.000	0.000	0.028	0.041	0.018	SN2013ha(IIn)	0.589	0.547	0.680	0.667	0.676	0.721	0.761
SN1992C(II)	0.183	0.284	0.294	0.321	0.289	0.228	0.259	SN2014F(II)	0.810	0.279	0.317	0.173	0.246	0.217	0.294
SN1992az(II)	0.374	0.285	0.297	0.295	0.256	0.227	0.163	SN2014bc(II)	0.934	0.925	0.894	0.886	0.868	0.882	0.889
SN1993J(IIb)	0.558	0.477	0.362	0.364	0.341	0.281	0.311	SN2014cn(II)	0.367	0.501	0.443	0.451	0.411	0.401	0.316
SN1994ak(II)	0.212	0.439	0.287	0.149	0.362	0.221	0.313	SN2014cv(IP)	0.575	0.344	0.651	0.663	0.679	0.678	0.720
SN1995V(II)	0.658	0.683	0.652	0.651	0.648	0.620	0.628	SN2015P(II)	0.000	0.052	0.250	0.271	0.000	0.292	0.050
SN1995Z(II)	0.273	0.597	0.546	0.428	0.474	0.481	0.393	SN2015V(II)	0.673	0.597	0.588	0.578	0.601	0.625	0.550
SN1996cc(II)	0.407	0.457	0.393	0.331	0.320	0.304	0.248	SN2015X(II)	0.355	0.355	0.250	0.248	0.180	0.182	0.175
SN1997bs(IIn)	0.344	0.385	0.392	0.387	0.378	0.324	0.346	SN2015am(II)	0.705	0.580	0.321	0.570	0.440	0.506	0.537
SN1998Y(II)	0.659	0.703	0.685	0.691	0.648	0.542	0.611	SN2015ba(II)	0.445	0.341	0.325	0.257	0.346	0.311	0.316
SN1998ar(II)	0.323	0.233	0.286	0.205	0.201	0.196	0.119	SN2015bh(II)	0.009	0.349	0.210	0.316	0.230	0.304	0.303
SN1999A(II)	0.472	0.428	0.402	0.417	0.456	0.349	0.264	SN2015cz(II)	0.442	0.406	0.348	0.405	0.390	0.364	0.351
SN1999bw(II)	0.294	0.344	0.326	0.261	0.209	0.163	0.195	SN2016aa(II)	0.000	0.754	0.440	0.375	0.380	0.264	0.229
SN1999dj(II)	0.411	0.236	0.177	0.314	0.188	0.190	0.161	SN2016bam(II)	0.444	0.378	0.482	0.292	0.265	0.256	0.129
SN1999ed(II)	0.486	0.534	0.489	0.481	0.403	0.401	0.301	SN2016bkv(II)	0.509	0.686	0.676	0.690	0.710	0.725	0.756
SN1999el(IIn)	0.507	0.428	0.373	0.455	0.463	0.469	0.464	SN2016bkk(IP)	0.506	0.419	0.510	0.533	0.496	0.577	0.452
SN1999gi(II)	0.811	0.822	0.833	0.839	0.808	0.837	0.753	SN2016bmd(IIb)	0.000	0.605	0.461	0.287	0.438	0.505	0.350
SN2000H(IIb)	0.255	0.257	0.241	0.265	0.199	0.255	0.232	SN2016brw(II)	0.582	0.469	0.542	0.523	0.447	0.457	0.483
SN2000dj(II)	0.254	0.224	0.246	0.206	0.213	0.177	0.151	SN2016ccf(II)	0.548	0.000	0.568	0.278	0.178	0.362	0.338
SN2000eo(IIn)	0.293	0.353	0.524	0.319	0.261	0.207	0.135	SN2016cok(II)	0.365	0.342	0.341	0.323	0.306	0.305	0.268
SN2000ez(II)	0.629	0.453	0.774	0.674	0.635	0.468	0.412	SN2016hrv(II)	0.730	0.815	0.690	0.613	0.630	0.671	0.619
SN2001R(II)	0.300	0.262	0.248	0.271	0.240	0.162	0.100	SN2016hrv(II)	0.298	0.289	0.362	0.445	0.234	0.347	0.227
SN2001cm(II)	0.649	0.000	0.436	0.541	0.349	0.426	0.294	SN2017ati(IIb)	0.405	0.869	0.381	0.087	0.039	0.000	0.000
SN2001dc(II)	0.345	0.463	0.380	0.316	0.407	0.483	0.428	SN2017czd(II)	0.825	0.853	0.804	0.860	0.815	0.772	0.776
SN2001ez(II)</															

Name(Type)	J0378	J0395	J0410	J0430	J0515	J0660	J0861	Name(Type)	J0378	J0395	J0410	J0430	J0515	J0660	J0861
SN2018imj(II)	0.124	0.240	0.179	0.160	0.171	0.206	0.122	SN2003cg(Ia)	0.311	0.334	0.357	0.380	0.411	0.498	0.528
SN2018ivc(II)	0.471	0.453	0.543	0.549	0.576	0.475	0.589	SN2003gt(Ia)	0.405	0.421	0.469	0.450	0.447	0.398	0.371
SN2018kg(II)	0.822	0.748	0.781	0.796	0.799	0.789	0.852	SN2003hm(Ia)	0.636	0.631	0.797	0.770	0.796	0.761	0.731
SN2018ow(l Ib)	0.416	0.565	0.417	0.506	0.529	0.517	0.426	SN2005ai(Ia)	0.443	0.000	0.264	0.108	0.267	0.189	0.052
SN2019bxq(II n)	0.792	0.757	0.777	0.755	0.753	0.722	0.753	SN2005bo(Ia)	0.000	0.523	0.491	0.514	0.533	0.475	0.492
SN2019el(II n)	0.714	0.000	0.000	0.258	0.374	0.425	0.541	SN2005cx(Ia)	0.125	0.138	0.112	0.115	0.121	0.150	0.177
SN2019fmb(II n)	0.595	0.484	0.721	0.386	0.625	0.390	0.127	SN2005dv(Ia)	0.466	0.547	0.650	0.597	0.633	0.526	0.573
SN2019fyd(II)	0.252	0.185	0.173	0.176	0.150	0.190	0.196	SN2005ev(Ia)	0.561	0.324	0.329	0.356	0.383	0.200	0.263
SN2019hyk(II)	0.393	0.000	0.298	0.231	0.250	0.216	0.181	SN2006D(Ia)	0.000	0.069	0.220	0.144	0.165	0.144	0.207
SN2019itw(l Ib)	0.792	0.755	0.631	0.673	0.557	0.486	0.518	SN2006dd(Ia)	0.404	0.694	0.471	0.549	0.685	0.714	0.757
SN2019ovr(II)	0.578	0.629	0.670	0.577	0.501	0.514	0.575	SN2007J(Ia)	0.335	0.544	0.216	0.174	0.176	0.261	0.218
SN2019upq(II)	0.488	0.121	0.000	0.514	0.305	0.255	0.492	SN2007ap(Ia)	0.293	0.060	0.089	0.058	0.047	0.054	0.052
SN2019xdf(II)	0.462	0.422	0.442	0.475	0.439	0.400	0.373	SN2007sa(Ia)	0.522	0.495	0.570	0.509	0.412	0.450	0.428
SN2020aapr(II)	0.065	0.545	0.374	0.406	0.460	0.643	0.610	SN2009hr(Ia)	0.000	0.000	0.499	0.322	0.555	0.000	0.048
SN2020acac(II)	0.671	0.607	0.835	0.842	0.883	0.912	0.849	SN2009ig(Ia)	0.300	0.229	0.322	0.355	0.358	0.417	0.400
SN2020dpw(II)	0.457	0.299	0.435	0.316	0.447	0.456	0.462	SN2009qn(Ia)	0.107	0.170	0.031	0.017	0.081	0.064	0.000
SN2020drl(II)	0.043	0.121	0.000	0.000	0.038	0.113	0.213	SN2010eb(Ia)	0.175	0.287	0.132	0.215	0.109	0.020	0.192
SN2020dvt(II)	0.694	0.395	0.285	0.597	0.500	0.472	0.760	SN2010jv(Ia)	0.609	0.645	0.629	0.630	0.612	0.607	0.609
SN2020fqv(l Ib)	0.777	0.789	0.804	0.808	0.814	0.768	0.770	SN2011aa(Iapec)	0.276	0.524	0.000	0.216	0.478	0.219	0.329
SN2020kb(II)	0.377	0.133	0.214	0.304	0.213	0.174	0.107	SN2011fe(Ia)	0.000	0.347	0.057	0.326	0.198	0.000	0.000
SN2020noc(II)	0.844	0.719	0.902	0.813	0.968	0.969	0.439	SN2011gb(Ia)	0.809	0.986	0.488	0.372	0.339	0.589	0.396
SN2020rue(II)	0.339	0.197	0.160	0.160	0.199	0.058	0.154	SN2011hd(Ia)	0.000	0.215	0.328	0.000	0.422	0.239	0.371
SN2020tlf(II)	0.517	0.513	0.459	0.440	0.351	0.354	0.354	SN2011lh(la-91T)	0.586	0.028	0.466	0.000	0.289	0.355	0.377
SN2020xqj(II)	0.698	0.606	0.730	0.701	0.823	0.894	0.853	SN2013fb(Ia)	0.616	0.000	0.075	0.365	0.182	0.196	0.190
SN2021afkk(II)	0.727	0.639	0.861	0.840	0.916	0.926	0.923	SN2013hg(Ia)	0.295	0.000	0.445	0.316	0.000	0.036	0.224
SN2021ass(II)	0.378	0.429	0.442	0.560	0.552	0.518	0.453	SN2014J(Ia)	0.444	0.485	0.415	0.406	0.419	0.454	0.504
SN2021bbm(II)	0.488	0.483	0.406	0.696	0.611	0.578	0.566	SN2014da(Ia-91bg)	0.808	0.881	0.702	0.862	0.821	0.766	0.781
SN2021eay(II)	0.647	0.628	0.601	0.635	0.655	0.707	0.719	SN2015ab(Ia)	0.418	0.318	0.480	0.431	0.501	0.464	0.000
SN2021lqr(II)	0.384	0.479	0.452	0.458	0.465	0.503	0.422	SN2016F(Ia)	0.000	0.216	0.105	0.076	0.107	0.053	0.033
SN2021yok(II)	0.431	0.552	0.464	0.397	0.449	0.510	0.438	SN2016cvn(Ia)	0.000	0.000	0.000	0.000	0.000	0.000	0.000
SN2022acfz(II)	0.883	0.844	0.864	0.895	0.895	0.910	0.928	SN2016iuh(Ia)	0.509	0.296	0.471	0.473	0.527	0.469	0.483
SN2022mji(II)	0.798	0.750	0.772	0.840	0.789	0.779	0.842	SN2017fcg(Ia)	0.000	0.798	0.743	0.284	0.685	0.649	0.474
SN2022ngb(l Ib)	0.471	0.357	0.347	0.371	0.366	0.416	0.373	SN2017gl(Ia)	0.926	0.853	0.874	0.827	0.882	0.868	0.654
SN2022prv(II)	0.342	0.542	0.370	0.382	0.337	0.281	0.285	SN2017gxq(Ia)	0.561	0.681	0.583	0.694	0.686	0.675	0.676
SN2022sjc(II)	0.345	0.187	0.131	0.091	0.065	0.066	0.046	SN2017hal(Ia)	0.000	0.158	0.193	0.232	0.221	0.254	0.203
SN2022zkd(II)	0.000	0.000	0.000	0.000	0.000	0.206	0.010	SN2017hij(Ia)	0.361	0.444	0.397	0.329	0.321	0.362	0.244
SN2023jo(II n)	0.935	0.935	0.948	0.955	0.961	0.936	0.956	SN2017igf(Ia)	0.137	0.422	0.489	0.463	0.453	0.588	0.550
iPTF13dkz(II)	0.634	0.471	0.564	0.611	0.823	0.815	0.653	SN2017iji(Ia)	0.838	0.834	0.824	0.821	0.820	0.818	0.823
ASASSN-15mc(Ia)	0.698	0.667	0.733	0.763	0.732	0.733	0.708	SN2017jav(Ia)	0.071	0.123	0.067	0.083	0.104	0.108	0.131
ASASSN-15ti(Ia)	0.350	0.354	0.066	0.002	0.000	0.019	0.000	SN2017if(Ia)	0.271	0.276	0.239	0.278	0.258	0.324	0.299
SN1921C(I)	0.000	0.240	0.252	0.170	0.252	0.050	0.081	SN2018bi(Ia)	0.316	0.480	0.436	0.552	0.699	0.641	0.470
SN1938A(I)	0.000	0.097	0.055	0.044	0.091	0.002	0.096	SN2018kp(Ia)	0.471	0.457	0.414	0.425	0.365	0.320	0.265
SN1945A(I)	0.511	0.403	0.624	0.662	0.649	0.601	0.567	SN2019arb(Ia)	0.573	0.409	0.606	0.564	0.585	0.525	0.555
SN1957A(Ia)	0.223	0.196	0.171	0.109	0.146	0.138	0.112	SN2019cth(Ia)	0.873	0.898	0.908	0.863	0.860	0.834	0.768
SN1957B(Ia)	0.341	0.282	0.371	0.405	0.407	0.389	0.377	SN2019gsc(Ia)	0.692	0.671	0.695	0.793	0.738	0.804	0.720
SN1961H(Ia)	0.849	0.847	0.836	0.826	0.811	0.771	0.744	SN2019tdf(Ia)	0.514	0.501	0.485	0.458	0.447	0.461	0.434
SN1963K(Ia)	0.401	0.278	0.180	0.145	0.205	0.243	0.240	SN2020akf(Ia)	0.490	0.524	0.423	0.545	0.497	0.542	0.491
SN1966G(I)	0.000	0.254	0.260	0.262	0.398	0.242	0.351	SN2020fcw(Ia)	0.509	0.511	0.579	0.604	0.655	0.688	0.741
SN1966J(Ia)	0.000	0.193	0.156	0.153	0.182	0.135	0.185	SN2020hni(Ia)	0.493	0.679	0.591	0.543	0.666	0.608	0.683
SN1970L(I)	0.583	0.118	0.000	0.206	0.000	0.004	0.000	SN2020jhf(Ia)	0.801	0.635	0.845	0.885	0.865	0.815	0.792
SN1971I(Ia)	0.164	0.091	0.033	0.073	0.074	0.044	0.035	SN2020scc(Ia)	0.269	0.000	0.343	0.220	0.161	0.120	0.068
SN1975G(Ia)	0.000	0.000	0.000	0.000	0.186	0.077	0.051	SN2021aaa(Ia)	0.720	0.646	0.717	0.781	0.756	0.683	0.677
SN1976G(Ia)	0.358	0.257	0.042	0.160	0.099	0.104	0.121	SN2021afsj(Ia)	0.172	0.171	0.189	0.185	0.160	0.192	0.219
SN1981B(Ia)	0.173	0.319	0.243	0.231	0.188	0.185	0.166	SN2021gmg(Ia)	0.667	0.691	0.600	0.638	0.588	0.562	0.562
SN1982C(Ia)	0.000	0.857	0.294	0.200	0.004	0.070	0.252	SN2021lja(Ia)	0.702	0.756	0.677	0.728	0.685	0.670	0.644
SN1982V(I)	0.405	0.251	0.460	0.640	0.499	0.622	0.425	SN2021wcu(Ia)	0.429	0.442	0.696	0.536	0.725	0.581	0.449
SN1982W(Ia)	0.306	0.271	0.124	0.483	0.091	0.228	0.235	SN2022aaq(Ia)	0.570	0.499	0.584	0.586	0.582	0.566	0.562
SN1986A(Ia)	0.608	0.721	0.679	0.659	0.611	0.589	0.545	SN2022hkc(Ia)	0.228	0.219	0.209	0.232	0.236	0.247	0.242
SN1989A(Ia)	0.469	0.941	0.239	0.265	0.309	0.219	0.150	SN2022mjk(Ia)	0.000	0.000	0.000	0.000	0.000	0.089	0.373
SN1989B(Ia)	0.737	0.735	0.679	0.669	0.615	0.614	0.587	iPTF13akk(Ia)	0.699	0.688	0.599	0.617	0.568	0.533	0.545
SN1989M(Ia)	0.703	0.732	0.656	0.639	0.593	0.577	0.531	iPTF13ebh(Ia)	0.000	0.484	0.349	0.367	0.268	0.339	0.327
SN1989P(Ia)	0.121	0.093	0.053	0.039	0.031	0.027	0.042	AT2014ge(Ib)	0.454	0.481	0.488	0.366	0.355	0.529	0.481
SN1990L(Ia)	0.000</														

Name(Type)	J0378	J0395	J0410	J0430	J0515	J0660	J0861	Name(Type)	J0378	J0395	J0410	J0430	J0515	J0660	J0861
SN2000fn(Ib)	0.471	0.329	0.436	0.504	0.445	0.422	0.314	SN2023ixf(II)	0.320	0.298	0.255	0.405	0.136	0.231	0.088
SN2001B(Ib)	0.507	0.512	0.501	0.466	0.418	0.000	0.446								
SN2001ef(Ic)	0.512	0.556	0.565	0.595	0.573	0.635	0.597								
SN2001ej(Ib)	0.429	0.470	0.459	0.505	0.567	0.495	0.578								
SN2001is(Ib)	0.377	0.368	0.396	0.407	0.336	0.391	0.285								
SN2002ap(Ic)	0.358	0.000	0.222	0.257	0.273	0.139	0.177								
SN2002cw(Ib)	0.548	0.373	0.438	0.243	0.318	0.151	0.139								
SN2002ho(Ic)	0.428	0.373	0.494	0.454	0.450	0.512	0.485								
SN2002ji(Ib)	0.258	0.262	0.297	0.254	0.262	0.241	0.200								
SN2002jz(Ib)	0.366	0.275	0.248	0.215	0.204	0.217	0.191								
SN2003aa(Ic)	0.376	0.361	0.353	0.367	0.325	0.344	0.249								
SN2003gk(Ib)	0.741	0.657	0.000	0.650	0.689	0.789	0.618								
SN2004ao(Ib)	0.186	0.215	0.128	0.109	0.073	0.091	0.067								
SN2004cc(Ib)	0.874	0.878	0.913	0.902	0.917	0.904	0.872								
SN2004dk(Ib)	0.617	0.552	0.579	0.508	0.420	0.517	0.320								
SN2004ge(Ic)	0.452	0.450	0.471	0.510	0.510	0.557	0.564								
SN2004gk(Ic)	0.753	0.670	0.815	0.793	0.767	0.775	0.799								
SN2004gn(Ib)	0.661	0.726	0.674	0.688	0.626	0.603	0.522								
SN2005aj(Ic)	0.084	0.072	0.052	0.059	0.058	0.081	0.100								
SN2005da(Ic)	0.215	0.124	0.034	0.000	0.042	0.021	0.029								
SN2005ek(Ic)	0.000	0.000	0.000	0.000	0.000	0.000	0.004								
SN2005kf(Ic)	0.546	0.579	0.604	0.568	0.606	0.607	0.601								
SN2006F(Ib)	0.345	0.294	0.175	0.167	0.158	0.133	0.000								
SN2006dg(Ic)	0.213	0.283	0.124	0.118	0.131	0.142	0.103								
SN2006eg(Ib-c)	0.418	0.424	0.597	0.610	0.611	0.640	0.647								
SN2006ei(Ic)	0.325	0.366	0.385	0.392	0.409	0.404	0.386								
SN2006ep(Ib)	0.000	0.157	0.103	0.206	0.216	0.137	0.151								
SN2006jc(Ibn)	0.198	0.129	0.238	0.000	0.208	0.193	0.202								
SN2006ld(Ib)	0.722	0.659	0.000	0.510	0.371	0.709	0.341								
SN2006lt(Ib)	0.000	0.000	0.000	0.316	0.000	0.000	0.415								
SN2006lv(Ib-c)	0.646	0.370	0.556	0.502	0.610	0.657	0.413								
SN2007C(Ib)	0.288	0.332	0.319	0.333	0.335	0.420	0.402								
SN2007fo(Ib)	0.650	0.696	0.656	0.669	0.616	0.501	0.553								
SN2007gr(Ic)	0.532	0.485	0.473	0.483	0.484	0.572	0.502								
SN2007tq(Ic)	0.358	0.568	0.358	0.374	0.165	0.357	0.290								
SN2007ru(Ic)	0.163	0.124	0.058	0.089	0.028	0.061	0.036								
SN2007tz(Ic)	0.774	0.722	0.723	0.738	0.704	0.692	0.611								
SN2007uy(Ib)	0.531	0.580	0.491	0.526	0.537	0.678	0.463								
SN2008D(Ib)	0.468	0.538	0.375	0.371	0.324	0.343	0.215								
SN2008ao(Ic)	0.163	0.116	0.120	0.109	0.065	0.065	0.000								
SN2008du(Ic)	0.497	0.513	0.550	0.534	0.518	0.481	0.490								
SN2008dv(Ic)	0.429	0.441	0.399	0.417	0.426	0.500	0.510								
SN2008eb(Ic)	0.443	0.482	0.471	0.469	0.464	0.430	0.453								
SN2008im(Ib)	0.192	0.282	0.350	0.249	0.219	0.156	0.000								
SN2009iz(Ib)	0.140	0.141	0.088	0.127	0.079	0.000	0.045								
SN2009lj(Ic)	0.120	0.173	0.151	0.145	0.129	0.136	0.069								
SN2009lw(Ib-IIb)	0.463	0.001	0.240	0.189	0.305	0.333	0.193								
SN2010X(Ic)	0.193	0.327	0.316	0.418	0.474	0.445	0.349								
SN2010do(Ic)	0.451	0.349	0.362	0.376	0.351	0.351	0.292								
SN2010gk(Ic)	0.823	0.812	0.840	0.852	0.809	0.776	0.734								
SN2010gr(Ib-c)	0.381	0.470	0.135	0.370	0.203	0.326	0.251								
SN2011it(Ic)	0.000	0.544	0.000	0.613	0.373	0.123	0.165								
SN2011jf(IbPec)	0.486	0.589	0.255	0.272	0.242	0.210	0.153								
SN2011jm(Ic)	0.968	0.931	0.914	0.923	0.930	0.921	0.733								
SN2012C(Ic)	0.659	0.750	0.634	0.655	0.628	0.597	0.629								
SN2012P(Ib-c)	0.740	0.750	0.652	0.607	0.589	0.706	0.473								
SN2012au(Ib)	0.000	0.803	0.791	0.786	0.760	0.738	0.719								
SN2012cw(Ic)	0.193	0.167	0.179	0.173	0.201	0.222	0.209								
SN2012ej(Ic)	0.336	0.377	0.323	0.376	0.333	0.377	0.325								
SN2014C(Ib)	0.353	0.690	0.432	0.624	0.554	0.589	0.582								
SN2014L(Ic)	0.750	0.769	0.732	0.735	0.705	0.745	0.690								
SN2014ad(Ic)	0.050	0.043	0.041	0.040	0.021	0.018	0.019								
SN2014ge(Ib)	0.511	0.405	0.486	0.495	0.322	0.508	0.337								
SN2015G(Ib)	0.376	0.009	0.209	0.387	0.120	0.130	0.055								
SN2015Q(Ib)	0.380	0.482	0.507	0.418	0.416	0.400	0.407								
SN2015U(Ibn)	0.231	0.284	0.350	0.412	0.489	0.526	0.577								
SN2015ah(Ib)	0.525	0.574	0.000	0.523	0.494	0.626	0.545								
SN2015ap(Ib-c)	0.824	0.569	0.880	0.820	0.925	0.958	0.704								
SN2016G(Ic)	0.387	0.389	0.321	0.337	0.309	0.375	0.293								
SN2016P(Ic)	0.870	0.823	0.796	0.776	0.709	0.798	0.508								
SN2016co(Ic)	0.546	0.430	0.356	0.485	0.381	0.246	0.287								
SN2017ewx(Ib)	0.612	0.602	0.543	0.538	0.559	0.000	0.442								
SN2017hcb(Ib)	0.682	0.735	0.774	0.764	0.703	0.620	0.623								
SN2018cow(Ic)	0.597	0.576	0.509	0.589	0.501	0.484	0.495								
SN2018dbg(Ibc)	0.964	0.959	0.955	0.950	0.941	0.938	0.932								
SN2018ebt(Ic)	0.493	0.000	0.214	0.130	0.133	0.128	0.114								
SN2018gwo(Ic)	0.295	0.000	0.000	0.225	0.176	0.089	0.108								
SN2018hdp(Ic)	0.578	0.556	0.610	0.595	0.616	0.590	0.644								
SN2019ccm(Ib)	0.487	0.369	0.474	0.459	0.519	0.593	0.578								
SN2019clq(Ib)	0.807	0.775	0.775	0.799	0.811	0.897	0.850								
SN2020hvp(Ib)	0.660	0.738	0.679	0.691	0.730	0.726	0.780								
SN2021mx(Ic)	0.569	0.539	0.637	0.582	0.720	0.721	0.765								
SN2022bdu(Ic)	0.621	0.648	0.579	0.595	0.540	0.585	0.540								
SN2022oqm(Ic)	0.023	0.340	0.497	0.169	0.178	0.000	0.076								
iPTF13bvn(Ib)	0.719	0.739	0.705	0.691	0.616	0.564	0.517								

Table A.4: NCR values for all the sample with the narrow-band filters after subtracting the correspondent underlying continuum.

Name(Type)	H α +[NII]	[OII]	Ca II triplet	H α	[NII]	Name(Type)	H α +[NII]	[OII]	Ca II triplet	H α	[NII]
ASASSN-14kg(II)	0.952	0.000	0.000	0.953	0.892	SN2005B(II)	0.000	0.000	0.000	0.000	0.000
ASASSN-15lf(II)	0.000	0.000	0.000	0.000	0.000	SN2005cs(II)	0.349	0.000	0.000	0.356	0.300
ASASSN-15tw(II)	0.171	0.000	0.000	0.179	0.030	SN2005db(IIIn)	0.633	0.000	0.000	0.640	0.596
ASASSN-16eu(II)	0.672	0.000	0.000	0.681	0.272	SN2005ip(IIIn)	0.742	0.000	0.000	0.744	0.692
ASASSN14az(IIb)	0.035	0.000	0.000	0.040	0.000	SN2005kj(IIIn)	0.000	0.000	0.000	0.000	0.000
ASASSN15bd(IIb)	0.753	0.584	0.000	0.759	0.659	SN2005lx(II)	0.458	0.861	0.000	0.374	0.426
AT2020drl(II)	0.000	0.000	0.000	0.000	0.000	SN2005mg(II)	0.466	0.727	0.000	0.421	0.000
PS15cwt(IIIn)	0.000	0.000	0.000	0.000	0.000	SN2006G(IIb)	0.000	0.000	0.000	0.000	0.000
SDSS-IIISN14215(II)	0.450	0.000	0.000	0.467	0.000	SN2006M(II)	0.749	0.308	0.000	0.751	0.782
SN1909A(II)	0.000	0.000	0.000	0.000	0.000	SN2006Q(II)	0.000	0.000	0.000	0.000	0.000
SN1921B(II)	0.109	0.000	0.000	0.129	0.000	SN2006W(II)	0.000	0.000	0.587	0.000	0.000
SN1937F(II)	0.000	0.000	0.000	0.000	0.000	SN2006at(II)	0.000	0.000	0.000	0.000	0.000
SN1940A(II)	0.000	0.881	0.000	0.000	0.000	SN2006bo(IIIn)	0.000	0.000	0.000	0.000	0.000
SN1941C(II)	0.321	0.000	0.000	0.331	0.276	SN2006iv(IIb)	0.000	0.000	0.000	0.000	0.000
SN1951H(II)	0.000	0.000	0.000	0.000	0.000	SN2006my(II)	0.874	0.413	0.926	0.876	0.856
SN1954C(II)	0.523	0.000	0.000	0.528	0.407	SN2007T(II)	0.469	0.000	0.000	0.474	0.416
SN1954J(II)	0.000	0.000	0.000	0.000	0.000	SN2007am(II)	0.253	0.000	0.000	0.274	0.048
SN1959D(II)	0.000	0.000	0.000	0.000	0.000	SN2007cm(II)	0.000	0.000	0.000	0.000	0.000
SN1961F(II)	0.752	0.709	0.000	0.758	0.606	SN2007pk(IIIn)	0.505	0.770	0.000	0.522	0.523
SN1961V(II)	0.000	0.000	0.000	0.000	0.000	SN2008aq(II-IIIb)	0.852	0.000	0.000	0.857	0.718
SN1964H(II)	0.000	0.000	0.000	0.000	0.000	SN2008ax(IIb)	0.053	0.300	0.000	0.057	0.030
SN1967H(II)	0.627	0.682	0.000	0.661	0.267	SN2008az(II)	0.000	0.000	0.000	0.000	0.000
SN1969L(II)	0.000	0.000	0.000	0.000	0.000	SN2008bo(IIb)	0.103	0.849	0.000	0.111	0.043
SN1970G(II)	0.000	0.000	0.000	0.000	0.000	SN2008ie(IIb)	0.857	0.000	0.000	0.859	0.807
SN1972Q(II)	0.000	0.839	0.000	0.000	0.000	SN2008ij(II)	0.349	0.000	0.000	0.362	0.172
SN1973R(II)	0.000	0.000	0.000	0.000	0.000	SN2008iz(II)	0.000	0.000	0.000	0.000	0.000
SN1975T(II)	0.313	0.982	0.000	0.319	0.162	SN2009ga(II)	0.000	0.000	0.000	0.000	0.000
SN1976F(II)	0.000	0.000	0.001	0.000	0.000	SN2009hd(II)	0.000	0.000	0.000	0.000	0.000
SN1978H(II)	0.381	0.718	0.000	0.395	0.230	SN2010gi(II)	0.000	0.000	0.000	0.000	0.000
SN1980D(II)	0.000	0.000	0.000	0.000	0.000	SN2010ic(II)	0.000	0.766	0.000	0.000	0.000
SN1981K(II)	0.443	0.000	0.000	0.486	0.082	SN2010ie(II)	0.000	0.000	0.000	0.000	0.000
SN1982F(II)	0.110	0.434	0.000	0.117	0.038	SN2010jl(IIIn)	0.000	0.596	0.000	0.000	0.000
SN1984E(II)	0.000	0.000	0.000	0.000	0.000	SN2011an(IIIn)	0.000	0.000	0.000	0.000	0.000
SN1986E(II)	0.000	0.000	0.000	0.000	0.000	SN2011dh(IIb)	0.000	0.000	0.000	0.000	0.000
SN1986f(II)	0.272	0.649	0.000	0.279	0.126	SN2013bu(II)	0.000	0.000	0.000	0.000	0.000
SN1987K(IIb)	0.964	0.574	0.979	0.965	0.956	SN2013cc(II)	0.235	0.000	0.000	0.256	0.000
SN1988A(II)	0.000	0.000	0.000	0.000	0.000	SN2013ej(II)	0.222	0.000	0.000	0.236	0.000
SN1988E(II)	0.000	0.000	0.000	0.000	0.000	SN2013fs(II)	0.000	0.000	0.668	0.000	0.000
SN1991ao(II)	0.000	0.000	0.000	0.000	0.000	SN2013ha(IIIn)	0.494	0.000	0.000	0.504	0.246
SN1992C(II)	0.000	0.000	0.000	0.000	0.000	SN2014F(II)	0.000	0.000	0.000	0.000	0.000
SN1992az(II)	0.132	0.000	0.000	0.153	0.000	SN2014bc(II)	0.633	0.925	0.000	0.687	0.155
SN1993J(IIb)	0.000	0.000	0.000	0.000	0.000	SN2014cn(II)	0.000	0.000	0.000	0.000	0.000
SN1994ak(II)	0.000	0.000	0.000	0.000	0.000	SN2014cv(IP)	0.686	0.000	0.000	0.689	0.620
SN1995V(II)	0.000	0.000	0.000	0.000	0.000	SN2015P(II)	0.000	0.000	0.000	0.000	0.000
SN1995Z(II)	0.000	0.000	0.000	0.000	0.000	SN2015V(II)	0.762	0.654	0.000	0.764	0.697
SN1996cc(II)	0.000	0.000	0.000	0.000	0.000	SN2015X(II)	0.000	0.000	0.000	0.000	0.000
SN1997bs(IIIn)	0.000	0.000	0.000	0.000	0.000	SN2015am(II)	0.000	0.000	0.000	0.000	0.000
SN1998Y(II)	0.112	0.418	0.000	0.118	0.109	SN2015ba(II)	0.566	0.000	0.000	0.571	0.446
SN1998ar(II)	0.000	0.000	0.000	0.000	0.000	SN2015bh(II)	0.000	0.000	0.000	0.000	0.000
SN1999A(II)	0.329	0.746	0.000	0.335	0.233	SN2015cz(II)	0.000	0.479	0.000	0.000	0.000
SN1999bw(II)	0.000	0.000	0.000	0.000	0.000	SN2016aa(II)	0.058	0.000	0.000	0.068	0.000
SN1999dj(II)	0.000	0.232	0.000	0.000	0.000	SN2016bam(II)	0.000	0.000	0.000	0.000	0.000
SN1999ed(II)	0.000	0.120	0.000	0.000	0.000	SN2016bkv(II)	0.081	0.000	0.000	0.100	0.000
SN1999el(IIIn)	0.242	0.129	0.000	0.279	0.000	SN2016bkx(IP)	0.657	0.840	0.000	0.664	0.547
SN1999gi(II)	0.726	0.709	0.000	0.745	0.395	SN2016bmd(IIb)	0.647	0.000	0.000	0.658	0.448
SN2000H(IIb)	0.000	0.000	0.000	0.000	0.000	SN2016bme(II)	0.000	0.000	0.000	0.000	0.000
SN2000dj(II)	0.000	0.000	0.000	0.000	0.000	SN2016brw(II)	0.000	0.000	0.000	0.000	0.000
SN2000eo(IIIn)	0.458	0.000	0.000	0.462	0.351	SN2016ccf(II)	0.497	0.737	0.000	0.502	0.354
SN2000ez(II)	0.207	0.269	0.000	0.217	0.071	SN2016cok(II)	0.000	0.000	0.000	0.000	0.000
SN2001R(II)	0.000	0.000	0.000	0.000	0.000	SN2016hrv(II)	0.000	0.000	0.000	0.000	0.000
SN2001cm(II)	0.677	0.000	0.000	0.682	0.558	SN2016iy(IIb)	0.198	0.000	0.000	0.239	0.000
SN2001dc(II)	0.040	0.000	0.000	0.084	0.000	SN2017ati(IIb)	0.000	0.736	0.000	0.000	0.000
SN2001ez(II)	0.680	0.525	0.000	0.702	0.000	SN2017czd(II)	0.000	0.578	0.000	0.000	0.000
SN2001fv(II)	0.429	0.000	0.000	0.434	0.344	SN2017gas(IIIn)	0.404	0.000	0.000	0.411	0.297
SN2002A(II)	0.000	0.138	0.000	0.000	0.000	SN2017gpn(IIb)	0.000	0.000	0.000	0.000	0.000
SN2002b2u(II)	0.000	0.000	0.000	0.000	0.000	SN2017gtd(IP)	0.791	0.614	0.822	0.795	0.756
SN2002kg(II)	0.000	0.141	0.000	0.000	0.000	SN2017hbg(II)	0.000	0.000	0.000	0.000	0.000
SN2003G(IIIn)	0.393	0.000	0.000	0.405	0.154	SN2017hkp(II)	0.000	0.000	0.000	0.000	0.000
SN2003bl(II)	0.000	0.406	0.000	0.000	0.000	SN2017hyh(IIb)	0.000	0.000	0.000	0.000	0.000
SN2003da(II)	0.000	0.703	0.000	0.000	0.000	SN2017jbl(IIb)	0.580	0.000	0.000	0.589	0.578
SN2003ef(II)	0.432	0.000	0.000	0.437	0.324	SN2017jfs(IIIn)	0.474	0.728	0.000	0.477	0.418
SN2003gd(II)	0.000	0.000	0.000	0.000	0.000	SN2018acf(II)	0.000	0.000	0.000	0.000	0.000
SN2004C(IIb)	0.907	0.000	0.000	0.908	0.882	SN2018afm(IIIn)	0.000	0.000	0.000	0.000	0.000
SN2004am(II)	0.000	0.000	0.000	0.000	0.000	SN2018aoq(II)	0.000	0.000	0.000	0.000	0.000
SN2004cm(II)	0.000	0.000	0.603	0.000	0.000	SN2018ccb(II)	0.000	0.000	0.000	0.000	0.000
SN2004dd(II)	0.312	0.167	0.000	0.324	0.376	SN2018cyy(II)	0.911	0.000	0.000	0.913	0.847
SN2004dg(II)	0.710	0.000	0.000	0.714	0.620	SN2018fmf(II)	0.690	0.000	0.000	0.697	0.471
SN2004dj(II)	0.000	0.214	0.000	0.000	0.000	SN2018fpb(IIb)	0.000	0.000	0.000	0.000	0.000
SN2004dw(II)	0.000	0.000	0.000	0.000	0.000	SN2018fru(II)	0.942	0.000	0.828	0.944	0.905
SN2004hx(II)	0.000	0.000	0.000	0.000	0.000	SN2018gj(IIb)	0.000	0.000	0.000	0.000	0.000

Name(Type)	H α +[NII]	[OII]	Ca II triplet	H α	[NII]	Name(Type)	H α +[NII]	[OII]	Ca II triplet	H α	[NII]
SN2018imj(II)	0.000	0.000	0.000	0.062	0.000	SN2003cg(Ia)	0.000	0.000	0.000	0.000	0.000
SN2018ivc(II)	0.105	0.000	0.000	0.109	0.061	SN2003gt(Ia)	0.000	0.000	0.000	0.000	0.000
SN2018kg(II)	0.793	0.000	0.000	0.803	0.535	SN2003hm(Ia)	0.871	0.000	0.000	0.874	0.808
SN2018ow(l Ib)	0.000	0.890	0.426	0.000	0.000	SN2005ai(Ia)	0.000	0.000	0.000	0.000	0.000
SN2019bxq(II n)	0.590	0.713	0.000	0.594	0.521	SN2005bo(Ia)	0.537	0.000	0.000	0.543	0.424
SN2019el(II n)	0.000	0.000	0.000	0.000	0.000	SN2005cx(Ia)	0.000	0.000	0.000	0.000	0.000
SN2019fmb(II n)	0.815	0.000	0.000	0.773	0.929	SN2005dv(Ia)	0.000	0.000	0.000	0.000	0.000
SN2019fyd(II)	0.000	0.000	0.000	0.000	0.000	SN2005ev(Ia)	0.000	0.029	0.000	0.000	0.000
SN2019hyk(II)	0.781	0.000	0.000	0.784	0.697	SN2006D(Ia)	0.000	0.000	0.000	0.000	0.000
SN2019itw(l Ib)	0.772	0.000	0.000	0.779	0.572	SN2006dd(Ia)	1.000	0.000	0.000	1.000	0.976
SN2019ovr(II)	0.542	0.000	0.000	0.547	0.433	SN2007J(Ia)	0.000	0.000	0.000	0.000	0.000
SN2019upq(II)	0.000	0.000	0.717	0.000	0.000	SN2007ap(Ia)	0.000	0.000	0.000	0.000	0.000
SN2019xdf(II)	0.247	0.601	0.000	0.254	0.166	SN2007sa(Ia)	0.773	0.000	0.000	0.777	0.603
SN2020aapr(II)	0.000	0.000	0.000	0.000	0.000	SN2009hr(Ia)	0.000	0.000	0.000	0.000	0.000
SN2020acac(II)	0.551	0.000	0.000	0.556	0.499	SN2009ig(Ia)	0.000	0.000	0.000	0.000	0.000
SN2020dpw(II)	0.092	0.006	0.000	0.092	0.000	SN2009nq(Ia)	0.000	0.000	0.000	0.000	0.000
SN2020drl(II)	0.192	0.000	0.000	0.216	0.000	SN2010eb(Ia)	0.000	0.000	0.000	0.000	0.000
SN2020dvt(II)	0.000	0.000	0.000	0.000	0.000	SN2010jv(Ia)	0.000	0.000	0.000	0.000	0.000
SN2020fqv(l Ib)	0.256	0.000	0.000	0.258	0.229	SN2011aa(Iapec)	0.000	0.000	0.000	0.000	0.000
SN2020kb(II)	0.000	0.000	0.000	0.000	0.000	SN2011fe(Ia)	0.000	0.000	0.000	0.000	0.000
SN2020noc(II)	0.793	0.000	0.000	0.793	0.796	SN2011gb(Ia)	0.000	0.000	0.000	0.000	0.000
SN2020rue(II)	0.000	0.000	0.000	0.000	0.000	SN2011hd(Ia)	0.000	0.000	0.859	0.000	0.000
SN2020tlf(II)	0.378	0.000	0.000	0.400	0.110	SN2011hr(la-91T)	0.000	0.000	0.000	0.000	0.000
SN2020xqj(II)	0.773	0.000	0.000	0.775	0.761	SN2013fb(Ia)	0.415	0.100	0.000	0.423	0.489
SN2021afkk(II)	0.744	0.338	0.000	0.750	0.661	SN2013hg(Ia)	0.000	0.291	0.000	0.000	0.000
SN2021ass(II)	0.000	0.000	0.000	0.000	0.000	SN2014J(Ia)	0.000	0.000	0.000	0.000	0.000
SN2021bbm(II)	0.000	0.000	0.000	0.000	0.000	SN2014da(Ia-91bg)	0.639	0.000	0.000	0.643	0.518
SN2021eay(II)	0.369	0.110	0.000	0.374	0.000	SN2015ab(Ia)	0.000	0.000	0.000	0.000	0.000
SN2021qvr(II)	0.335	0.000	0.000	0.366	0.111	SN2016F(Ia)	0.000	0.000	0.000	0.000	0.000
SN2021yok(II)	0.647	0.000	0.000	0.656	0.607	SN2016evn(Ia)	0.000	0.000	0.000	0.000	0.000
SN2022acfz(II)	0.816	0.854	0.000	0.819	0.756	SN2016iuh(Ia)	0.000	0.000	0.000	0.000	0.000
SN2022mji(II)	0.286	0.532	0.000	0.290	0.224	SN2017fgc(Ia)	0.244	0.000	0.000	0.270	0.000
SN2022ngb(l Ib)	0.483	0.484	0.000	0.490	0.364	SN2017gld(Ia)	0.862	0.000	0.948	0.866	0.693
SN2022prv(II)	0.000	0.000	0.000	0.000	0.000	SN2017gxq(Ia)	0.601	0.000	0.000	0.612	0.234
SN2022sje(II)	0.000	0.000	0.000	0.000	0.000	SN2017hal(Ia)	0.381	0.000	0.000	0.384	0.290
SN2022zkd(II)	0.000	0.000	0.000	0.000	0.000	SN2017hij(Ia)	0.000	0.000	0.000	0.000	0.000
SN2023jo(II n)	0.779	0.000	0.000	0.783	0.704	SN2017igf(Ia)	0.139	0.000	0.000	0.155	0.000
iPTF13dkz(II)	0.208	0.000	0.000	0.217	0.105	SN2017iji(Ia)	0.000	0.000	0.000	0.000	0.000
ASASSN-15mc(Ia)	0.676	0.000	0.000	0.680	0.680	SN2017jav(Ia)	0.000	0.000	0.000	0.000	0.000
ASASSN-15ti(Ia)	0.000	0.000	0.000	0.000	0.000	SN2017if(Ia)	0.076	0.000	0.000	0.115	0.000
SN1921C(I)	0.109	0.000	0.000	0.129	0.000	SN2018bi(Ia)	0.000	0.511	0.000	0.000	0.000
SN1938A(I)	0.000	0.000	0.000	0.000	0.000	SN2018kp(Ia)	0.059	0.000	0.000	0.038	0.000
SN1945A(I)	0.000	0.000	0.000	0.000	0.000	SN2019arb(Ia)	0.000	0.000	0.000	0.000	0.000
SN1957A(Ia)	0.000	0.000	0.000	0.000	0.000	SN2019cth(Ia)	0.751	0.000	0.748	0.755	0.668
SN1957B(Ia)	0.000	0.000	0.000	0.000	0.000	SN2019gsc(Ia)	0.567	0.000	0.000	0.574	0.681
SN1961H(Ia)	0.000	0.000	0.000	0.000	0.000	SN2019tdf(Ia)	0.322	0.000	0.000	0.328	0.220
SN1963K(Ia)	0.000	0.000	0.000	0.000	0.000	SN2020akf(Ia)	0.875	0.000	0.000	0.875	0.828
SN1966G(I)	0.000	0.000	0.000	0.000	0.000	SN2020fcw(Ia)	0.000	0.000	0.000	0.000	0.000
SN1966J(Ia)	0.000	0.000	0.000	0.000	0.000	SN2020hni(Ia)	0.000	0.000	0.000	0.000	0.000
SN1970L(I)	0.000	0.445	0.000	0.000	0.000	SN2020jhf(Ia)	0.531	0.000	0.000	0.536	0.886
SN1971I(Ia)	0.000	0.000	0.000	0.000	0.000	SN2020scc(Ia)	0.000	0.000	0.000	0.000	0.000
SN1975G(Ia)	0.000	0.000	0.000	0.000	0.000	SN2021aaa(Ia)	0.469	0.000	0.219	0.474	0.563
SN1976G(Ia)	0.000	0.000	0.000	0.000	0.000	SN2021afsj(Ia)	0.000	0.000	0.153	0.000	0.000
SN1981B(Ia)	0.000	0.290	0.000	0.000	0.000	SN2021gmg(Ia)	0.277	0.572	0.000	0.282	0.203
SN1982C(Ia)	0.000	0.000	0.000	0.000	0.000	SN2021jag(Ia)	0.572	0.970	0.000	0.576	0.491
SN1982V(I)	0.481	0.000	0.622	0.489	0.405	SN2021wcu(Ia)	0.299	0.000	0.000	0.271	0.452
SN1982W(Ia)	0.000	0.000	0.000	0.000	0.000	SN2022aaq(Ia)	0.000	0.000	0.000	0.000	0.000
SN1986A(Ia)	0.167	0.000	0.000	0.186	0.005	SN2022hkc(Ia)	0.000	0.000	0.000	0.000	0.000
SN1989A(Ia)	0.000	0.000	0.000	0.000	0.000	SN2022mj(k)	0.000	0.000	0.000	0.000	0.000
SN1989B(Ia)	0.000	0.000	0.000	0.000	0.000	iPTF13akk(Ia)	0.671	0.000	0.000	0.376	0.000
SN1989M(Ia)	0.000	0.000	0.000	0.000	0.000	iPTF13ebh(Ia)	0.000	0.000	0.000	0.000	0.000
SN1989P(Ia)	0.000	0.000	0.000	0.000	0.000	AT2014ge(lb)	0.716	0.000	0.000	0.721	0.598
SN1990L(Ia)	0.000	0.000	0.000	0.000	0.000	CSS14(lb)	0.269	0.000	0.000	0.273	0.184
SN1991F(Ia)	0.000	0.000	0.000	0.000	0.000	PTF09dfk(lb)	0.000	0.632	0.000	0.000	0.000
SN1991IT(Ia)	0.404	0.000	0.000	0.412	0.223	PTF12gzk(lc)	0.680	0.115	0.000	0.682	0.707
SN1991bg(Ia)	0.000	0.000	0.000	0.000	0.000	SN1954A(lb)	0.000	0.000	0.351	0.000	0.000
SN1991bi(Ia)	0.000	0.000	0.000	0.000	0.000	SN1962L(ic)	0.000	0.000	0.000	0.000	0.000
SN1995al(Ia)	0.296	0.000	0.000	0.304	0.192	SN1972R(lb)	0.000	0.000	0.000	0.000	0.000
SN1997bm(Ia)	0.000	0.000	0.000	0.000	0.000	SN1976B(lb)	0.000	0.000	0.000	0.000	0.000
SN1997dp(Ia)	0.000	0.000	0.000	0.000	0.000	SN1984L(lb)	0.595	0.441	0.000	0.601	0.495
SN1998dk(Ia)	0.129	0.524	0.000	0.062	0.000	SN1985F(lb)	0.739	0.821	0.000	0.762	0.485
SN1998eb(Ia)	0.000	0.785	0.000	0.000	0.000	SN1988ac(lbc)	0.608	0.794	0.000	0.615	0.490
SN1998es(Iapec)	0.074	0.000	0.000	0.076	0.039	SN1990B(lc)	0.517	0.000	0.000	0.520	0.458
SN1999by(Ia)	0.000	0.000	0.000	0.000	0.000	SN1991ar(lb)	0.990	0.000	0.000	0.990	0.958
SN1999da(Ia)	0.000	0.000	0.000	0.000	0.000	SN1994I(ic)	0.512	0.879	0.000	0.520	0.386
SN1999ej(Ia)	0.000	0.000	0.000	0.000	0.000	SN1997dc(lb)	0.000	0.000	0.000	0.000	0.000
SN1999gr(Ia)	0.153	0.000	0.000	0.160	0.005	SN1997dq(lc)	0.158	0.000	0.000	0.162	0.118
SN2000E(Ia)	0.207	0.000	0.000	0.220	0.000	SN1997ef(lc)	0.784	0.000	0.000	0.787	0.845
SN2000fd(Ia)	0.000	0.000	0.117	0.000	0.000	SN1998cc(lb)	0.000	0.000	0.000	0.000	0.000
SN2001ed(Ia)	0.000	0.000	0.000	0.000	0.000	SN1998ey(lc)	0.000	0.000	0.000	0.000	0.000
SN2002cs(Ia)	0.000	0.000	0.000	0.000	0.000	SN1999dn(lb)	0.039	0.197	0.000	0.043	0.007
SN2002dl(Ia)	0.000	0.000	0.000	0.000	0.000	SN1999eh(lb)	0.392	0.000	0.00		

Name(Type)	H α +[NII]	[OIII]	Ca II triplet	H α	[NII]	Name(Type)	H α +[NII]	[OIII]	Ca II triplet	H α	[NII]
SN2000fn(Ib)	0.526	0.000	0.000	0.530	0.573	SN2023ixf(II)	0.201	0.298	0.047	0.192	0.157
SN2001B(Ib)	0.000	0.421	0.446	0.000	0.000						
SN2001ef(Ic)	0.576	0.000	0.000	0.588	0.326						
SN2001ej(Ib)	0.172	0.436	0.000	0.180	0.089						
SN2001is(Ib)	0.198	0.000	0.000	0.190	0.000						
SN2002ap(Ic)	0.000	0.000	0.000	0.000	0.000						
SN2002cw(Ib)	0.000	0.000	0.000	0.000	0.000						
SN2002ho(Ic)	0.000	0.000	0.000	0.000	0.000						
SN2002ji(Ib)	0.074	0.000	0.000	0.080	0.000						
SN2002jz(Ib)	0.000	0.403	0.000	0.000	0.000						
SN2003aa(Ic)	0.287	0.000	0.000	0.308	0.048						
SN2003gk(Ib)	0.699	0.515	0.618	0.710	0.577						
SN2004ao(Ib)	0.000	0.000	0.000	0.000	0.000						
SN2004cc(Ib)	0.648	0.000	0.000	0.651	0.591						
SN2004dk(Ib)	0.730	0.000	0.000	0.735	0.576						
SN2004ge(Ic)	0.000	0.201	0.000	0.000	0.000						
SN2004gk(Ic)	0.710	0.000	0.000	0.712	0.635						
SN2004gn(Ib)	0.514	0.000	0.000	0.522	0.367						
SN2005aj(Ic)	0.000	0.000	0.000	0.000	0.000						
SN2005da(Ic)	0.000	0.000	0.000	0.000	0.000						
SN2005ek(Ic)	0.000	0.000	0.000	0.000	0.000						
SN2005kf(Ic)	0.000	0.000	0.000	0.000	0.000						
SN2006F(Ib)	0.000	0.000	0.000	0.000	0.000						
SN2006dg(Ic)	0.000	0.000	0.000	0.000	0.000						
SN2006eg(Ib-c)	0.515	0.144	0.000	0.523	0.297						
SN2006ei(Ic)	0.000	0.000	0.000	0.000	0.000						
SN2006ep(Ib)	0.000	0.000	0.000	0.000	0.000						
SN2006jc(Ibn)	0.000	0.000	0.000	0.000	0.000						
SN2006ld(Ib)	0.865	0.728	0.000	0.867	0.803						
SN2006lt(Ib)	0.000	0.000	0.501	0.000	0.000						
SN2006lv(Ib-c)	0.424	0.000	0.000	0.441	0.402						
SN2007C(Ib)	0.000	0.023	0.000	0.000	0.000						
SN2007fo(Ib)	0.166	0.283	0.000	0.179	0.067						
SN2007gr(Ic)	0.000	0.208	0.000	0.000	0.000						
SN2007tq(Ic)	0.776	0.000	0.000	0.585	0.684						
SN2007ru(Ic)	0.000	0.000	0.000	0.000	0.000						
SN2007tz(Ic)	0.665	0.652	0.000	0.669	0.597						
SN2007uy(Ib)	0.719	0.000	0.000	0.722	0.709						
SN2008D(Ib)	0.180	0.000	0.000	0.185	0.246						
SN2008ao(Ic)	0.000	0.000	0.000	0.000	0.000						
SN2008du(Ic)	0.481	0.394	0.000	0.487	0.390						
SN2008dv(Ic)	0.324	0.000	0.000	0.337	0.072						
SN2008eb(Ic)	0.325	0.000	0.000	0.329	0.269						
SN2008im(Ib)	0.148	0.000	0.000	0.163	0.000						
SN2009iz(Ib)	0.000	0.000	0.045	0.000	0.000						
SN2009lj(Ic)	0.000	0.000	0.000	0.000	0.000						
SN2009lw(Ib-IIb)	0.373	0.280	0.000	0.396	0.019						
SN2010X(Ic)	0.000	0.000	0.349	0.000	0.000						
SN2010do(Ic)	0.299	0.000	0.000	0.303	0.231						
SN2010gk(Ic)	0.616	0.641	0.000	0.622	0.571						
SN2010gr(Ib-c)	0.145	0.532	0.000	0.113	0.000						
SN2011it(Ic)	0.000	0.000	0.000	0.000	0.000						
SN2011jf(IbPec)	0.000	0.000	0.000	0.000	0.000						
SN2011jm(Ic)	0.845	0.766	0.000	0.851	0.705						
SN2012C(Ic)	0.456	0.000	0.000	0.472	0.472						
SN2012P(Ib-c)	0.825	0.000	0.000	0.828	0.755						
SN2012au(Ib)	0.570	0.000	0.000	0.576	0.452						
SN2012cw(Ic)	0.000	0.000	0.000	0.000	0.000						
SN2012ej(Ic)	0.410	0.000	0.000	0.432	0.000						
SN2014C(Ib)	0.000	0.000	0.000	0.000	0.000						
SN2014L(Ic)	0.533	0.916	0.000	0.566	0.196						
SN2014ad(Ic)	0.000	0.000	0.000	0.000	0.000						
SN2014ge(Ib)	0.782	0.000	0.000	0.786	0.679						
SN2015G(Ib)	0.133	0.000	0.000	0.163	0.000						
SN2015Q(Ib)	0.239	0.000	0.000	0.254	0.019						
SN2015U(Ibn)	0.000	0.000	0.000	0.000	0.000						
SN2015ah(Ib)	0.916	0.000	0.545	0.908	0.925						
SN2015ap(Ib-c)	0.966	0.285	0.000	0.967	0.933						
SN2016G(Ic)	0.317	0.236	0.000	0.424	0.000						
SN2016P(Ic)	0.628	0.410	0.000	0.631	0.549						
SN2016coi(Ic)	0.000	0.000	0.413	0.000	0.000						
SN2017ewx(Ib)	0.000	0.000	0.000	0.000	0.000						
SN2017hcb(Ib)	0.620	0.000	0.000	0.624	0.565						
SN2018cow(Ic)	0.781	0.958	0.588	0.786	0.641						
SN2018dbg(Ibc)	0.797	0.606	0.000	0.799	0.752						
SN2018ebt(Ic)	0.000	0.000	0.000	0.000	0.000						
SN2018gwo(Ic)	0.000	0.000	0.000	0.000	0.000						
SN2018hdp(Ic)	0.579	0.557	0.000	0.583	0.533						
SN2019ccm(Ib)	0.272	0.000	0.578	0.299	0.000						
SN2019clq(Ib)	0.710	0.656	0.000	0.711	0.676						
SN2020hvp(Ib)	0.000	0.000	0.000	0.000	0.000						
SN2021mxz(Ic)	0.366	0.000	0.000	0.370	0.353						
SN2022bdu(Ic)	0.000	0.000	0.000	0.000	0.000						
SN2022oqm(Ic)	0.000	0.000	0.000	0.000	0.000						
iPTF13bvn(Ib)	0.466	0.000	0.000	0.471	0.352						

Table A.5: Results of the SED fitting with all 12 filters.

Name	Type	$\log < t_* \text{ (yr)} >$	$A_V \text{ (mag)}$	$\log \text{SFR}$	$\log M$	Name	Type	$\log < t_* \text{ (yr)} >$	$A_V \text{ (mag)}$	$\log \text{SFR}$	$\log M$
SN2021yok	II	6.60 ^{0.08} _{-0.13}	2.10 ^{0.03} _{-0.15}	0.55 ^{0.19} _{-0.23}	6.85 ^{0.07} _{-0.12}	SN2016bkv	II	9.05 ^{0.03} _{-2.40}	0.00 ^{-0.00} _{-0.00}	-1.53 ^{2.13} _{-0.03}	7.22 ^{0.02} _{-0.11}
SN2022prv	II	6.80 ^{1.31} _{-0.17}	0.80 ^{0.41} _{-0.80}	-0.44 ^{0.18} _{-1.29}	6.06 ^{0.05} _{-0.16}	SN1982F	II	7.00 ^{0.03} _{-0.10}	0.30 ^{0.06} _{-0.17}	0.05 ^{0.16} _{-0.10}	6.74 ^{0.06} _{-0.05}
SN1998ar	II	6.60 ^{0.10} _{-0.11}	1.40 ^{0.03} _{-0.17}	0.12 ^{0.27} _{-0.27}	6.42 ^{0.04} _{-0.19}	SN2008ax	IIb	7.00 ^{0.03} _{-1.30}	0.30 ^{0.06} _{-0.16}	0.04 ^{0.16} _{-0.09}	6.74 ^{0.06} _{-0.05}
SN1990L	Ia	7.65 ^{0.05} _{-0.10}	0.00 ^{0.00} _{-0.00}	-3.31 ^{0.07} _{-0.03}	3.99 ^{0.07} _{-0.04}	SN1985F	Ib	7.00 ^{1.34} _{-0.10}	0.70 ^{-0.70} _{-0.70}	0.20 ^{0.11} _{-0.11}	6.90 ^{0.05} _{-0.00}
SN2019ltw	IIb	6.55 ^{0.01} _{-0.30}	1.40 ^{0.05} _{-0.09}	0.93 ^{0.52} _{-0.91}	7.18 ^{0.24} _{-0.02}	SN1971I	Ia	6.55 ^{0.09} _{-0.05}	2.00 ^{-0.19} _{-0.19}	-0.09 ^{0.04} _{-0.18}	6.16 ^{0.14} _{-0.08}
SN2018cow	Ic	9.50 ^{0.02} _{-2.47}	0.00 ^{1.43} _{-0.00}	-2.16 ^{1.79} _{-0.02}	6.87 ^{0.02} _{-0.28}	SN2018acj	II	9.00 ^{0.01} _{-0.06}	0.00 ^{0.00} _{-0.00}	-2.25 ^{0.06} _{-0.01}	6.85 ^{0.00} _{-0.05}
SN2020aac	II	8.40 ^{0.02} _{-0.78}	0.00 ^{1.50} _{-0.00}	-1.35 ^{1.74} _{-0.03}	6.72 ^{0.05} _{-0.05}	SN2020lf	II	7.00 ^{0.03} _{-0.10}	0.50 ^{0.08} _{-0.08}	-0.31 ^{0.11} _{-0.04}	6.38 ^{0.06} _{-0.03}
SN2006W	II	9.35 ^{0.06} _{-0.16}	0.00 ^{0.00} _{-0.00}	-2.71 ^{0.15} _{-0.09}	7.02 ^{0.05} _{-0.07}	SN2017cdz	II	6.65 ^{0.05} _{-0.05}	0.90 ^{0.04} _{-0.04}	0.32 ^{0.06} _{-0.44}	6.67 ^{0.03} _{-0.14}
SN2008az	II	9.50 ^{0.02} _{-2.90}	0.00 ^{2.23} _{-0.00}	-1.33 ^{2.40} _{-0.01}	7.70 ^{0.02} _{-0.33}	SN1966J	Ia	7.05 ^{0.02} _{-0.10}	0.50 ^{0.06} _{-0.09}	-1.36 ^{0.14} _{-0.01}	5.38 ^{0.06} _{-0.01}
SN2016brw	II	8.75 ^{0.02} _{-2.13}	0.00 ^{1.67} _{-0.00}	-1.50 ^{1.99} _{-0.04}	7.02 ^{0.03} _{-0.14}	SN1999bw	II	7.00 ^{1.19} _{-0.37}	0.70 ^{-0.70} _{-0.70}	-0.70 ^{0.54} _{-0.04}	6.00 ^{0.19} _{-0.00}
SN2005kf	Ic	9.30 ^{0.03} _{-0.41}	0.00 ^{0.00} _{-0.00}	-1.44 ^{0.03} _{-0.08}	7.41 ^{0.02} _{-0.06}	SN2002bu	II	8.95 ^{0.19} _{-0.00}	0.00 ^{0.00} _{-0.00}	-2.70 ^{0.07} _{-0.03}	5.96 ^{0.03} _{-0.06}
SN2019hyk	II	6.25 ^{0.03} _{-0.33}	1.20 ^{0.02} _{-0.56}	0.43 ^{0.36} _{-1.39}	6.38 ^{0.07} _{-0.73}	SN2002cs	Ia	6.55 ^{3.16} _{-0.01}	3.00 ^{0.03} _{-0.00}	0.30 ^{0.15} _{-0.22}	6.55 ^{0.46} _{-0.01}
SN2018dbg	Ibc	8.65 ^{0.33} _{-1.70}	0.20 ^{0.92} _{-0.20}	-0.41 ^{1.36} _{-0.25}	7.82 ^{0.07} _{-0.10}	SN2014bc	II	9.70 ^{0.04} _{-0.34}	0.00 ^{0.00} _{-0.00}	-0.91 ^{0.04} _{-0.05}	8.59 ^{0.10} _{-0.10}
SN2001fv	II	8.65 ^{0.01} _{-0.34}	0.00 ^{0.00} _{-0.00}	-1.70 ^{0.08} _{-0.04}	6.53 ^{0.04} _{-0.08}	SN1981K	II	9.45 ^{0.02} _{-2.83}	0.00 ^{0.00} _{-0.00}	-1.44 ^{2.35} _{-0.05}	7.57 ^{0.01} _{-0.27}
SN2014ge	Ib	6.55 ^{0.10} _{-0.02}	1.80 ^{0.03} _{-0.00}	0.34 ^{0.01} _{-0.18}	6.59 ^{0.06} _{-0.08}	SN2005cs	II	6.65 ^{2.00} _{-0.09}	1.60 ^{0.04} _{-0.06}	0.61 ^{0.11} _{-0.81}	6.96 ^{0.17} _{-0.03}
SN2020jhf	Ia	9.15 ^{0.01} _{-0.01}	0.00 ^{0.00} _{-0.00}	-1.95 ^{0.01} _{-0.01}	7.60 ^{0.02} _{-0.02}	SN1945A	I	9.30 ^{0.01} _{-0.17}	0.00 ^{0.00} _{-0.00}	-1.77 ^{0.06} _{-0.06}	7.79 ^{0.01} _{-0.01}
SN2019upq	II	6.40 ^{0.03} _{-0.04}	0.60 ^{0.00} _{-0.17}	-0.94 ^{0.03} _{-0.09}	5.15 ^{0.03} _{-0.05}	SN2011dh	IIb	7.00 ^{0.05} _{-0.38}	0.40 ^{0.05} _{-0.16}	-0.47 ^{0.54} _{-0.10}	6.22 ^{0.20} _{-0.05}
SN2020fcw	Ia	9.75 ^{0.31} _{-0.06}	0.00 ^{0.00} _{-0.00}	-5.70 ^{1.75} _{-0.01}	8.97 ^{0.16} _{-0.03}	SN1994I	Ic	9.60 ^{0.03} _{-0.36}	0.00 ^{0.00} _{-0.00}	-0.95 ^{0.03} _{-0.04}	8.28 ^{0.02} _{-0.11}
SN1989A	Ia	8.80 ^{0.01} _{-0.13}	0.00 ^{0.00} _{-0.00}	-2.39 ^{0.07} _{-0.03}	6.29 ^{0.01} _{-0.12}	SN1997ef	Ic	6.60 ^{0.06} _{-0.04}	1.40 ^{0.01} _{-0.16}	0.04 ^{0.20} _{-0.11}	6.34 ^{0.20} _{-0.04}
SN2020xqj	II	9.05 ^{0.08} _{-1.98}	0.00 ^{0.00} _{-0.00}	-1.89 ^{0.09} _{-0.04}	7.18 ^{0.06} _{-0.06}	SN1997bm	Ia	8.95 ^{0.09} _{-0.00}	0.00 ^{0.00} _{-0.00}	-2.63 ^{0.06} _{-0.01}	6.35 ^{0.00} _{-0.06}
SN2014cn	II	6.65 ^{1.88} _{-0.09}	1.40 ^{0.03} _{-1.40}	0.03 ^{0.12} _{-1.69}	6.38 ^{0.00} _{-0.00}	SN2016iuh	Ia	9.55 ^{0.09} _{-0.20}	0.00 ^{0.00} _{-0.00}	-2.37 ^{0.11} _{-0.09}	7.55 ^{0.08} _{-0.08}
SN1999gr	Ia	7.65 ^{0.01} _{-0.05}	0.50 ^{0.25} _{-0.29}	-2.74 ^{0.10} _{-0.25}	4.56 ^{0.10} _{-0.08}	SN2019arb	Ia	9.30 ^{0.01} _{-0.08}	0.00 ^{0.00} _{-0.00}	-2.48 ^{0.21} _{-0.00}	7.72 ^{0.00} _{-0.03}
SN1982C	Ia	7.45 ^{0.13} _{-0.11}	1.50 ^{0.05} _{-0.02}	-1.73 ^{0.08} _{-0.12}	5.36 ^{0.06} _{-0.03}	SN2015ba	II	9.35 ^{0.12} _{-0.29}	0.00 ^{0.00} _{-0.00}	-2.08 ^{0.04} _{-0.09}	7.06 ^{0.04} _{-0.04}
SN2017iji	Ia	9.10 ^{0.01} _{-0.04}	0.00 ^{0.00} _{-0.00}	-0.65 ^{0.02} _{-0.02}	8.74 ^{0.01} _{-0.01}	SN1996cc	II	7.00 ^{0.04} _{-0.24}	0.40 ^{0.02} _{-0.17}	-0.59 ^{0.09} _{-0.00}	6.10 ^{0.01} _{-0.01}
SN2015X	II	6.60 ^{2.91} _{-0.04}	2.30 ^{0.00} _{-2.30}	0.58 ^{0.01} _{-0.19}	6.87 ^{0.32} _{-0.05}	SN2019cth	Ia	6.60 ^{0.08} _{-0.03}	2.10 ^{0.02} _{-0.18}	0.99 ^{0.18} _{-0.08}	7.29 ^{0.02} _{-0.02}
SN2011hn	II	6.65 ^{0.01} _{-0.08}	1.10 ^{0.06} _{-0.10}	-0.29 ^{0.12} _{-0.01}	6.06 ^{0.08} _{-0.01}	SN2007T	II	6.65 ^{0.04} _{-0.17}	1.50 ^{0.04} _{-0.17}	0.20 ^{0.48} _{-0.08}	6.54 ^{0.30} _{-0.03}
SN2013hg	Ia	7.25 ^{0.34} _{-0.16}	1.40 ^{0.26} _{-0.50}	-1.79 ^{0.24} _{-0.38}	5.14 ^{0.10} _{-0.06}	SN1999by	Ia	9.50 ^{0.05} _{-0.37}	0.00 ^{0.00} _{-0.00}	-2.21 ^{0.04} _{-0.03}	6.93 ^{0.03} _{-0.07}
SN1941C	II	6.65 ^{0.28} _{-0.08}	1.10 ^{0.02} _{-0.69}	-0.93 ^{0.11} _{-0.45}	5.41 ^{0.06} _{-0.33}	SN1957A	Ia	9.35 ^{0.12} _{-0.31}	0.00 ^{0.00} _{-0.00}	-2.44 ^{0.04} _{-0.16}	6.79 ^{0.00} _{-0.27}
SN2019tdf	Ia	6.70 ^{1.75} _{-0.08}	1.80 ^{0.01} _{-1.63}	0.19 ^{0.01} _{-1.73}	6.58 ^{0.13} _{-0.12}	SN1972R	Ib	6.40 ^{2.98} _{-0.04}	2.50 ^{0.05} _{-2.50}	0.28 ^{0.94} _{-0.04}	6.38 ^{0.04} _{-0.04}
SN2018ccb	II	9.70 ^{0.08} _{-1.00}	0.20 ^{0.06} _{-0.20}	-2.67 ^{0.57} _{-0.18}	6.59 ^{0.07} _{-0.21}	SN2014cv	IIP	10.05 ^{0.00} _{-0.30}	0.00 ^{0.00} _{-0.00}	-2.32 ^{0.41} _{-0.00}	8.37 ^{0.06} _{-0.07}
SN2022mji	II	9.40 ^{0.03} _{-2.77}	0.00 ^{0.06} _{-0.00}	-1.27 ^{0.29} _{-0.03}	7.67 ^{0.02} _{-0.25}	SN2021afsj	Ia	6.65 ^{0.29} _{-0.07}	1.80 ^{0.01} _{-0.01}	0.24 ^{0.08} _{-0.48}	6.59 ^{0.10} _{-0.02}
SN1970L	I	6.95 ^{0.10} _{-0.12}	0.30 ^{0.00} _{-0.30}	-1.99 ^{0.21} _{-0.20}	4.64 ^{0.12} _{-0.07}	SN2000dv	Ib	6.65 ^{0.07} _{-0.07}	1.50 ^{0.00} _{-0.00}	0.47 ^{0.08} _{-0.08}	6.82 ^{0.05} _{-0.04}
SN1991bi	Ia	9.20 ^{0.01} _{-0.04}	0.00 ^{0.00} _{-0.00}	-2.24 ^{0.04} _{-0.04}	7.50 ^{0.01} _{-0.01}	SN2016bme	II	6.25 ^{0.05} _{-0.22}	2.20 ^{0.08} _{-0.10}	0.35 ^{0.21} _{-0.05}	6.30 ^{0.04} _{-0.01}
SN2006M	II	6.60 ^{0.03} _{-0.05}	0.70 ^{0.01} _{-0.01}	0.04 ^{0.05} _{-0.05}	6.34 ^{0.04} _{-0.04}	SN2019gsc	Ia	7.05 ^{0.03} _{-0.11}	0.10 ^{0.07} _{-0.07}	-0.66 ^{0.16} _{-0.01}	6.08 ^{0.06} _{-0.01}
SN2002cw	Ib	6.65 ^{0.25} _{-0.06}	1.90 ^{0.03} _{-0.65}	-0.13 ^{0.07} _{-0.37}	6.22 ^{0.04} _{-0.09}	SN20220qm	Ic	6.55 ^{0.01} _{-0.37}	0.30 ^{0.09} _{-0.11}	-1.15 ^{0.43} _{-0.01}	5.05 ^{0.08} _{-0.01}
SN2021wcu	Ia	6.60 ^{0.02} _{-0.09}	0.90 ^{0.00} _{-0.12}	-0.58 ^{0.11} _{-0.02}	5.73 ^{0.04_{-0.03}}	SN1963K	Ia	9.15 ^{0.08} _{-0.08}	0.00 ^{0.04} _{-0.00}	-2.57 ^{0.15} _{-0.00}	6.98 ^{0.01} _{-0.02}
SN2001ej	Ib	6.50 ^{0.01} _{-0.17}	1.60 ^{0.04} _{-0.15}	0.87 ^{0.35} _{-0.10}	7.07 ^{0.08} _{-0.08}	SN1975T	II	6.50 ^{0.04} _{-0.04}	1.70 ^{0.07} _{-0.17}	-0.37 ^{0.20} _{-0.20}	5.83 ^{0.09} _{-0.09}
SN2016bmd	IIb	9.05 ^{0.01} _{-0.08}	0.00 ^{0.00} _{-0.00}	-2.79 ^{0.09} _{-0.09}	6.44 ^{0.01} _{-0.06}	SN1975G	Ia	7.45 ^{0.08} _{-0.08}	1.40 ^{0.10} _{-0.10}	-2.11 ^{0.05} _{-0.13}	5.00 ^{0.12} _{-0.02}
SN2015U	Ibn	9.95 ^{0.09} _{-0.38}	0.40 ^{0.18} _{-0.00}	-2.11 ^{0.20} _{-0.01}	8.49 ^{0.06} _{-0.06}	SN1999A	II	8.75 ^{0.06} _{-0.14}	0.00 ^{0.00} _{-0.00}	-2.02 ^{0.07} _{-0.01}	6.57 ^{0.01} _{-0.12}
SN2010jv	Ia	9.50 ^{0.24} _{-0.16}	0.00 ^{0.00} _{-0.00}	-1.74 ^{0.11} _{-0.08}	8.27 ^{0.10} _{-0.08}	SN2022zkd	II	6.50 ^{0.01} _{-0.04}	0.00 ^{0.00} _{-0.00}	-1.74 ^{0.04} _{-0.03}	4.46 ^{0.04} _{-0.03}
SN2015bh	II	9.00 ^{0.00} _{-0.15}	0.00 ^{0.00} _{-0.00}	-1.87 ^{0.04} _{-0.06}	6.91 ^{0.01} _{-0.04}	SN1980D	II	6.50 ^{0.01} _{-0.22}	1.00 ^{0.05} _{-0.05}	-0.55 ^{0.06} _{-0.01}	5.65 ^{0.02} _{-0.01}
SN2007uy	Ib	6.65 ^{0.08} _{-0.08}	1.70 ^{0.01} _{-0.16}	0.32 ^{0.04} _{-0.04}	6.67 ^{0.05} _{-0.04}	SN2015Q	Ib	6.95 ^{1.54} _{-0.33</sub}			

Name	Type	$\log < t_*(yr) >$	A_V (mag)	$\log \text{SFR}$	$\log M$	Name	Type	$\log < t_*(yr) >$	A_V (mag)	$\log \text{SFR}$	$\log M$
SN2002A	II	8.80 ^{0.17} _{-0.04}	0.00 ^{0.00} _{-0.00}	-1.61 ^{0.07} _{-0.01}	7.06 ^{0.05} _{-0.03}	SN2018fpb	IIb	7.05 ^{0.14} _{-0.02}	0.50 ^{0.18} _{-0.21}	-0.36 ^{0.27} _{-0.21}	6.38 ^{0.12} _{-0.04}
SN2016bkx	IIP	6.65 ^{0.05} _{-0.06}	0.70 ^{0.03} _{-0.20}	0.15 ^{0.06} _{-0.12}	6.50 ^{0.01} _{-0.07}	SN1999ej	Ia	9.60 ^{0.02} _{-0.38}	0.00 ^{0.00} _{-0.00}	-3.07 ^{0.21} _{-0.05}	6.76 ^{0.01} _{-0.01}
SN2020drl	II	7.00 ^{0.07} _{-0.13}	0.00 ^{0.01} _{-0.00}	-0.88 ^{1.35} _{-0.00}	5.81 ^{1.63} _{-0.00}	SN2015cz	II	9.35 ^{0.12} _{-0.22}	0.00 ^{0.00} _{-0.00}	-1.99 ^{0.05} _{-0.05}	7.52 ^{0.03} _{-0.07}
SN2005B	II	6.60 ^{0.03} _{-0.04}	0.60 ^{0.03} _{-0.17}	-1.29 ^{0.02} _{-0.10}	5.00 ^{0.05} _{-0.05}	SN2020lkb	II	8.40 ^{0.07} _{-0.11}	0.00 ^{0.00} _{-0.00}	-2.04 ^{0.05} _{-0.05}	6.06 ^{0.06} _{-0.06}
SN2005ai	Ia	9.70 ^{0.01} _{-0.12}	1.40 ^{0.12} _{-0.27}	-7.44 ^{1.22} _{-0.04}	6.46 ^{0.07} _{-0.10}	SN2007pk	IIn	6.95 ^{0.95} _{-0.07}	0.60 ^{0.05} _{-0.60}	0.10 ^{0.11} _{-0.11}	6.74 ^{0.14} _{-0.09}
SN2011aa	Iapc	7.05 ^{0.09} _{-0.00}	0.30 ^{0.02} _{-0.19}	-1.22 ^{0.00} _{-0.13}	5.52 ^{0.01} _{-0.04}	iPTF13dkz	II	6.00 ^{0.52} _{-0.00}	2.00 ^{0.02} _{-0.00}	1.17 ^{0.07} _{-0.07}	6.87 ^{0.00} _{-0.26}
SN2019clq	Ib	6.65 ^{0.07} _{-0.00}	0.70 ^{0.04} _{-0.00}	0.03 ^{0.01} _{-0.03}	6.37 ^{0.06} _{-0.01}	SN2016F	Ia	8.75 ^{0.02} _{-0.09}	0.00 ^{0.00} _{-0.00}	-2.47 ^{0.04} _{-0.04}	6.12 ^{0.04} _{-0.04}
SN2008bo	IIb	8.75 ^{0.24} _{-0.45}	0.40 ^{0.18} _{-0.40}	-1.59 ^{0.23} _{-0.39}	6.72 ^{0.10} _{-0.01}	SN2006ei	Ic	6.50 ^{0.07} _{-0.14}	2.80 ^{0.02} _{-0.12}	7.10 ^{0.02} _{-0.05}	
SN2008ij	II	9.75 ^{0.05} _{-0.25}	0.00 ^{0.00} _{-0.00}	-2.30 ^{0.03} _{-0.02}	6.99 ^{0.04} _{-0.07}	SN2000dj	II	6.50 ^{0.18} _{-0.22}	1.80 ^{0.02} _{-0.21}	-0.32 ^{0.28} _{-0.30}	5.88 ^{0.40} _{-0.11}
SN2018fmf	II	7.00 ^{0.05} _{-0.06}	0.60 ^{0.02} _{-0.23}	-0.66 ^{0.06} _{-0.14}	6.03 ^{0.13} _{-0.05}	SN2007J	Ia	7.15 ^{0.90} _{-1.15}	1.00 ^{0.78} _{-0.77}	-0.97 ^{1.67} _{-0.88}	5.86 ^{0.54} _{-0.01}
SN2010gi	II	6.65 ^{0.10} _{-0.06}	1.50 ^{0.04} _{-0.20}	0.34 ^{0.62} _{-0.06}	6.68 ^{0.31} _{-0.12}	iPTF13ebh	Ia	9.35 ^{0.01} _{-0.08}	0.00 ^{0.00} _{-0.00}	-3.43 ^{0.20} _{-0.00}	7.05 ^{0.01} _{-0.01}
SN2017tgt	Ia	9.35 ^{0.03} _{-0.32}	0.00 ^{0.00} _{-0.00}	-2.25 ^{0.08} _{-0.08}	6.71 ^{0.05} _{-0.05}	SN1976F	II	6.50 ^{0.36} _{-0.36}	0.00 ^{0.00} _{-0.00}	-2.62 ^{0.03} _{-0.03}	3.59 ^{0.08} _{-0.01}
SN2018gj	IIb	6.50 ^{0.01} _{-0.04}	0.00 ^{0.00} _{-0.00}	-1.35 ^{0.01} _{-0.01}	4.85 ^{0.01} _{-0.01}	SN1938A	I	10.10 ^{0.01} _{-0.04}	3.00 ^{0.02} _{-0.08}	-16.61 ^{0.03} _{-0.02}	7.26 ^{0.02} _{-0.02}
SN2019bxq	IIn	6.55 ^{0.03} _{-0.10}	2.20 ^{0.01} _{-0.13}	1.66 ^{0.08} _{-0.27}	7.91 ^{0.03} _{-0.22}	SN2011gb	Ia	6.50 ^{0.00} _{-0.07}	1.30 ^{0.06} _{-0.09}	-0.29 ^{0.07} _{-0.04}	5.91 ^{0.04} _{-0.03}
SN2004dd	II	7.00 ^{1.29} _{-0.05}	0.70 ^{0.04} _{-0.00}	-0.35 ^{0.01} _{-0.07}	6.35 ^{0.18} _{-0.04}	SN2006Q	II	10.05 ^{0.01} _{-0.14}	0.00 ^{0.00} _{-0.00}	-1.93 ^{0.37} _{-0.01}	8.76 ^{0.02} _{-0.02}
SN1998dk	Ia	6.65 ^{0.05} _{-0.21}	1.90 ^{0.06} _{-0.00}	0.58 ^{0.31} _{-0.17}	6.99 ^{0.02} _{-0.03}	ASASSN-14kg					
SN2009ig	Ia	9.45 ^{0.22} _{-0.00}	0.00 ^{0.00} _{-0.00}	-2.78 ^{0.07} _{-0.11}	7.04 ^{0.06} _{-0.09}	SN1999dj	II	8.70 ^{0.02} _{-0.19}	0.00 ^{0.00} _{-0.00}	-2.08 ^{0.04} _{-0.04}	6.43 ^{0.04} _{-0.04}
SN2004hx	II	6.50 ^{0.09} _{-0.01}	1.20 ^{0.01} _{-0.19}	-1.07 ^{0.01} _{-0.18}	5.13 ^{0.00} _{-0.08}	SN2002fb	Ia	9.85 ^{0.04} _{-2.80}	0.00 ^{0.00} _{-0.00}	-3.57 ^{3.55} _{-1.74}	7.37 ^{0.01} _{-0.01}
SN1995V	II	6.65 ^{0.36} _{-0.04}	1.90 ^{0.05} _{-0.90}	0.46 ^{0.01} _{-0.28}	6.81 ^{0.21} _{-0.07}	SN2006td	Ia	9.20 ^{0.01} _{-0.05}	0.00 ^{0.00} _{-0.00}	-2.77 ^{0.06} _{-0.05}	6.97 ^{0.05} _{-0.05}
SN2018ivc	II	9.55 ^{0.02} _{-0.32}	0.00 ^{0.00} _{-0.00}	-0.88 ^{0.05} _{-0.03}	8.37 ^{0.05} _{-0.07}	SN2005cx	Ia	6.60 ^{0.05} _{-0.02}	2.60 ^{0.01} _{-0.19}	1.14 ^{0.15} _{-0.11}	7.44 ^{0.02} _{-0.01}
SN1991ar	Ib	6.50 ^{0.00} _{-0.36}	1.40 ^{0.03} _{-0.00}	0.19 ^{0.57} _{-0.03}	6.39 ^{0.02} _{-0.01}	SN1992az	II	6.70 ^{0.13} _{-0.13}	2.10 ^{0.08} _{-0.27}	0.19 ^{0.04} _{-0.29}	6.59 ^{0.04} _{-0.16}
SDSS-II-SNS-I4215											
SN2006G	IIb	9.05 ^{0.01} _{-0.04}	0.00 ^{0.00} _{-0.00}	-2.52 ^{0.01} _{-0.08}	6.72 ^{0.01} _{-0.04}	SN2010gr	Ib-c	7.05 ^{0.19} _{-0.05}	1.60 ^{0.05} _{-0.28}	-0.69 ^{1.60} _{-0.28}	6.05 ^{0.56} _{-0.09}
SN1966G	I	9.10 ^{0.00} _{-0.08}	0.00 ^{0.00} _{-0.00}	-2.64 ^{0.01} _{-0.01}	6.74 ^{0.04} _{-0.00}	SN2004dw	II	10.10 ^{0.01} _{-0.10}	0.00 ^{0.00} _{-0.00}	-2.97 ^{0.08} _{-0.02}	7.00 ^{0.01} _{-0.07}
SN2022mjk	Ia	6.55 ^{0.04} _{-0.04}	3.00 ^{0.00} _{-3.00}	-0.75 ^{0.01} _{-0.54}	5.50 ^{0.33} _{-0.02}	SN2016hrv	II	6.65 ^{0.29} _{-0.10}	2.00 ^{0.04} _{-0.74}	0.61 ^{0.07} _{-0.07}	6.96 ^{0.02} _{-0.17}
SN2014da	Ia-91bg	9.65 ^{0.04} _{-0.17}	0.00 ^{0.00} _{-0.00}	-2.19 ^{0.19} _{-0.23}	8.56 ^{0.01} _{-0.09}	SN2000ez	II	6.95 ^{0.01} _{-0.09}	0.00 ^{0.00} _{-0.00}	-0.47 ^{0.07} _{-0.07}	6.17 ^{0.03} _{-0.00}
SN2006ld	Ib	6.60 ^{0.00} _{-0.08}	0.50 ^{0.04} _{-0.09}	-0.66 ^{0.28} _{-0.01}	5.64 ^{0.23} _{-0.01}	SN1988ac	Ibc	6.70 ^{0.02} _{-0.11}	0.10 ^{0.07} _{-0.08}	0.01 ^{0.17} _{-0.00}	6.40 ^{0.08} _{-0.01}
SN2009hr	Ia	10.10 ^{0.01} _{-0.01}	3.00 ^{0.02} _{-0.08}	-16.44 ^{0.02} _{-0.01}	7.43 ^{0.02} _{-0.02}	SN2011fe	Ia	6.00 ^{0.46} _{-0.00}	0.00 ^{0.00} _{-0.00}	-2.72 ^{0.05} _{-0.05}	2.98 ^{0.01} _{-0.11}
SN2017fgc	Ia	7.70 ^{0.04} _{-0.02}	0.40 ^{0.01} _{-0.23}	-2.16 ^{0.03} _{-0.01}	5.19 ^{0.04} _{-0.04}	SN2023ixf	II	6.00 ^{0.00} _{-0.00}	0.70 ^{0.00} _{-0.50}	0.42 ^{0.05} _{-0.05}	6.12 ^{0.01} _{-0.41}
SN2003hm	Ia	9.30 ^{0.15} _{-0.09}	0.00 ^{0.00} _{-0.00}	-1.80 ^{0.07} _{-0.07}	7.76 ^{0.09} _{-0.09}	SN1909A	II	6.00 ^{0.00} _{-0.00}	0.00 ^{0.00} _{-0.00}	-2.72 ^{0.05} _{-0.05}	2.98 ^{0.07} _{-0.11}
ASASSN-15mc											
SN1976G	Ia	9.45 ^{0.14} _{-0.00}	0.00 ^{0.00} _{-0.00}	-2.74 ^{0.05} _{-0.04}	6.69 ^{0.03} _{-0.06}	SN1951H	II	6.50 ^{0.02} _{-0.09}	0.00 ^{0.00} _{-0.00}	-0.13 ^{0.15} _{-0.05}	6.07 ^{0.05} _{-0.00}
SN2010eb	Ia	7.55 ^{0.03} _{-0.13}	0.80 ^{0.05} _{-0.25}	-2.31 ^{0.13} _{-0.14}	4.89 ^{0.03} _{-0.03}	SN1970G	II	6.00 ^{0.33} _{-0.00}	0.00 ^{0.00} _{-0.00}	0.13 ^{0.00} _{-0.00}	5.83 ^{0.00} _{-0.00}
SN2018hd	Ic	6.65 ^{0.06} _{-0.20}	1.90 ^{0.05} _{-0.62}	1.61 ^{0.10} _{-0.43}	7.95 ^{0.11} _{-0.09}	SN1991bg	Ia	9.25 ^{0.09} _{-0.03}	0.00 ^{0.00} _{-0.00}	-2.55 ^{0.32} _{-0.34}	7.41 ^{0.09} _{-0.09}
SN2008ie	IIb	9.25 ^{0.01} _{-0.08}	0.00 ^{0.08} _{-0.00}	-2.97 ^{0.18} _{-0.01}	6.98 ^{0.01} _{-0.02}	SN2004gk	Ic	9.25 ^{0.05} _{-2.63}	0.00 ^{0.00} _{-0.00}	-2.49 ^{0.01} _{-0.01}	7.47 ^{0.09} _{-0.00}
SN1998es	Iapc	9.10 ^{0.25} _{-0.06}	0.00 ^{0.00} _{-0.00}	-2.30 ^{0.19} _{-0.01}	7.08 ^{0.01} _{-0.06}	SN2013am	II	9.30 ^{0.23} _{-0.07}	0.00 ^{0.00} _{-0.00}	-1.94 ^{0.10} _{-0.05}	7.62 ^{0.00} _{-0.00}
SN2001ed	Ia	6.90 ^{0.20} _{-0.20}	1.20 ^{0.01} _{-0.04}	0.26 ^{0.29} _{-0.15}	6.82 ^{0.11} _{-0.11}	SN1997bs	IIn	9.00 ^{0.09} _{-0.09}	0.00 ^{0.00} _{-0.00}	-1.65 ^{0.03} _{-0.03}	7.31 ^{0.03} _{-0.03}
SN2003G	IIIn	6.00 ^{0.63} _{-0.00}	2.30 ^{0.03} _{-0.25}	1.28 ^{0.10} _{-1.00}	6.98 ^{0.04} _{-0.29}	SN1989B	Ia	6.65 ^{2.61} _{-0.08}	2.00 ^{0.04} _{-0.04}	1.14 ^{0.11} _{-2.20}	7.49 ^{0.29} _{-0.01}
SN2017glq	Ia	6.95 ^{0.44} _{-0.00}	0.70 ^{0.10} _{-0.00}	-0.08 ^{0.08} _{-0.08}	6.56 ^{0.27} _{-0.05}	SN2009hd	II	8.35 ^{0.76} _{-0.14}	0.40 ^{1.50} _{-0.00}	-0.71 ^{1.74} _{-2.20}	7.32 ^{0.26} _{-0.00}
SN2015ap	Ib-c	6.05 ^{0.55} _{-0.11}	0.20 ^{0.01} _{-0.14}	0.55 ^{0.14} _{-0.05}	6.30 ^{0.01} _{-0.01}	SN1973R	II	9.35 ^{0.39} _{-0.14}	0.00 ^{0.00} _{-0.08}	-1.88 ^{0.07} _{-0.41}	7.47 ^{0.11} _{-0.11}
SN2005mg	II	6.75 ^{0.21} _{-0.11}	3.00 ^{0.02} _{-0.00}	1.14 ^{0.05} _{-0.07}	7.59 ^{0.04_{-0.07}}	SN2016cok	II	6.65 ^{1.95} _{-0.07}	1.70 ^{0.00} _{-0.00}	0.52 ^{0.03} _{-0.03}	6.86 ^{0.01} _{-0.01}
SN2013fs	II	10.10 ^{0.09} _{-0.14}	0.00 ^{0.00} _{-0.00}	-2.55 ^{0.01} _{-0.01}	7.76 ^{0.02} _{-0.13}	SN2001ez	II	10.10 ^{0.02} _{-0.30}	0.00 ^{0.00} _{-0.00}	-2.44 ^{2.98} _{-2.20}	7.53 ^{0.07} _{-0.04}
SN2006dg	Ic	8.75 ^{0.06} _{-0.10}	0.00 ^{0.00} _{-0.00}	-2.15 ^{0.08} _{-0.05}	6.43 ^{0.08} _{-0.04}	SN2001is	Ib	6.50 ^{0.40} _{-0.40}	2.10 ^{0.02} _{-0.00}	0.19 ^{0.51} _{-0.04}	6.39 ^{0.07} _{-0.51}
SN2003gd	II	6.60<									

Name	Type	$\log < t_*(yr) >$	A_V (mag)	$\log \text{SFR}$	$\log M$
SN2008im	Ib	7.20 ^{0.15} _{-0.07}	3.00 ^{0.02} _{-0.12}	-1.16 ^{0.04} _{-0.14}	5.71 ^{0.08} _{-0.01}
SN2008eb	Ic	6.80 ^{0.25} _{-0.04}	3.00 ^{0.03} _{-0.51}	0.80 ^{0.01} _{-0.46}	7.29 ^{0.01} _{-0.19}
SN2008du	Ic	6.95 ^{1.33} ₋₁₇	0.80 ^{0.43} _{-0.80}	-0.19 ^{0.35} _{-0.19}	6.45 ^{0.18} _{-0.02}
SN2007rz	Ic	6.25 ^{0.62} _{-0.12}	2.80 ^{0.03} _{-0.42}	1.48 ^{0.18} _{-0.97}	7.43 ^{0.02} _{-0.36}
SN2006bo	IIIn	6.00 ^{0.84} _{-0.00}	0.70 ^{0.08} _{-0.60}	-0.68 ^{0.06} _{-1.43}	5.02 ^{0.06} _{-0.47}
SN2003gt	Ia	9.85 ^{0.10} _{-0.37}	0.00 ^{0.00} _{-0.00}	-2.47 ^{0.16} _{-0.02}	7.49 ^{0.06} _{-0.16}
SN2005aj	Ic	8.15 ^{0.09} _{-0.12}	3.00 ^{0.02} _{-0.09}	-1.96 ^{0.04} _{-0.05}	5.85 ^{0.07} _{-0.06}
SN2004gn	Ib	9.70 ^{0.09} _{-0.25}	0.00 ^{0.00} _{-0.00}	-2.20 ^{0.05} _{-0.14}	7.72 ^{0.08} _{-0.07}
SN1991T	Ia	9.85 ^{0.02} _{-0.40}	0.00 ^{0.00} _{-0.00}	-2.37 ^{0.03} _{-0.06}	7.11 ^{0.03} _{-0.11}
SN1981B	Ia	6.60 ^{2.22} _{-0.01}	1.80 ^{0.05} _{-1.80}	-0.29 ^{0.00} _{-2.14}	6.01 ^{0.19} _{-0.05}
SN2001B	Ib	7.10 ^{1.01} _{-0.05}	1.30 ^{0.00} _{-0.83}	-0.37 ^{0.04} _{-0.36}	6.41 ^{0.13} _{-0.04}
SN2002ji	Ib	6.65 ^{0.17} _{-2.46}	1.50 ^{0.09} _{-0.09}	0.20 ^{0.01} _{-0.01}	6.54 ^{0.30} _{-0.00}
SN2000fn	Ib	6.60 ^{2.46} _{-0.02}	2.00 ^{0.03} _{-2.00}	0.41 ^{0.00} _{-2.22}	6.71 ^{0.18} _{-0.06}
SN2000H	IIlb	7.60 ^{0.25} _{-0.34}	2.10 ^{0.26} _{-0.25}	-1.24 ^{0.29} _{-0.21}	6.02 ^{0.08} _{-0.02}
SN2018imj	II	7.20 ^{1.13} _{-0.15}	2.40 ^{0.17} _{-0.86}	-1.19 ^{0.21} _{-0.91}	5.68 ^{0.28} _{-0.03}
SN1999el	IIIn	10.05 ^{0.04} _{-0.01}	1.80 ^{0.00} _{-0.00}	-2.54 ^{0.09} _{-0.09}	7.45 ^{0.01} _{-0.01}
SN2020dpw	II	10.10 ^{0.01} _{-0.04}	2.30 ^{0.12} _{-0.26}	-2.48 ^{0.13} _{-0.13}	7.50 ^{0.01} _{-0.05}
SN2000E	Ia	8.20 ^{0.71} _{-0.11}	3.00 ^{0.02} _{-0.09}	-1.81 ^{0.04} _{-0.21}	6.06 ^{0.41} _{-0.06}
SN2015G	Ib	7.75 ^{0.36} _{-0.07}	2.70 ^{0.01} _{-0.25}	-2.48 ^{0.04} _{-0.22}	4.93 ^{0.11} _{-0.04}
PTF09dfk	Ib	8.45 ^{0.15} _{-1.81}	0.00 ^{0.00} _{-1.52}	-1.29 ^{1.79} _{-0.01}	6.86 ^{0.12} _{-0.05}
SN1999dn	Ib	6.70 ^{0.12} _{-0.12}	1.70 ^{0.00} _{-0.30}	0.63 ^{0.34} _{-0.34}	7.03 ^{0.17} _{-0.17}
SN2007fo	Ib	6.55 ^{0.03} _{-0.48}	1.80 ^{0.06} _{-0.08}	0.86 ^{0.00} _{-0.00}	7.11 ^{0.00} _{-0.00}
SN1998ey	Ic	6.55 ^{0.01} _{-0.55}	2.60 ^{0.06} _{-0.09}	0.40 ^{0.64} _{-0.01}	6.65 ^{0.11} _{-0.01}
PTF12gzk	Ic	6.55 ^{0.00} _{-0.01}	0.00 ^{0.02} _{-0.00}	-0.85 ^{0.12} _{-0.01}	5.40 ^{0.05} _{-0.01}
ASASSN14az	IIlb	7.70 ^{0.01} _{-0.09}	1.50 ^{0.00} _{-0.19}	-2.63 ^{0.08} _{-0.08}	4.72 ^{0.01} _{-0.06}
SN2003gk	Ib	6.60 ^{0.02} _{-0.33}	1.90 ^{0.05} _{-0.10}	0.48 ^{0.58} _{-0.03}	6.77 ^{0.28} _{-0.02}
SN2015ah	Ib	6.45 ^{0.09} _{-0.02}	1.90 ^{0.02} _{-0.20}	0.25 ^{0.00} _{-0.19}	6.40 ^{0.00} _{-0.08}
SN2006my	II	7.60 ^{0.01} _{-0.04}	0.40 ^{0.08} _{-0.00}	1.55 ^{0.05} _{-0.05}	8.80 ^{0.06} _{-0.05}
SN1987K	IIlb	7.60 ^{0.01} _{-0.04}	0.30 ^{0.00} _{-0.18}	1.67 ^{0.04} _{-0.05}	8.92 ^{0.04} _{-0.05}
SN1988E	II	9.55 ^{0.00} _{-0.31}	0.00 ^{0.00} _{-0.00}	-2.28 ^{0.06} _{-0.35}	7.63 ^{0.00} _{-0.11}
SN2011jm	Ic	6.65 ^{0.07} _{-0.22}	0.80 ^{0.05} _{-0.17}	-0.08 ^{0.32} _{-0.19}	6.27 ^{0.11} _{-0.10}
ASASSN-15ti	Ia	6.45 ^{1.13} _{-0.05}	0.00 ^{0.00} _{-0.00}	-1.90 ^{0.05} _{-1.24}	4.25 ^{0.04} _{-0.5}
SN2008ao	Ic	8.30 ^{0.24} _{-0.01}	1.30 ^{0.00} _{-0.00}	-1.59 ^{0.22} _{-0.22}	6.39 ^{0.07} _{-0.03}
SN2003cg	Ia	9.80 ^{0.17} _{-0.27}	0.00 ^{0.11} _{-0.34}	-2.43 ^{0.22} _{-0.22}	8.23 ^{0.08} _{-0.03}
SN1984E	II	6.50 ^{0.13} _{-0.02}	2.20 ^{0.03} _{-0.18}	0.18 ^{0.01} _{-0.24}	6.38 ^{0.16} _{-0.09}
SN2012cw	Ic	9.25 ^{0.17} _{-0.32}	0.00 ^{0.00} _{-0.00}	-2.42 ^{0.09} _{-0.05}	7.00 ^{0.08} _{-0.01}
SN2003ef	II	9.10 ^{0.09} _{-0.10}	0.00 ^{0.00} _{-0.00}	-1.84 ^{0.13} _{-0.04}	7.35 ^{0.02} _{-0.05}
SN2016cvn	Ia	9.40 ^{0.00} _{-0.20}	0.00 ^{0.00} _{-0.00}	-1.95 ^{0.05} _{-0.15}	7.71 ^{0.03} _{-0.08}
SN2005bo	Ia	9.00 ^{0.04} _{-0.14}	0.00 ^{0.00} _{-0.00}	-1.82 ^{0.07} _{-0.05}	7.04 ^{0.03} _{-0.05}
ASASSN-15tw	II	6.65 ^{0.28} _{-0.05}	1.10 ^{0.03} _{-0.65}	-0.61 ^{0.05} _{-0.43}	5.74 ^{0.04} _{-0.14}
SN2008aq	II-IIIb	6.60 ^{0.05} _{-0.02}	1.00 ^{0.02} _{-0.23}	-0.37 ^{0.00} _{-0.13}	5.93 ^{0.00} _{-0.09}
SN2016aa	II	6.65 ^{0.28} _{-0.05}	1.10 ^{0.03} _{-0.65}	-0.61 ^{0.05} _{-0.43}	5.74 ^{0.04} _{-0.14}
SN2015P	II	6.95 ^{0.03} _{-0.33}	0.30 ^{0.58} _{-0.17}	-1.44 ^{0.44} _{-0.40}	5.20 ^{0.15} _{-0.05}
SN2018ebt	Ic	6.30 ^{0.58} _{-0.05}	2.90 ^{0.01} _{-0.65}	-0.16 ^{0.09} _{-0.46}	5.84 ^{0.05} _{-0.58}
SN2017jfs	IIIn	6.95 ^{0.03} _{-0.33}	0.60 ^{0.63} _{-0.12}	0.20 ^{0.48} _{-0.09}	6.84 ^{0.18} _{-0.03}
SN1986E	II	9.20 ^{0.00} _{-0.04}	0.00 ^{0.00} _{-0.00}	-2.59 ^{0.01} _{-0.01}	7.15 ^{0.00} _{-0.01}
SN2014L	Ic	6.65 ^{0.33} _{-0.09}	1.90 ^{0.04} _{-0.80}	1.04 ^{0.12} _{-0.53}	7.39 ^{0.09} _{-0.01}
SN1986I	II	6.80 ^{1.05} _{-0.19}	1.10 ^{0.12} _{-1.10}	0.48 ^{0.12} _{-1.21}	6.98 ^{0.21} _{-0.21}
SN1967H	II	6.55 ^{0.05} _{-0.18}	0.80 ^{0.01} _{-0.12}	0.48 ^{0.30} _{-0.20}	6.73 ^{0.21} _{-0.07}
SN1972Q	II	7.05 ^{0.11} _{-0.10}	0.30 ^{0.00} _{-0.11}	-0.67 ^{0.10} _{-0.04}	6.07 ^{0.05} _{-0.03}
SN2005kj	IIIn	9.15 ^{0.07} _{-0.06}	0.00 ^{0.00} _{-0.00}	-2.04 ^{0.12} _{-0.01}	7.51 ^{0.00} _{-0.03}
SN2005ip	IIIn	6.60 ^{2.93} _{-0.03}	2.40 ^{0.03} _{-2.40}	0.58 ^{0.00} _{-2.53}	6.88 ^{0.27} _{-0.06}
SN2005ek	Ic	8.75 ^{0.08} _{-0.17}	1.00 ^{0.13} _{-0.16}	-2.55 ^{0.15} _{-0.12}	6.04 ^{0.07} _{-0.09}
SN2004dk	Ib	6.10 ^{0.83} _{-0.03}	2.50 ^{0.02} _{-0.25}	0.64 ^{0.12} _{-0.29}	6.44 ^{0.04} _{-0.44}
SN2020hvp	Ib	9.40 ^{0.03} _{-0.11}	0.30 ^{0.00} _{-0.14}	-3.37 ^{0.54} _{-0.30}	7.43 ^{0.04} _{-0.04}
SN2006eg	Ib-c	6.60 ^{3.21} _{-0.01}	2.60 ^{0.06} _{-2.60}	0.45 ^{0.00} _{-2.70}	6.75 ^{0.42} _{-0.02}
PS15cwt	IIIn	6.80 ^{0.47} _{-0.51}	1.60 ^{0.22} _{-0.78}	-0.81 ^{0.94} _{-0.71}	5.69 ^{0.47} _{-0.27}
SN1969L	II	6.55 ^{0.02} _{-0.10}	0.20 ^{0.12} _{-0.12}	-2.10 ^{0.18} _{-0.01}	4.15 ^{0.10} _{-0.00}
SN1961V	II	6.45 ^{0.18} _{-0.09}	1.60 ^{0.00} _{-0.16}	-0.45 ^{0.49} _{-0.49}	5.70 ^{0.02} _{-0.29}
SN2007gr	Ic	9.00 ^{0.04} _{-2.37}	0.00 ^{0.13} _{-0.16}	-1.57 ^{2.04} _{-0.06}	7.02 ^{0.02} _{-0.20}
SN2015ab	Ia	9.45 ^{0.60} _{-0.03}	0.00 ^{0.00} _{-0.00}	-2.76 ^{0.12} _{-0.21}	7.38 ^{0.22} _{-0.00}
SN2006F	Ib	8.10 ^{0.22} _{-0.34}	2.30 ^{0.16} _{-0.36}	-0.69 ^{0.22} _{-0.25}	7.05 ^{0.08} _{-0.10}
SN2018ow	IIlb	9.30 ^{0.76} _{-2.24}	0.60 ^{0.20} _{-0.33}	-3.27 ^{0.40} _{-0.21}	6.55 ^{0.31} _{-0.05}
SN2016G	Ic	6.50 ^{0.18} _{-0.18}	2.70 ^{0.01} _{-0.20}	0.66 ^{0.44} _{-0.44}	6.86 ^{0.24} _{-0.24}
SN2016coi	Ic	6.60 ^{0.07} _{-0.09}	1.70 ^{0.01} _{-0.18}	-0.68 ^{0.20} _{-0.11}	5.62 ^{0.20} _{-0.05}
SN2014ad	Ic	8.35 ^{0.16} _{-0.16}	0.00 ^{0.00} _{-0.00}	-1.19 ^{0.03} _{-0.10}	6.85 ^{0.13} _{-0.02}
SN2009iz	Ib	7.00 ^{0.06} _{-0.04}	0.30 ^{0.00} _{-0.23}	-1.33 ^{0.01} _{-0.01}	5.37 ^{0.02} _{-0.09}
SN2007ru	Ic	6.25 ^{0.56} _{-0.25}	2.80 ^{0.11} _{-0.42}	-0.17 ^{0.28} _{-0.07}	5.78 ^{0.11} _{-0.19}
SN2007iq	Ic	6.00 ^{0.73} _{-0.00}	2.00 ^{0.05} _{-0.27}	0.05 ^{0.05} _{-1.01}	5.75 ^{0.05} _{-0.20}
SN2005da	Ic	10.10 ^{0.01} _{-0.04}	0.10 ^{0.36} _{-0.93}	-17.91 ^{0.28} _{-0.03}	5.96 ^{0.20} _{-0.05}
SN1999ed	II	6.95 ^{1.13} _{-0.15}	1.10 ^{0.09} _{-0.97}	-0.54 ^{0.15} _{-1.05}	6.10 ^{0.08} _{-0.08}
SN2004ge	Ic	10.00 ^{0.04} _{-3.37}	0.00 ^{0.00} _{-0.00}	-2.12 ^{0.01} _{-0.11}	7.49 ^{0.01} _{-0.55}
SN2000eo	IIIn	6.65 ^{0.11} _{-0.13}	1.90 ^{0.06} _{-0.27}	-0.59 ^{0.37} _{-0.13}	5.75 ^{0.31} _{-0.01}
SN1984L	Ib	6.65 ^{0.33} _{-0.03}	0.80 ^{0.02} _{-0.75}	-0.26 ^{0.05} _{-0.53}	6.09 ^{0.06} _{-0.19}
SN1962L	Ic	7.00 ^{1.23} _{-0.09}	0.60 ^{0.06} _{-0.60}	-1.14 ^{0.10} _{-0.03}	5.55 ^{0.25} _{-0.01}
SN1989M	Ia	9.45 ^{0.03} _{-0.37}	0.00 ^{0.00} _{-0.00}	-1.92 ^{0.03} _{-0.03}	7.40 ^{0.01} _{-0.01}
SN1998A	II	9.00 ^{0.36} _{-0.09}	0.00 ^{0.00} _{-0.00}	-2.10 ^{0.07} _{-0.13}	7.24 ^{0.12} _{-0.08}
SN1961H	Ia	9.35 ^{0.17} _{-0.04}	0.00 ^{0.00} _{-0.00}	-1.77 ^{0.19} _{-0.01}	8.71 ^{0.11} _{-0.00}
SN2004ao	Ib	6.60 ^{2.83} _{-0.04}	2.30 ^{0.03} _{-0.30}	-0.18 ^{0.04} _{-0.46}	6.12 ^{0.27} _{-0.05}
SN2006D	Ia	9.35 ^{0.89} _{-2.76}	0.00 ^{0.00} _{-1.65}	-2.76 ^{0.33} _{-0.01}	6.75 ^{0.09} _{-0.32}
SN2012au	Ib	8.95 ^{0.23} _{-2.32}	0.00 ^{0.00} _{-0.00}	-3.57 ^{0.05} _{-0.05}	4.93 ^{0.06} _{-0.16}
SN2007C	Ib	8.90 ^{0.08} _{-0.08}	0.00 ^{0.00} _{-0.00}	-1.57 ^{0.06} _{-0.00}	7.30 ^{0.00} _{-0.06}
SN2002jz	Ib	7.65 ^{0.02} _{-0.11}	2.30 ^{0.06} _{-0.09}	-1.96 ^{0.07} _{-0.00}	5.34 ^{0.02} _{-0.03}